Dr. Sanford,
Best Wishes.
Jeffrie

A GEOTHERMAL STUDY IN WEST-CENTRAL NEW MEXICO

by

Jeffrie D. Minier

Submitted in Partial Fulfillment of
the Requirements for the Degree of
Doctor of Philosophy

NEW MEXICO INSTITUTE OF MINING AND TECHNOLOGY

Socorro, New Mexico

December 1987

TABLE OF CONTENTS

	Page
Acknowledgements	iii
List of Figures	iv
List of Tables	v
Abstract	vi
Introduction	1
Tectonic Setting	5
Heat-Flow Data and Analyses	9
Coal Maturation Data and Analyses	52
Discussion	84
Conclusions	100
Appendix I - Heat Flow	103
Appendix II - Coal Maturation	122
Appendix III - Thermal Conductivity and Temperature Data	126
References	219

ACKNOWLEDGEMENTS

I thank Dr. Marshall Reiter, my advisor, for the guidance and encouragement which made the completion of this work possible. I also thank the other members of the advisory committee: Dr. Charles Chapin, Dr. Allan Gutjahr, Dr. Fred Phillips and Dr. Allan Sanford. Special thanks are extended to my parents for their support and encouragement. I am also grateful to my wife Leanna. Dr. Dan Stephens is gratefully acknowledged for his support.

This material is based upon work supported by the National Science Foundation under Grant No. EAR-8308367 and by the New Mexico Bureau of Mines and Mineral Resources. The following are thanked for permission to collect and present the data in this report: the Bureau of Land Management, the New Mexico Bureau of Mines and Mineral Resources, J.C. Brown, W. Green, D. Parker and H. Towner. Field assistance was provided by M.A. Reiter, M.W. Barroll and S. Jarpe. B.R. Broadwell aided with thermal conductivity measurement. D.T. Kendrick, Dr. Fred Kuellmer and B. Maiga provided assistance with vitrinite reflectance sample preparation and measurement. I gratefully acknowledge Frank Campbell for making coal samples, proximate analysis data and geophysical logs available to me as well as for providing field assistance. I also thank O.J. Anderson, F. Campbell and Dr. W.J. Stone for valuable discussions.

LIST OF FIGURES

		Page
Figure 1	Colorado Plateau Region and Study area	2
Figure 2	Heat-Flow Data and Volcanic Ages	13
Figure 3	Thermal Conductivity vs Saturation	16
Figure 4a	Temperature Increase at Depth	27
4b	Inferred Roof Thickness	30
Figure 5a	Temperature Effect of Sill Intrusion	33
5b	Sill Solidification vs. Conduction Cooling	34
Figure 6	Heat Flow in Southern Study Area	37
Figure 7a	Rectangular Prism	38
7b	Surface Heat-Flow Anomaly (width = 30 km)	40
7c	Surface Heat-Flow Anomaly (width = 10 km)	42
7d	Surface Heat-Flow Anomaly (width = 2 km)	44
Figure 8a	Thermal Convection in a Permeable Layer	47
8b	Thermal Gradient Required For Convection	48
Figure 9	Coal Maturation Data Regions	53
Figure 10	Volatile Matter vs. Vitrinite Reflectance	65
Figure 11	Surface Paleotemperature and Elevation	69
Figure 12	Coal Burial History Models	70
Figure 13a	Coal Temperatures at 1 km Due to Sill	77
13b	Coal Temperatures at 2 km Due to Sill	78
Figure 14	Inferred Basement Fault Pattern	93
Figure 15	Monoclines in Study Area	95
Figure 16	Histogram of Heat-Flow Values	99

LIST OF TABLES

		Page
Table 1	Heat-Flow Data	10
Table 2	Potassium-Argon Data	18
Table 3	Coal Data Summary	54
Table 4	Vitrinite Reflectance Measurement	56
Table 5	Analysis of Variance	59
Table 6	"F" Test Analysis	61
Table 7	"t" Test Analysis	63
Table 8	Summary of Burial Model Calculations	73
Table 9	Summary of Sill Emplacement Models	80
Table 10	Summary of Prismatic Intrusion Models	82

ABSTRACT

More than thirty new heat-flow data obtained in west-central New Mexico on the southern boundary of the Colorado Plateau (CP) demonstrate considerable spatial variability. A number of the heat-flow data suggest that the regional heat flow for the southern CP may be similar to that of the Plateau interior ($\lesssim$65 mW/m2). The relatively short distance from some of the sites with high heat flows to sites with low or intermediate heat flows suggests the presence of shallow, recent intrusions ($\lesssim$1 Ma) or shallow ground-water movement beneath the zone of heat-flow measurement. High heat flow at sites located within, and also away from, the volcanically-active Jemez lineament may be controlled by basement fault zones. Six new K-Ar dates indicate Pliocene and Pleistocene volcanic activity along the Jemez lineament between the White Mountains-Springerville and Zuni-Bandera volcanic fields. Low-rank, bituminous coals have been deposited across the study area (late Cretaceous). Predictions of coal maturation levels using relatively shallow coal burial histories ($\sim$1 km) are consistent with observed maturation values if a steady-state heat flow of 67 to 75 mW/m2 is assumed. However, if deeper coal burial histories (between 1 to 2 km) are more appropriate, then consistency between observed and predicted

maturation levels may be obtained by assuming a steady-state heat flow similar to that reported for the interior CP ($\lesssim$ 65 mW/m2). Profound regional trends in heat flow and coal maturation are not observed in the study area. Therefore it seems likely that any major post-Cretaceous thermal events associated with the Jemez lineament, or southern Plateau boundary, have been initiated relatively recently and/or occur at relatively great depths.

INTRODUCTION

Models for the tectonic evolution of the Colorado Plateau (CP, Figure 1) are constrained by geological and geophysical data. In particular, measurements of the present-day heat flow may provide considerable information regarding the occurrence, or lack of, significant thermal processes in the Plateau region (Bird, 1979; Reiter and others, 1979; Bodell and Chapman, 1982; Reiter and Clarkson, 1983; Eggleston and Reiter, 1984). However, the ability of heat-flow data to define heat-flow trends which might differentiate between the various thermal models is often diminished by a poor geographic distribution of the data and or ground-water movement (Mansure and Reiter, 1979; Bodell and Chapman, 1982).

The tectonic evolution of the CP, as well as the geologic relationships between the CP and the surrounding physiographic provinces, have been the subject of many geoscientific investigations (see Thompson and Zoback, 1979, for a summary of studies in the CP). For example, several investigations have characterized the transition between the CP and the Basin and Range Province (BRP) as a 50-100 km wide zone where crustal thinning is occurring. These studies suggest that the boundary of the CP is migrating toward the Plateau interior (Keller and others, 1979; Kelley, 1979; Thompson and Zoback, 1979; Aldrich and Laughlin, 1984; Eggleston and Reiter, 1984). Other investigators suggest that the southeastern boundary of the CP may

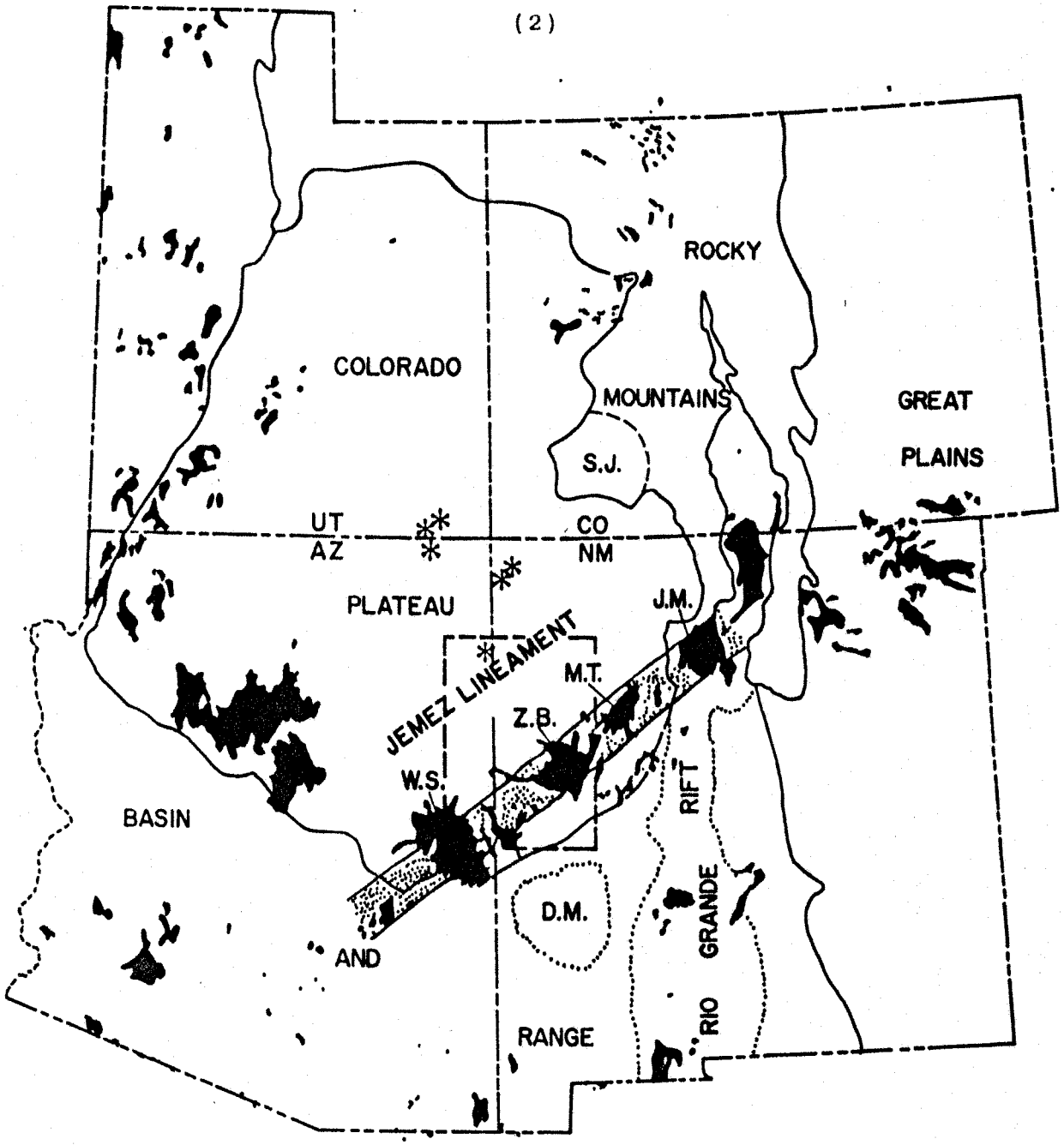

Figure 1. Map showing distribution of late Cenozoic (≈11 Ma, shaded areas) volcanic fields in Arizona, Colorado, New Mexico and Utah (after Aldrich and Laughlin, 1984). Volcanic field names: W.S., White Mountains-Springerville; Z.B., Zuni-Bandera; M.T., Mount Taylor; J.M., Jemez Mountains. D.M. and S.J. indicate the location and approximate areal extent of the Datil-Mogollon and San Juan volcanic fields. Asterisks indicate Oligocene volcanic rocks (Naeser, 1971). The Jemez lineament is located by the stippled area. The study area is located between the W.S. and Z.B. volcanic fields (box, dashed line).

be characterized as a deeply penetrating zone of weakness in the lithosphere (the Jemez lineament, Figure 1) which controls magma intrusion and influences crustal deformation (Chapin and others, 1978; Baldridge, 1979).

This paper discusses new and previous heat-flow data, new K-Ar dates, and coal maturation data in an area of west-central New Mexico on the southern periphery of the CP. Of particular interest is the spatial variability of the heat-flow data and possible temporal relationships between heat-flow anomalies and recent volcanic activity. Models regarding the tectonic evolution of the CP are examined for consistency with the data in the study area. The findings of the present study along the southern CP transition zone are also compared with geophysical investigations in other peripheral regions of the CP. It will be of interest to note if the data permit any conclusions about crustal thinning and geologic boundary migration or pre--existing zones of weakness in the study area along the southern CP.

This study attempts to identify past and present trends in the thermal regime of the southern CP using both heat--flow and coal maturation data. Heat-flow data relate to recent near-surface thermal processes and also, to some extent, earlier thermal events which occurred at greater depths. Over thirty new heat-flow data have been obtained which significantly improve the data distribution in the

study area. A heat-flow correction for vertical ground--water movement in the zone of measurement is applied to the heat-flow data in order to estimate the perturbing effect of energy transport by ground-water movement. Coal maturation data provide an estimate of the the total amount of heating which has occurred in the study area since late Cretaceous time. Analytical models are applied to the data as a means of estimating depth, lateral continuity and timing of possible thermal events in the region under study.

TECTONIC SETTING

The study area is located in west-central New Mexico on the southern periphery of the CP (Figure 1). The CP is an uplifted, relatively undeformed crustal block. Upper Cretaceous coal beds are present within the southeastern CP (e.g. Molenaar, 1977). The formation of the principal structural features (monoclines, uplifts, and basins) occurred during Laramide time (Kelley, 1955; Eardley, 1962); uplift of the Plateau as a whole followed later (approx. 24 to 5 Ma; Luchitta, 1972; McKee and McKee, 1972; Chapin and Seager, 1975). Monoclines on the CP are thought to reflect movement along high-angle Precambrian fault zones which were reactivated by northeast-southwest regional compression in Laramide time (Davis, 1978). The CP is bounded on the east by the southern Rocky Mountains and the Rio Grande rift (RGr), and on the south and west by the Basin and Range Province (BRP; Thompson and Burke, 1974; Eaton, 1979). To the north the CP borders the middle Rocky Mountains and the Wyoming basin.

The geophysical characteristics of the CP, such as crustal thickness, upper mantle seismic velocity, and heat flow, appear to be intermediate between those characteristic of the southern Great Plains and the RGr/BRP (Thompson and Zoback, 1979). In addition, the CP is relatively

quiescent seismically with perhaps modest late Cenozoic faulting and volcanism. Where heat-flow data exist, high values are restricted to the Plateau's peripheral regions (Keller and others, 1979; Eggleston and Reiter, 1984). For example, high heat flow along the western boundary of the CP with the BRP suggests a 50-100 km wide transition zone where crustal thinning is occurring, i.e. the boundary of the CP seems to be migrating toward the Plateau interior (Keller and others, 1979; Kelley, 1979; Thompson and Zoback, 1979; Aldrich and Laughlin, 1984; Eggleston and Reiter, 1984). The interior of the CP is a region of modest tectonic activity relative to the BRP. The Plateau, located between two zones of crustal extension (i.e. the RGr and BRP) demonstrates crustal compression (Smith and Sbar, 1974; Zoback and Zoback, 1980). More recent data, however, indicate that the CP is characterized by an extensional stress regime with the least horizontal principal stress oriented approximately north-northeast (Aldrich and others, 1987). Gravity data suggest that the CP is in isostatic equilibrium (Thompson and Zoback, 1979).

Cenozoic volcanism in the southern CP appears to have occurred during two distinct periods. Late Eocene to early Miocene volcanic rocks ($\sim$40-23 Ma) are present in the Datil-Mogollon volcanic field and east of Quemado (Figure 1; Elston, 1976; Laughlin and others, 1983). Tertiary volcanic activity also occurred in the Four Corners area and the San

Juan volcanic field (Pohlman, 1967; Armstrong, 1969; Naeser, 1971; Steven, 1975). Pliocene and Pleistocene volcanism is reflected by a northeast-trending alignment of volcanic fields on the southeastern periphery of the CP which defines the Jemez lineament (JL, Figure 1; Mayo, 1958; Chapin and others, 1978; Aldrich and Laughlin, 1984). The JL is approximately coincident with a Precambrian age province boundary (Lipman and Mehnert, 1979; Van Schmus and Bickford, 1981; Laughlin and others, 1982; Chapin and Cather, 1983). The Precambrian province boundary seems to have acted as a zone of crustal weakness, which was activated during late Cenozoic time by a changing regional stress regime and has leaked magmas to the surface (Chapin and others, 1978; Baldridge, 1979; Zoback and others, 1981; Aldrich and Laughlin, 1984). Geologic stress indicators suggest that the JL is a zone of transition between the regional compressive stress regime of the interior CP and the extensional stress regime of the RGr/BRP (Aldrich and Laughlin, 1984); although more recent data may make this conclusion suspect (Aldrich and others, 1987).

Th JL, part of which is represented by the northeast trending volcanic rocks in the study area (Figure 1), is associated with anomalously high electrical conductivity at relatively shallow depths between Mount Taylor and Springerville, AZ (Ander and others, 1984). This observation suggest magma intrusion in the crust along the lineament in

this area (Ander and others, 1984). A gravity anomaly over the Zuni-Bandera volcanic field, in the eastern part of the study area, is probably caused by a shallow (approximately 5 km) mafic intrusion unrelated, however, to recent basaltic volcanism (Ander and Heustis, 1982). Alternatively, the lack of differentiation in the McCarty's basalt flow of the Zuni-Bandera volcanic field suggests that the magma was imported rapidly from the mantle, without residing in crustal holding chambers long enough for significant differentiation to occur (Renault, 1970). The possible presence of recent shallow magmas will be addressed in the present manuscript by considering the heat-flow data obtained for this study. Analyses of coal maturation data are presented as constraints on potential thermal histories for the study area.

HEAT-FLOW DATA AND ANALYSES

Heat flow has been measured at several sites in the study area by obtaining the product of the temperature gradient and the appropriate rock thermal conductivity. Since measurements are obtained in the very uppermost portion of the earth's crust, heat-flow data are essentially boundary values. Therefore heat-flow data will relate to thermal processes which operate within and below the earth's crust such as volcanism, crustal thinning, and magma emplacement. Because chronologic control on volcanic events may be provided by radiometric dating of volcanic rocks, additional volcanic age data have been collected during this study. Heat-flow measurements and radiometric dates form an integrated database for analyses which are compared with the results of various models.

PRESENTATION OF THE HEAT-FLOW DATA

Table 1 presents basic heat-flow data from new sites in the study area (Figure 2). Temperature measurements were made every 2-10 m. The temperature gradients were determined by the measurement interval endpoint temperatures (which in all cases agree with the least-mean-square

Table 1. Heat-Flow Data

Well Location (N lat, W long)	Depth Interval (m)	M	*Thermal Conductivity (W/mK) Range	NC	Harmonic Mean	Arithmetic Mean	Temperature Gradient (C/km) NT	End-Point Method	L.R. Method	Heat Flow (mW/m2) Interval	GW	Corr	Best
1. Agua Fria	31- 75	a	1.15-1.86	6	1.59	1.63	23	33.4	33.4± 0.7	53.1	37.9± 9.0	91.0	
34.34, 108.82	88-109	w	0.37-2.91	3	2.64	2.87	5	50.0	52.6± 2.6	132.0	40.6±33.4		112.5
2. Blaine's Lake	29-101	a	1.17-1.93	16	1.46	1.51	19	42.8	44.0± 0.4	62.5	11.9± 8.3**		
34.31, 108.79	118-199	w	1.46-2.75	14	1.85	1.89	17	38.4	41.4± 0.7	71.0	6.2± 9.3**		71.0
3. Cabin Spring	30- 44	a	1.31-2.07	5	1.53	1.60	8	27.3	27.8± 0.3	41.8	-27.7± 4.0**		
34.63, 108.73	53- 68	w	1.95-2.42	4	2.19	2.21	4	33.3	34.6± 2.0	72.9	-23.5± 0.1**		72.9
4. Cerro Prieto 1	25- 35	a	1.48-2.30	5	1.94	1.99	6	45.6	46.8± 3.8	88.5	-32.6±25.0**		88.5
34.56, 108.59													
5. Cerro Prieto 2	27- 39	a	1.08-1.69	5	1.33	1.36	7	12.8	12.6± 1.2	17.0	32.2± 3.0	48.0	48.0
34.57, 108.59													
6. Cimmaron Mesa	35- 51	w	1.76-2.17	5	1.86	1.87	9	29.2	30.2± 1.1	54.3	-31.6±16.6**		54.3
34.32, 108.85													
7. Fence Lake	50- 75	w	1.80-2.99	7	2.20	2.26	6	30.6	30.9± 1.7	67.3	56.4± 7.8	123.7	123.7
34.66, 108.62													
8. Garcia Lake	33- 43	w	1.90-3.45	5	2.98	3.01	5	17.5	17.5± 0.4	52.2	13.9± 0.8	66.1	66.1
34.53, 108.45													
9. Gobbler Knob	30-110	a	1.37-1.92	12	1.71	1.73	9	27.8	28.9± 1.3	47.5	29.7±11.5	77.2	
34.63, 108.45	140-230	w	1.84-2.79	10	2.20	2.24	10	35.7	34.6± 1.5	78.5	39.5±21.7**		78.5
10.Half-Lonesome	30- 55	a	1.61-1.78	3	1.69	1.69	4	15.8	16.2± 1.2	26.7	16.0± 0.0	42.7	42.7
Windmill, 34.59, 108.69													
11.Red Hill	29- 54	a	1.10-1.84	6	1.39	1.45	6	39.2	38.1± 2.4	54.5	55.2± 4.0	109.7	
34.26, 108.93	68-124	w	1.81-2.60	9	2.20	2.23	12	40.8	39.9± 1.3	89.8	27.8±26.4**		89.8
12.Route 32	53-179	w	0.37-2.18	15	1.78	1.86	26	42.3	42.9± 0.6	75.3	19.0± 6.8	94.3	94.3
34.40, 108.62													
13.Zuni Salt Lake 1	27- 45	a	1.23-1.77	7	1.40	1.42	10	56.4	54.5± 3.5	80.1	142.6±14.2	222.7	
34.40, 108.67	61- 67	a	1.40-1.77	2	1.56	1.59	5	68.7	68.6± 9.6	107.2	63.3± 0.7	170.1	170.1
14.Zuni Salt Lake 2	29- 63	a	1.23-1.77	11	1.46	1.49	18	44.5	43.9± 0.5	65.0	29.8±13.7**		
34.41, 108.69	77- 85	a	1.59-1.97	3	1.67	1.67	5	32.4	32.9± 0.5	54.1	-2.1± 1.9**		59.6
15.Zuni Salt Lake 3	27- 57	a	1.12-1.97	11	1.58	1.62	16	44.2	43.5± 0.5	69.8	30.7±13.3	100.5	100.5
34.40, 108.70													

16. LANL #1 34.12, 109.13	21- 52	w?	2.09-2.35	3	2.29 (2.08)	2.30 (2.08)	5	74.1	75.6± 1.8	169.7 (154.1)	NE***		169.7?
17. LANL #2 34.14, 109.13	55-122	w?	2.09-3.72	8	2.17 (1.89)	2.21 (1.90)	12	121.6	129.0± 3.1	280.0 (229.8)	NE***		280.0?
18. LANL #3 34.29, 108.76	110-195	w?	1.46-2.75	14	(1.85)	(1.89)	15	37.9	37.2± 0.3	(70.1)	-5.1± 7.0**		70.1
19. LANL #4 34.27, 108.71	91-287	w	2.09	1	2.09 (1.84)	2.09 (1.84)	33	35.2	34.9± 0.2	73.6 (64.8)	5.1±10.2**		73.6
20. LANL #8 34.91, 108.84	64-122	w?	2.09	1	2.09 (1.84)	2.09 (1.84)	13	63.6	63.8± 1.1	132.9 (117.0)	-58.3±12.8	191.2	191.2
21. LANL #10 34.92, 108.69	39-142	a	1.50-2.68	4	2.55 (1.87)	2.61 (1.89)	23	24.7	25.1± 3.0	62.9 (46.2)	262.4±13.2	325.3	
	147-162	w?	3.72	1	3.72 (2.79)	3.72 (2.79)	4	20.1	21.6± 2.4	74.9 (56.1)	-9.9± 0.1**		74.9
22. LANL #12 35.14, 108.83	268-341	a	2.68	1	2.68 (1.92)	2.68 (1.92)	13	25.1	25.0± 0.3	67.3 (48.2)	-2.1±11.9**		67.3
23. LANL #13 35.11, 108.65	83-105	a	1.50	1	1.50 (1.37)	1.50 (1.37)	10	67.3	69.1± 1.2	101.0 (92.2)	-29.8±14.2**		
	108-115	w?	2.09	1	2.09 (1.84)	2.09 (1.84)	4	54.8	57.4± 3.9	114.5 (100.8)	0.0± 0.8**		107.8
24. LANL #15 35.27, 108.63	17- 34	a	1.50-2.68	14	1.66 (1.46)	1.76 (1.49)	6	33.5	33.0± 0.4	55.6 (48.9)	18.0± 9.5**		55.6
25. LANL #18 35.23, 108.60	24- 45	a	0.35-2.44	6	1.52 (1.32)	1.69 (1.39)	9	49.8	50.1± 1.5	75.7 (65.7)	45.3±32.7**		75.7
26. LANL #20 35.59, 108.30	280-475	w	2.80-3.72	4	3.56 (2.60)	3.58 (2.64)	33	16.2	16.2± 0.3	57.7 (42.1)	-16.6±16.6**		57.7
27. LANL #21 35.59, 108.33	280-433	a	1.50-2.44	5	2.27 (1.55)	2.33 (1.55)	26	20.8	20.9± 0.1	47.2 (32.2)	-21.3± 9.4**		47.2
28. LANL #24 35.49, 108.75	67-122	a	0.35-2.68	8	1.57 (1.38)	1.83 (1.51)	10	30.8	30.8± 0.5	48.4 (42.5)	-6.5± 6.8**		48.4
29. LANL #25 35.50, 108.67	59-122	w?	0.35-2.68	4	1.90 (1.69)	2.10 (1.83)	14	29.2	30.7± 2.5	55.5 (49.3)	-108.3±18.3	163.8	163.8
30. LANL #26 35.54, 108.60	134-183	w	2.09-3.72	17	2.42 (2.09)	2.57 (2.15)	9	23.0	22.8± 0.7	55.7 (47.8)	-6.8±14.7**		55.7
31. LANL #28 35.50, 108.21	427-793	w	2.09-3.72	35	2.55 (2.14)	2.76 (2.23)	56	38.4	38.3± 0.2	97.9 (82.2)	19.9±14.5**		97.9
32. LANL #29 35.53, 108.12	402-524	w	2.09-3.72	10	2.60 (2.24)	2.76 (2.30)	21	19.6	20.3± 0.4	51.0 (43.9)	-3.9± 8.1**		51.0

33. Huckleberry Federal #1 34.41, 108.48	1063-1398	w	2.08-3.13	6	2.57	2.63	2	18.2	25.1****	64.5	NA	64.5
34. Spanel & Heinze, SFP #1-9617 34.54, 107.98	1194-1642	w	1.62-2.94	8	2.31	2.41	2	17.4	23.9****	55.2	NA	55.2
35. Sun No. 1	823-1463	w	1.93-2.11	5	2.01	2.02	22	51.8	51.1± 0.1	104.1	-5.6± 4.6**	104.1
San Agustin	155-1644	w	1.93-2.43	6	2.06	2.07	2	24.2	31.5****	64.9	NA	
	1644-3202	w	0.99-4.07	14	2.27	2.70	2	36.7	40.9****	92.8	NA	
	3202-3745	w	2.69-3.94	5	3.14	3.17	2	63.4	64.3****	201.9	NA	
	1644-3745	w	0.99-4.07	19	2.45	2.82	2	43.6	47.0****	115.2	NA	
	155-3745	w	0.99-4.07	20	2.24	2.56	2	35.6	40.6****	90.9	NA	

Note: M - medium in which the temperature measurements were made: a = air, w = water.
Range - range of thermal conductivity values within the heat-flow measurement depth interval.
NC - number of thermal conductivity layers within the heat-flow measurement depth interval.
NT - number of temperature measurements within the heat-flow measurement depth interval.
End-Point - temperature gradient determined by the first and last temperature measurements for that depth interval.
L.R. - best fit (linear regression) gradient ± standard deviation for all the temperature-depth data in that interval.
Interval - heat flow determined by harmonic mean thermal conductivity and the end-point temperature gradient.
GW - estimate ± standard deviation of ground-water correction for heat flow (after Mansure and Reiter, 1979).
Corr - interval heat flow with ground-water correction.
Best - estimated heat flow for that site.

*Thermal conductivity calculated from measurements on representative rock samples. Mean conductivities obtained by considering percent of interval for each rock type as determined from lithologic and geophysical logs, and drill cuttings. Whole rock conductivities for wells 16, 17, and 19-32 estimated from average of measurements for each rock type (Reiter and Tovar, 1982) represented in the lithologic log. Numbers in parentheses are thermal conductivity estimates obtained from average of measured values from the study area. Conductivities for wells 14 and 15 estimated from measurements of samples from well 13. Conductivities for well 18 estimated from measurements of samples from well 2. In-situ saturation estimated to be 0.5 (Stone, 1984) where temperature measurements were made in air, 1.0 otherwise. Porosities generally estimated from density logs. Porosity of coal determined from density bottle measurements.

**Not estimated for one of the following reasons: 1) standard deviation of ground-water correction is greater than about 0.5 of the value of the ground-water correction, 2) magnitude of correction not well determined due to small number of temperature measurements in that depth interval, or 3) upward movement of water in the liquid state is unlikely in the vadose zone, vapor transport is not considered. See text for discussion of ground-water correction.

***NE - not estimated since temperature logs were made shortly after well drilling and completion (20-48 hours).

****Temperature gradient corrected after Kehle in Eggleston and Reiter (1984).

Figure 2. Location of heat-flow data and new volcanic ages in the study area (Decker and Birch, 1974; Reiter and others, 1975; Reiter and Shearer, 1979; Levitte and Gambill, 1980; Sass and others, 1982; Minier and others, 1987; this study). Volcanic age data are located by solid dots (Ma). Heat-flow data are located by triangles (mW/m2). The letters G, S, Q and Z indicate the locations of Gallup, Springerville, Quemado and Zuni. Map after Wilson and others (1969), Callender and others (1983) and Aldrich and Laughlin (1984).

approximation of the gradient to within 8 %). The intervals chosen for measurement were determined by linear temperature gradient and depth considerations. For some sites the temperature gradient has been estimated using bottom-hole temperatures obtained in petroleum tests (Table 1). The estimated gradients often provide useful information since temperatures at great depths are less likely to perturbed by near-surface processes (Reiter and Tovar, 1982; Reiter and others, 1985). Temperature gradient measurement and heat-flow calculation are discussed by Roy and others (1968) and Reiter and others (1975; Appendix I).

Thermal conductivity samples representing distinct rock types (as indicated on geophysical logs) were obtained from drill cuttings (Table 1). The thermal conductivity measurement technique for fragment samples is described by Reiter and Hartman (1971) and Sass and others (1971). The harmonic mean thermal conductivities over the temperature measurement intervals are calculated according to the percentage of each rock type within the interval (Table 1; Appendix I). The calculation of thermal conductivity incorporates the assumption that the rocks in-situ are 100 or 50 percent water saturated when the corresponding temperature measurements were made in water or air, respectively. The degree of saturation of rock units above the water table is expected to vary between sites and between rock types. However, because data required to determine the degree of

saturation were not available, the value of 50 percent saturation has been estimated in order to determine thermal conductivity (Stone, 1984). Figure 3 illustrates the relationship between thermal conductivity and the degree of water saturation. One may see the values of thermal conductivity become less as saturation decreases for any given porosity.

Vertical ground-water movement corrections for the heat-flow data are presented in Table 1 (Appendix I). The ground-water correction is the estimated amount of heat "ΔQ" which is transported across a layer of thickness "Δz" by steady-state ground-water flow of vertical specific discharge "v", i.e.

$$\Delta Q = rcv\Delta T \qquad (1)$$

where "r" and "c" are the density and specific heat, respectively, of the ground water, and "ΔT" is the temperature difference across the layer "Δz" (Lachenbruch and Sass, 1977). The parameter "rcv" is estimated from the slope of "Q" versus "T" across the layer of interest (Mansure and Reiter, 1979). Hence, "ΔQ" in equation 1 may be estimated. The ground-water corrections are presented in the present study for sites where vertical ground-water movement is reasonably well defined. For example, corrections were not estimated when the standard deviation of

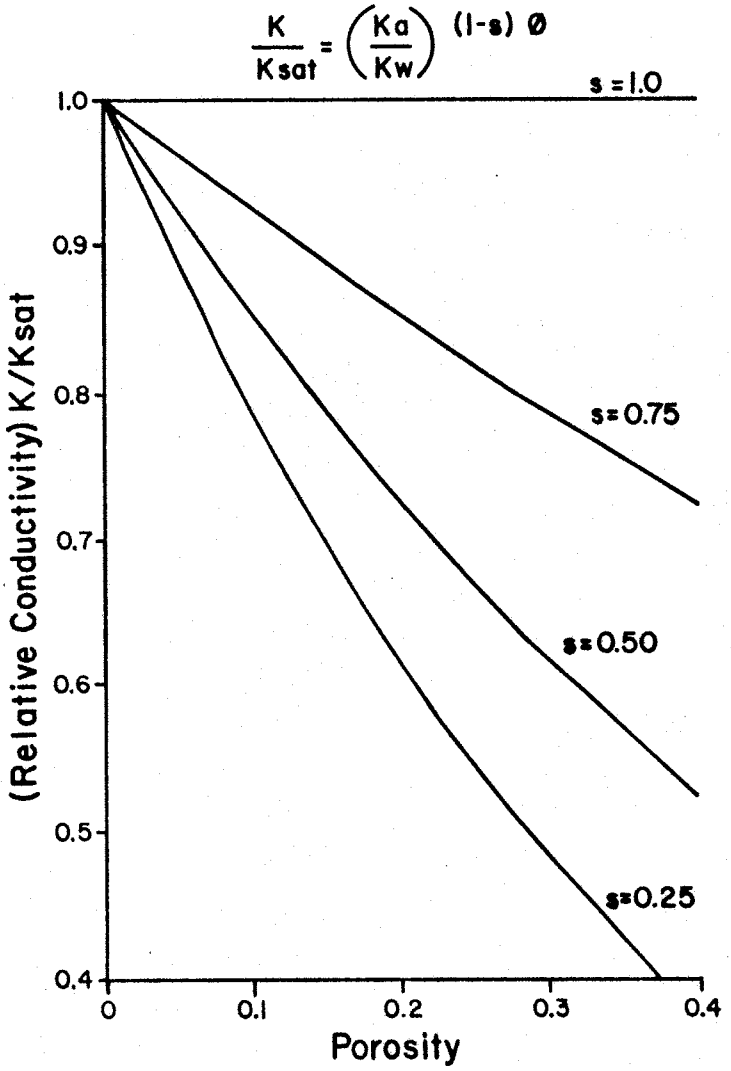

Figure 3. Relative thermal conductivity K/Ksat as a function of porosity ϕ and saturation s. Relative conductivity is the ratio of the conductivity of a partially saturated rock (K where s is less than 1) to the conductivity of the same rock fully saturated (Ksat, s=1). The curves are determined by the equation in the figure which has been obtained from the geometric mean conductivity (e.g. see Sass and others, 1971).

the slope ($\Delta Q/\Delta T$, which may be used to define the vertical ground-water flow, see equation 1) was greater than 0.5 of the value of the slope ($\Delta Q/\Delta T$). The magnitude of the ground-water correction presented in Table 1 illustrates the significance of the effect that ground-water movement can have on heat-flow measurements.

The vertical ground-water corrections estimated for the heat-flow data range from 0 to greater than 100 mW/m2 (Table 1). The estimates of vertical specific discharge obtained from the ground-water correction range from 0 to about 1 m/y and are not inconsistent with the limited amount of hydrologic data in the area. Vertical hydraulic gradients have been estimated from water level data presented by Summers (1972) for the Zuni Pueblo and include values up to 0.42. Vertical hydraulic gradients of similar magnitude have been estimated in the Salt Lake coal field (McGurk and Stone, 1986 in Stone and McGurk, 1987). Specific discharges of 0.01 to >1.0 m/y may result from a hydraulic gradient of 0.42 in relatively permeable shales and sandstones (hydraulic conductivity = 1.0 E-08 to > 1.0 E-06 cm/s, Freeze and Cherry, 1979).

Radiometric dates for volcanic ages as young as $\sim$ 0.10 Ma may be determined by the potassium-argon (K-Ar) dating technique. New K-Ar dates for volcanic rocks from west-central New Mexico are presented in Table 2 and Figure 2

Table 2. Potassium-Argon Data (Minier and others, 1987)

Sample Location N. lat., W. long. section of township,range	Sample Description	K-analyses (%) individual	mean	Radiogenic Ar-40 (x1E-12 m/g) Individual	Mean	Atmospheric Ar-40 (%) Individual	Mean	Age (m.y.)
Cerro Pomo, NM	Groundmass feldspar	1.382	1.378	3.242	3.238	95.6	95.6	1.35±0.21
34.36, 108.74	concentrate, basaltic	1.368		3.138		95.8		
28 of 2N, 18W	andesite	1.379		3.333		95.5		
		1.385						
El Porticito, NM	Groundmass feldspar	0.722	0.726	7.082	7.131	73.9	73.3	5.66±0.20
34.39, 108.57	concentrate, basalt	0.723		7.173		72.6		
24 of 2N, 17W		0.729		7.147		73.2		
		0.729		7.121		73.4		
Eagle Peak, NM	Groundmass felspar	0.950	0.944	10.88	10.96	35.1	34.8	6.69±0.17
34.39, 108.68	concentrate, basalt	0.942		10.92		35.2		
23 of 2N, 18W		0.939		11.04		34.5		
				11.02		34.2		
Cerro Prieto, NM	Groundmass feldspar	1.678	1.677	17.46	17.41	23.3	22.8	5.98±0.14
34.56, 108.57	concentrate, basaltic	1.678		17.07		23.2		
24 of 4N, 17W	andesite	1.675		17.67		21.9		
				17.42		22.9		
Red Hill, NM	Groundmass feldspar	1.131	1.127	1.980	2.014	97.1	97.1	1.03±0.22
34.28, 108.88	concentrate, basaltic	1.122		2.048		97.0		
26 of 1N, 20W	andesite	1.127		2.015		97.1		
Blaine's Lake, NM	Groundmass feldspar	0.374	0.369	0.506	0.787	98.5	97.7	1.23±0.23
34.31, 108.73	concentrate, basalt	0.356		0.734		97.8		
14 of 1N, 19W		0.376		0.957		97.2		
				0.952		97.2		

Decay constants used: λ_β =4.963E-10/y
λ_e =0.581E-10/y
λ =5.544E-10/y
40K/K=1.167E-04 atom/atom

(see also Minier and others, 1987). Analytical data for the new K-Ar dates and the decay constants used in the calculations are also presented in Table 2.

OVERVIEW OF THE DATA

The new K-Ar age data indicate volcanic activity in the study area during latest Miocene and early Pleistocene time (Decade of North American Geology time scale, 1983; Figure 2). Similar dates have been reported southwest and northeast of the study area in the Springerville and Zuni-Bandera volcanic fields (Laughlin and others, 1979, 1980; Callender and others, 1983; Aubele and others, 1986). Late Pliocene volcanic rocks with dates of ~ 1 Ma also occur west of Quemado and in the Zuni-Bandera volcanic field (Figure 2). Sites where latest Miocene dates occur (~6 Ma) are generally located northwest of Quemado (Figure 2). There does not seem to be a well-defined age progression of volcanism along the JL in the study area. On a larger scale, the lack of any consistent age progression of volcanism along the JL as a whole makes unlikely the hypothesis that the JL reflects the trace of a mantle plume (Suppe and others, 1975; Lipman and Mehnert, 1979).

The mean heat flow for the study area is 90 mW/m2 (s.d. = 42 mW/m2, n=63, Figure 2). Excluding the anomalous data (values greater than one standard deviation from the mean) the mean heat flow for the study area becomes 80 mW/m2

(s.d. = 20 mW/m2, n=51, Figure 2). The heat-flow values in the study area are generally greater than the average of heat-flow values reported for the interior CP (~58-65 mW/m2) and are more similar to the higher heat flow mean in the southern BRP (~86 mW/m2; Reiter and others, 1975; Reiter and Shearer, 1979; Bodell and Chapman, 1982; Reiter and Mansure, 1983). Two heat-flow sites located west of Quemado exhibit high values (>100 mW/m2, Figure 2); a third nearby site has a significantly lower value (71 mW/m2; Figure 2). Within 10 km of these three heat-flow sites are volcanic rocks where K-Ar ages have been determined (sites with values of 1.03, 1.23 and 1.35 Ma, Table 2). High temperature gradients, due to magmatic intrusion into the upper crust and/or ground-water advection of heat, may locally elevate the surface heat flow in the area. The relatively short distance (~5 km) between the two higher heat-flow sites and the intermediate heat-flow site suggests that the mechanism which is elevating the heat flow in this area (ground-water convection and/or magma intrusion) occurs at relatively shallow crustal depths.

Similar heat-flow distributions observed in other parts of the study area also suggest the presence of shallow crustal heat sources (Figure 2). For example, north of Quemado near the late Tertiary-Quaternary Zuni-Bandera volcanic field, a high heat-flow site (124 mW/m2) is within 10-15 km of two sites with significantly lower values (sites

with values of 73 and 79 mW/m2; Figure 2). Similarly in the north-central study area two high heat-flow sites (98 mW/m2) away from extensive volcanism are within 5-10 km of sites with lower heat-flow values (sites with values of 47, 51 and 58 mW/m2; Figure 2).

The heat-flow values generally increase as the Pliocene volcanic centers are approached (Figure 2). For example, consider the heat-flow profile determined by the four heat-flow sites in the southeastern part of the study area (sites with values of 65, 61, 83 and 94 mW/m2). Heat-flow sites in proximity to extensive volcanism often have values characteristic of the BRP while sites at greater distances (for example east of Quemado and in the north-western part of the study area) have values which are more characteristic of the interior CP.

QUALITATIVE CONSIDERATIONS OF THERMAL MODELS FOR THE COLORADO PLATEAU PERIPHERY

Heat-flow values in the interior CP are consistent with suggestions that the Plateau interior is in transient thermal reponse to mid-Tertiary lithospheric thinning (Bodell and Chapman, 1982; Reiter and Clarkson, 1983). Crustal thinning of the northwestern CP boundary is suggested by seismic studies, high elevation, normal faulting, volcanism and high heat flow (90-100 mW/m2; Keller and others, 1979; Bodell and Chapman, 1982; Eggleston and

Reiter, 1984). The present study area, located on the southern CP boundary, is to a lesser extent characterized by high elevation, some normal faulting, volcanism, and moderately elevated heat flow with locally high values (76-85 mW/m2 vs. > 100 mW/m2; Callender and others, 1983; Figure 2). These characteristics suggest that lithosperic thinning, and perhaps crustal thinning, may be occurring in the study area. The heat-flow values in the study area are generally greater than values in the non-volcanic interior of the Plateau and less than values in the north--western periphery of the CP. This observation indicates that the process of lithospheric thinning, or crustal thinning, in the study area may be in a stage intermediate between that of the Plateau's interior and northwestern periphery. For example, perhaps the initiation of the thinning event occurred earlier in the northwestern periphery of the CP. Alternatively the initial lithospheric thickness may have been less in the northwestern periphery of the CP as compared to the study area. For comparison, Reiter and Minier (1985) illustrate the thermal response due to a temperature increase at depth as a function of time and initial lithospheric thickness. A quantitative model for lithospheric thinning is considered later in this manuscript.

In an alternative model for the tectonic development of the southeastern CP boundary Chapin and others (1978) and

Aldrich and Laughlin (1984) suggest that the JL is a zone of weakness which has been reactivated by changes in the regional stress regime. The hypothesis that major volcanism initiated about 7-4 Ma with increasing extension across the JL is supported by stress data and radiometric dates (Aldrich and Laughlin, 1984; Minier and others, 1987). Localized volcanism along the lineament may be expected to be associated with geothermal anomalies superimposed upon a regional or background heat flow. Heat-flow values in the southern half of the study area, i.e. in proximity to the Jemez lineament, range from less than 70 mW/m2 to greater than 100 mW/m2 (Figure 2). In this area low to intermediate heat-flow values (<70 mW/m2; Figure 2) are generally located at greater distances from centers of recent volcanism than are higher heat-flow values (> 70 mW/m2; Figure 2). There are, however, sites within the volcanically active Jemez zone which have heat-flow values characteristic of the non-volcanic regions of the interior Plateau. The data suggest the possibility that background heat flow in the Quemado area may be similar to that of the Plateau interior, with elevated heat-flow values resulting from proximity to recent volcanism. Analyses of the heat-flow anomalies associated with isolated thermal events, such the emplacement of magma into the crust, are presented below.

GEOTHERMAL MODELS - OVERVIEW

Several one- and three-dimensional heat-conduction models are now examined to provide interpretations of the thermal regime in the study area. Interpretation of heat-flow data necessarily involves a number of simplifying assumptions in order to model and to begin to understand thermal systems which are inhomogeneous, geometrically--complicated, and poorly known in detail. Except for very simple cases, models which account for inhomogeneity and complicated geometries typically involve numerical methods. Although three-dimensional effects may be important and should be considered, complicated three-dimensional numerical analyses may not be justified with the present uncertainty in system parameters such as geometry, physical properties, and the heat-flow data. K-Ar ages from volcanic rocks provide chronologic control on volcanic events; the timing of volcanism, although a simplification, is often used to estimate the initiation or cessation of the associated thermal event (Bodell and Chapman, 1982; Reiter and Clarkson, 1983).

The transport of heat by ground-water convection is not addressed quantitatively in the following analyses. However, an estimate is made to indicate if ground-water convection is likely to be induced by geothermal gradients in the study area. Heat transport by ground-water convection generally occurs in the upper crust where porosity and

hydraulic conductivity are greatest (see Freeze and Cherry, 1979), and where heat-flow measurements are made. Hydrothermal convection (vs. heat conduction) can greatly influence the thermal regime of the crust in certain areas (Lachenbruch and Sass, 1977). The effect of crustal heat sources on surface heat flow may be exaggerated or attenuated by ground-water convection (see for example, Donaldson, 1962; Norton and Knight, 1977). High temperature gradients may also induce free ground-water convection (Donaldson, 1962; Turcotte and Schubert, 1982). The effect of ground-water covection presents a difficult problem since solutions are described by the coupled partial differential equations for heat and mass transport. Solutions usually require numerical methods. At present, numerical simulations are not pursued due to the lack of hydrologic data in the study area. As such the present study proceeds with thermal conduction models, however, as mentioned above, an estimate of geothermal gradients inducing free ground-water convection in the study area will be given.

ONE-DIMENSIONAL ISOTHERMAL MODEL

Geothermal studies in the San Juan basin and Four Corners area of the CP suggest that the regional heat flow in the southern San Juan basin (at the northern boundary of the study area) is 67-70 mW/m2, only slightly higher than the mean heat flow for some of the other non-volcanic

regions of the CP ($\leq$65 mW/m2; Bodell and Chapman, 1982; Reiter and Mansure, 1983; Clarkson, 1984). Furthermore, coal maturation data in the southern San Juan basin are consistent with a thermal history in which the surface heat flow has been approximately steady-state since the late Cretaceous ($\sim$67 mW/m2 for various burial histories; Clarkson, 1984). Therefore, because of the proximity of the southern San Juan basin to the study area, it may be reasonable to apply a one-dimensional isothermal model which evolves from steady-state to begin a thermal analysis of the regional heat flow in the study area.

Consider first the effect likely to be observed in surface heat flow due to a thermal disturbance at some depth. Perhaps the simplest case is the one-dimensional, heat conduction solution for an instantaneous increase in temperature at depth which is thereafter held constant (Figure 4a). Such a model might represent an extensive shallow magma sill which is continually being replenished, or perhaps lithospheric or crustal thinning where Moho or upper asthenospheric temperatures remain constant after an initial increase in temperature at depth (Lachenbruch and others, 1976; Reiter and Minier, 1985). This model may be used to estimate the depth to a temperature disturbance if estimates of the time of initiation of the thermal event and the magnitude of the resultant heat-flow anomaly are available. The surface heat-flow anomaly (heat flow above

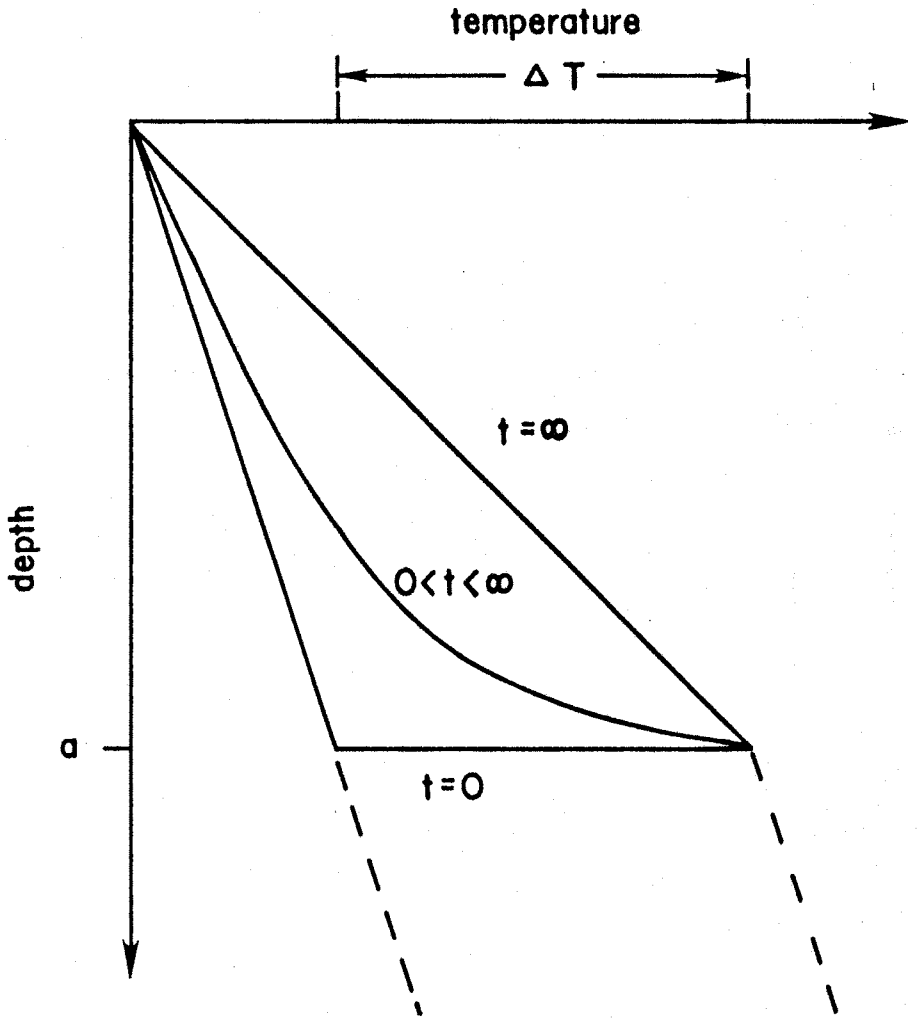

Figure 4a. Illustration of temperature versus depth at several times "t" after an instantaneous temperature increase "Δ T" at depth "a". "a" is the roof thickness. (after Lachenbruch and others, 1976).

the regional value) may be estimated from heat-flow measurements. The timing of volcanism as determined by radiometric dates may be used to estimate the initiation of the thermal event.

Values for several model parameters must be obtained in order to evaluate the anomalous heat flows resulting from a one-dimensional thermal model. For example, the approximate upper temperature limit for basaltic/mafic magmas is about 1200 °C (Jaeger, 1964). A reasonable estimate of the background, or initial, surface heat flow for the study area would be about 65 mW/m2 (Figure 2; Clarkson, 1984). Thus, an average crustal thermal conductivity value of 2.5 W/m°C (Chapman and Pollock, 1977) results in a background temperature gradient of 26 °C/km. The anomalous heat flow at the ground surface (z=0) at any time "t" after initiation of the thermal event is given by

$$Q(\ell) = Q_0\left[\, 1 + 2 \sum_{n=1}^{\infty} (-1)^n \exp\left(\frac{-n^2 \pi^2 \ell^2}{4a^2}\right) \right] \qquad (2)$$

where "Qo", the anomalous steady-state heat flow due to an anomalous temperature "ΔT" at depth "a", is

$$Q_0 = K\,(\Delta T/a) \qquad (3)$$

The characteristic conduction length "l" is given by

$$\ell(t) = (4kt)^{1/2} \qquad (4)$$

The constants "k" and "K" are, respectively, thermal diffusivity and thermal conductivity (Lachenbruch and others, 1976; Figure 4a). The roof thickness "a" is the depth to the thermal disturbance, which may be obtained from equation 2 if one knows the time since the initiation of the thermal event (estimated from volcanic radiometric dates) and the magnitude of the heat-flow anomaly (estimated from heat-flow measurements). Figure 4b illustrates the roof thickness as a function of time for several observed surface heat-flow anomalies.

The one-dimensional isothermal model is now applied to the heat-flow data in the study area (Figure 2). Several of the data sites in the study area have heat-flow values significantly greater than 65 mW/m2 (Figure 2, Table 1). K-Ar dates in the area are approximately 1 and 6 Ma (Table 2). If, for example, the elevated regional heat flow in south-western part of the study area is 105 mW/m2, then the anomalous heat flow is estimated to be 40 mW/m2 (105 minus 65 mW/m2; however, more heat-flow data are needed to determine with confidence the heat flow for this area). Therefore, if the initiation of the thermal event is estimated from the K-Ar dates (1 or 6 Ma) the roof thickness

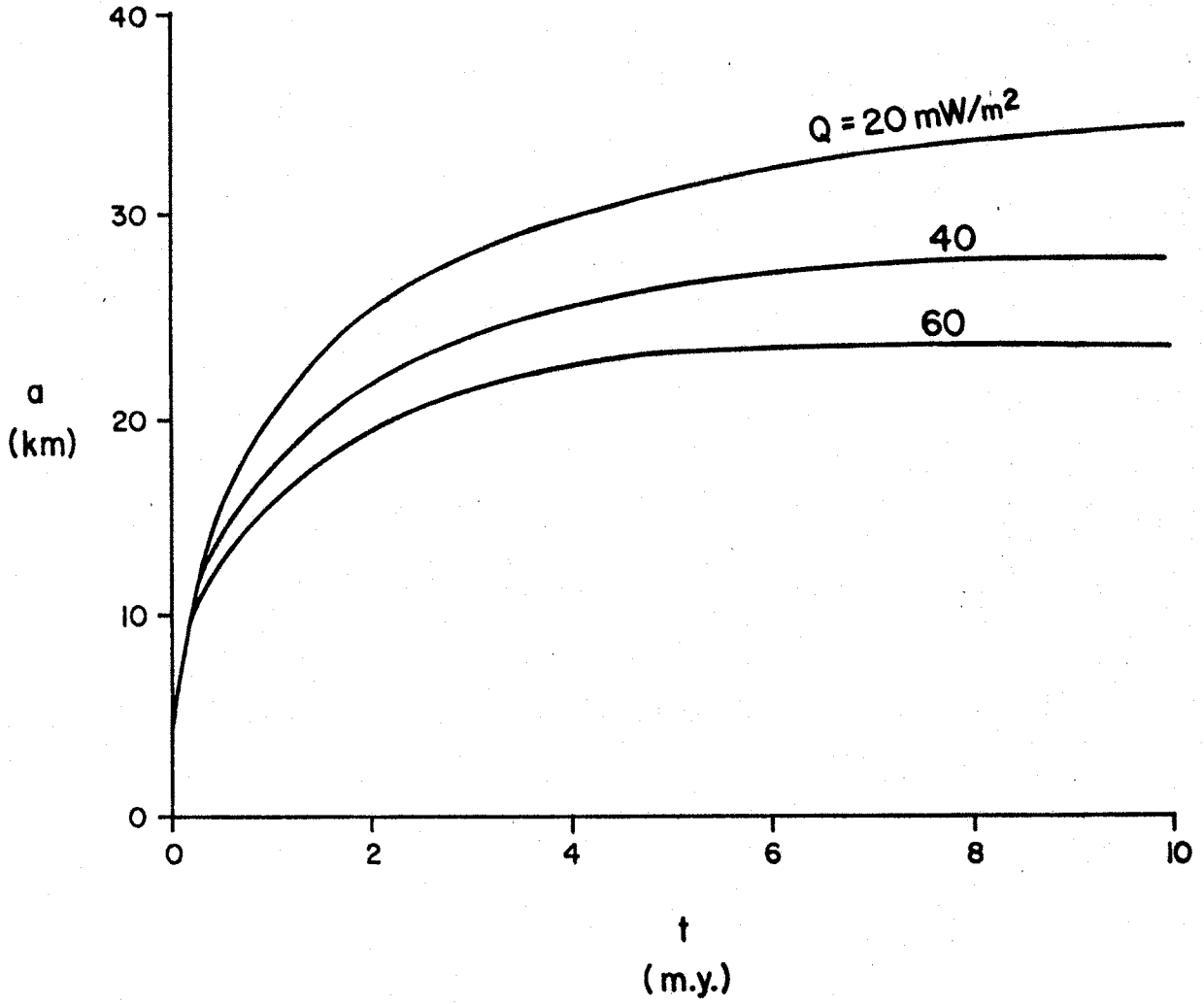

Figure 4b. Graph of roof thickness "a" as a function of time "t" for several surface heat-flow anomalies "Q". See equation 2 in text. Background heat flow = 65 mW/m2 (thermal conductivity = 2.5 W/m°C, thermal gradient = 26 C/km, surface temperature = 10 ° C). Temperature at depth "a" = 1200 ° C. Thermal diffusivity = 0.011 E-04 m2/s.

would be estimated as being about 17 or 27 km, respectively (Figure 4b).

The one-dimensional isothermal analysis is a limiting case solution and may be apropriate for regional crustal thinning or lithospheric thinning. However, it should be noted that spatial variations in heat-flow data in the study area suggest that the thermal sources are to some extent laterally heterogeneous. Additional processes which may significantly affect the spatial variability of heat flow include the release of latent heat of fusion (during solidification of magma) and the subsequent cooling of laterally discontinuous intrusions. First, however, a simplified example of latent heat release in one-dimensional conductive cooling is considered.

ONE-DIMENSIONAL CONSIDERATION OF THE RELEASE OF LATENT HEAT

The significance of the release of latent heat during solidification of an intrusion is now considered. A limiting case estimate of the time required to solidify an intrusion can be approximated by solving the one-dimensional heat conduction equation with the condition that the heat conducted away from the solidification boundary is equal to the heat released by the solidifying magma (Turcotte and Schubert, 1982). The time "ts" required to solidify a sill of thickness "2b" is

$$t_s = \frac{b^2}{4k\lambda_2^2} \qquad (5)$$

where

$$\frac{L\sqrt{\pi}}{c\,(T_m - T_o)} = \frac{e^{-\lambda_2^2}}{\lambda_2\,(1 + \mathrm{erf}\,\lambda_2)} \qquad (6)$$

may be solved for "λ_2" by iterative numerical calculations (Turcotte and Schubert, 1982, "L" is the latent heat of solidification, "c" is the specific heat of the magma, "Tm" is the melting temperature of the magma, "To" is the initial temperature of the country rock, and erf is the error function). It is assumed for this solution that the temperature anomaly due to the sill is zero at an infinite distance from the sill. The solidification time of an intrusion will not be greatly affected by proximity to the ground surface when the roof thickness is greater than the characteristic conduction length "ℓ" (equation 4), and when the magma thickness is less than twice the roof thickness "a" (Figure 5a; Lachenbruch and others, 1976). Equation 5 is a limiting case estimate of the solidification time since heat transport by ground-water advection and lateral conduction (neglected in this case) would tend to decrease the solidification time of a finite body. Consider as a numerical example a 2 km thick intrusion buried at 5 km depth initially at 1200 ^{o}C. The anomalous temperature distribution at the time of complete solidification of the

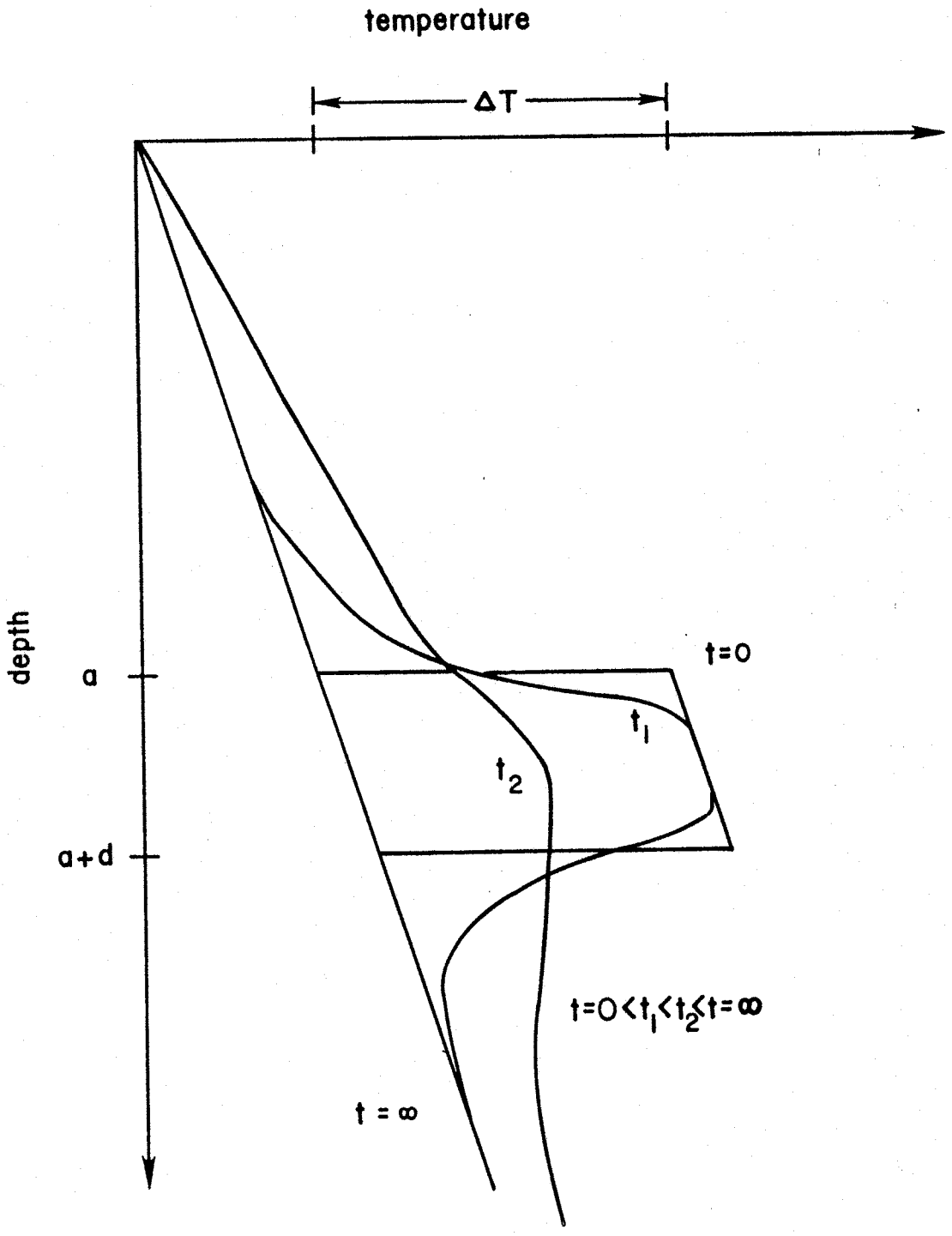

Figure 5a. Illustration of temperature versus depth at several times "t" after an instantaneous temperature increase "Δ T" at depth "a" to "a+d" (after Lachenbruch and others, 1976).

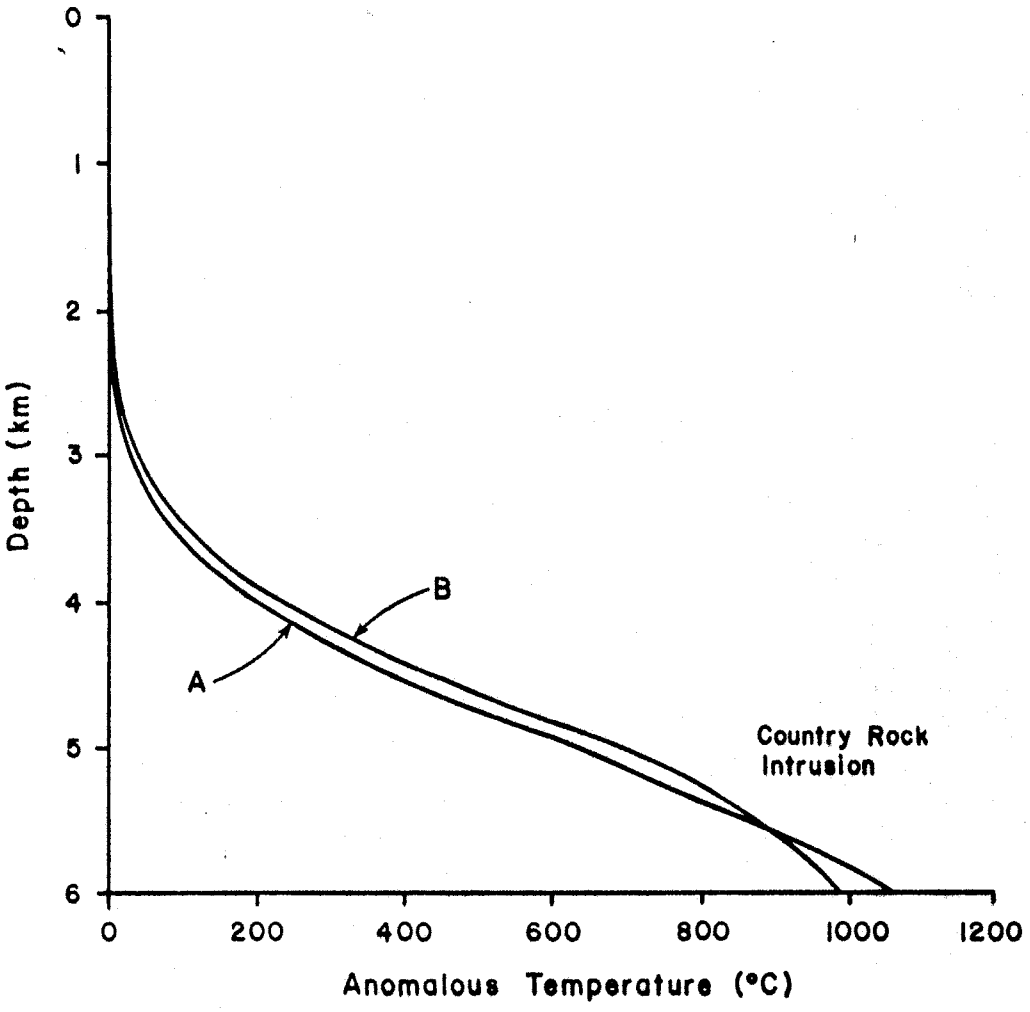

Figure 5b. Anomalous temperature distributions as functions of depth:
i) Curve A, at the time of complete solidification of a 2 km thick sill. Burial depth = 5 km. Time of solidification = 0.015 m.y. after emplacement. Melt temperature "Tm" = 1200 °C. Background temperature = 140 °C (estimated by multiplying background thermal gradient by depth and adding the surface temperature). Specific heat "c" = 1.1 kJ/kg°C. Latent heat "L" = 334 kJ/kg. Thermal diffusivity = 0.011 E-04 m2/s. Initial anomalous temperature = 1060°C (estimated by subtracting the background temperature from the melt temperature).
ii) Curve B, for pure conduction cooling (no latent heat) of a 2 km thick slab. Time after emplacement = 0.015 m.y. Burial depth = 5 km. Initial anomalous temperature = 1460 °C (initial slab temperature = 1600°C).

sill is illustrated in Figure 5b (curve A). The anomalous temperature at depth (a-y) after instantaneous emplacement of the sill up to the time of complete solidification is

$$T = T_o + (T_m - T_o) \frac{\operatorname{erfc}\left(\frac{y}{2\sqrt{kt}}\right)}{1 + \operatorname{erf} \lambda_2} \qquad (7)$$

where y=0 at the interface between the magma and country rock and y<0 in the country rock (Turcotte and Schubert, 1982). The time to solidify the intrusion is not greatly affected by proximity to the ground surface and is about 0.015 m.y. (equation 5, curve A in Figure 5b).

Analytical solutions which incorporate latent heat effects are not valid after complete solidification, i.e. when latent heat of fusion is no longer produced (Turcotte and Schubert, 1982). At the time of complete solidification, a large amount of heat will still remain in the intrusion; the temperature of the intrusion will typically be much higher than the ambient temperature of the country rock. Further cooling of the intrusion by heat conduction may be reflected in the surface heat flow. The effect of the release of latent heat by a solidifying intrusion on the temperature of the country rock (away from the intrusion) may approximately be accounted for by increasing the initial magma temperature by 300 to 400 °C in the pure conduction solution (Jaeger, 1964). For example, Figure 5b (curves A and B) illustrates that the temperature

distribution at the time of complete solidification, incoporating latent heat, is approximately matched by the pure conduction solution when the initial magma temperature is elevated by 400 °C; better fitting at depths < 3km. Therefore, conduction analyses with an appropriate temperature increase can approximate the effects of latent heat at some distance from the heat source. As such, the following three-dimensional analysis will account for latent heat by increasing the initial magma temperature in the conduction solution.

THREE-DIMENSIONAL FINITE SOURCE MODEL

As previously mentioned, spatial variability of the heat-flow and gravity data suggest that heat sources within the study area are laterally discontinuous. Near the Zuni-Bandera volcanic field is a northeast-trending gravity anomaly (length ~ 90 km, width ~ 30 km) thought to reflect the presence of a shallow, mafic intrusion emplaced before Laramide deformation (Figure 6, Ander and Heustis, 1982). Models based upon the gravity data indicate the minimum thickness of the intrusion is about 2 km; the maximum depth of burial is about 3-5 km (Ander and Heustis, 1982). Cerro Prieto, a volcanic neck which intruded through Cretaceous sediments about 6 Ma, is located within the gravity anomaly (Table 2; CPr in Figure 6). K-Ar dates in the Zuni-Bandera volcanic field are generally less than 3.8 Ma (Callender and

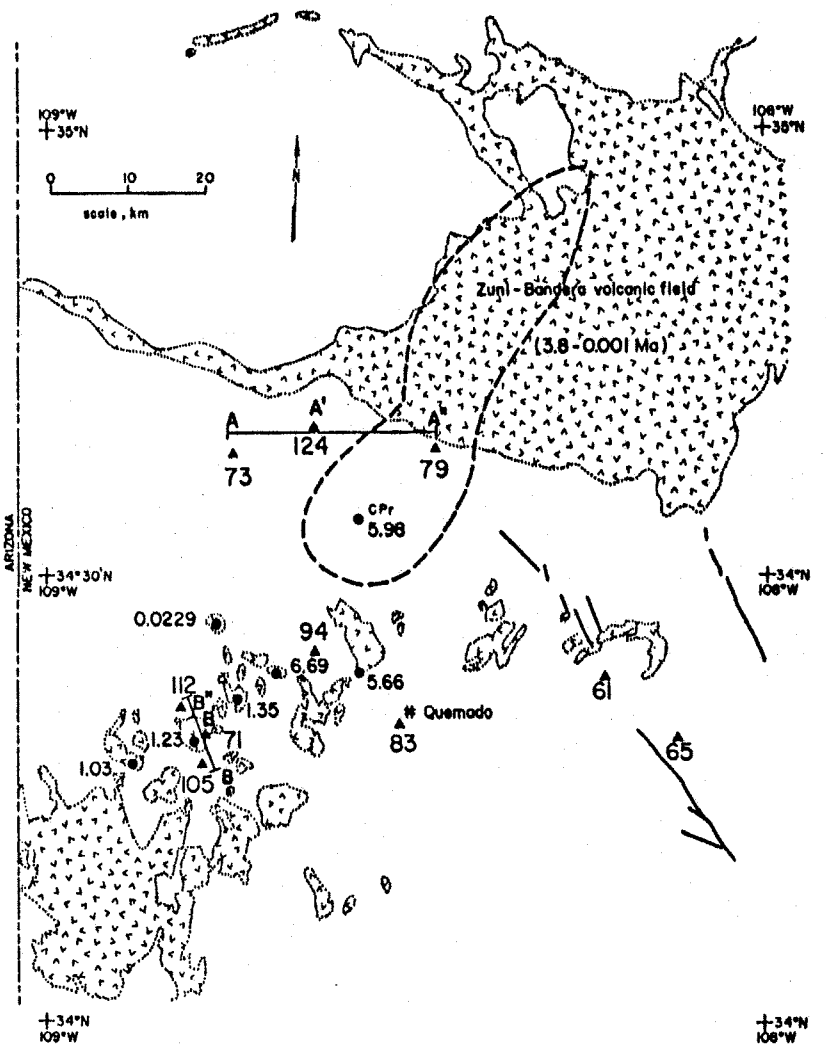

Figure 6. Location of volcanic ages and heat-flow data in the southern part of the study area (Bradbury, 1966; Reiter and others, 1975; Reiter and Shearer, 1979; Minier and others, 1987; this study). Volcanic age data are located by solid dots (Ma). Heat-flow data are located by triangles (mW/m2). The heavy solid lines represent mid-Tertiary dikes (~ 28 Ma, Laughlin and others, 1983). Dashed outline marks location of -210 mgal contour of the gravity anomaly discussed in the text (Ander and Heustis, 1984). CPr is Cerro Prieto volcanic neck (Table 2). Profiles AA", BB" pertain to thermal models discussed in the text. Map after Callender and others, 1983).

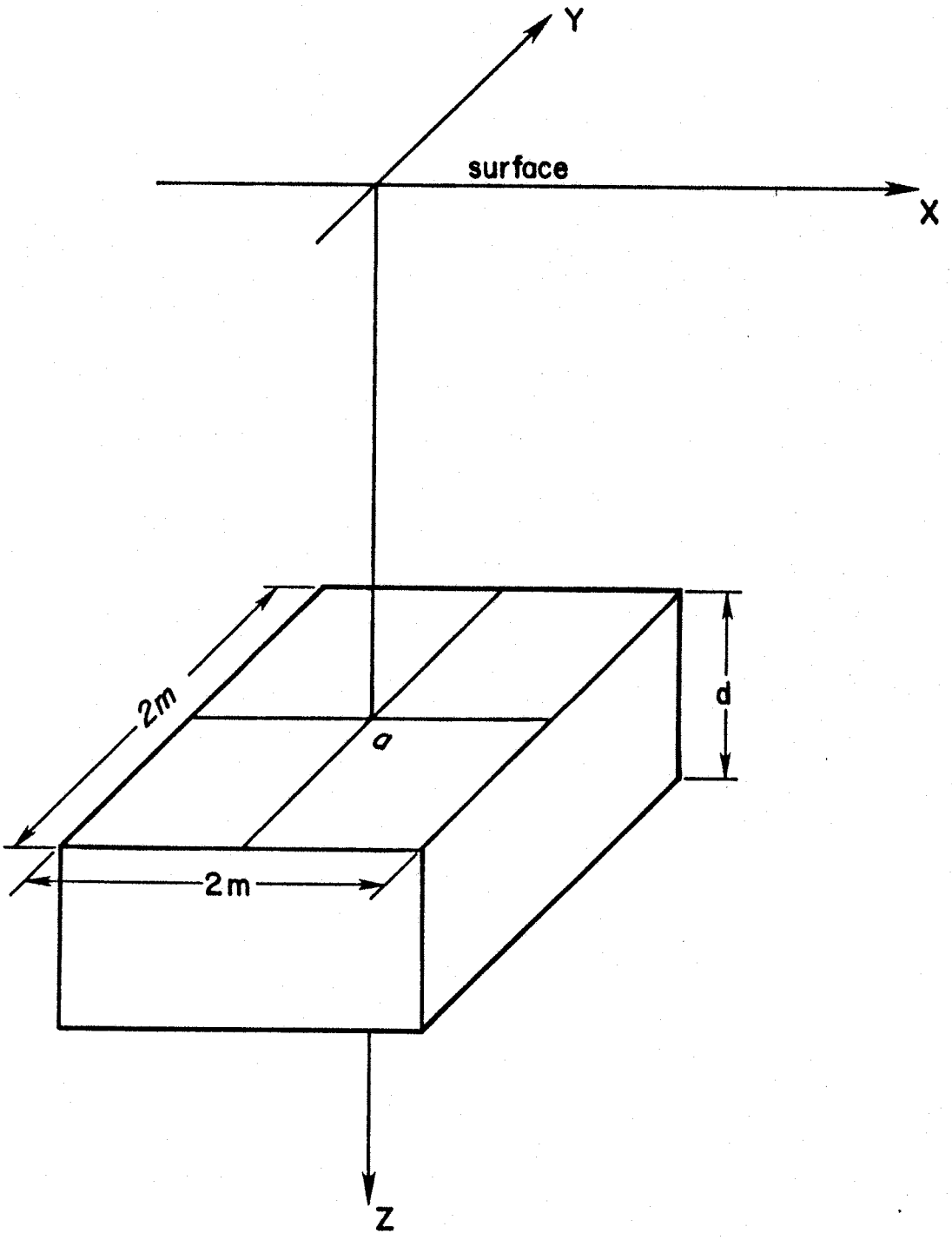

Figure 7a. Illustration of rectangular prism buried at depth "a". Prism thickness is "d". Length and width of prism are "2m" (after Lachenbruch and others, 1976).

others, 1983).

In order to estimate the surface heat-flow anomaly resulting from the cooling and solidification of a laterally discontinuous magmatic intrusion consider the case of instantaneous emplacement of a square prism of magma which is at its melting temperature (Figure 7a). In the absence of ground-water convection, cooling will occur through vertical and lateral heat conduction. The surface heat-flow anomaly (along an axis of symmetry, Figure 7a) due to a cooling prismatic temperature anomaly is given by Lachenbruch and others (1976) as

$$Q(\ell) = Q_o \frac{2a}{\ell \sqrt{\pi}} \left\{ \exp\left(\frac{-a^2}{\ell^2}\right) - \exp\left[\frac{-a^2}{\ell^2}\left(1+\frac{d}{a}\right)^2\right] \right\} \bar{E} \qquad (8)$$

where

$$E(x,\ell,m) = \frac{1}{2} \operatorname{erf}\frac{m}{\ell}\left[\operatorname{erf}\frac{m}{\ell}\left(1-\frac{x}{m}\right) + \operatorname{erf}\frac{m}{\ell}\left(1+\frac{x}{m}\right)\right] \qquad (9)$$

and "m" is half the distance across the intrusion which has thickness "d" ("x" is the horizontal distance away from the center of the intrusion along an axis of symmetry, Figure 7a; the remaining symbols are defined with equations 2-4). To incorporate the effect of latent heat released during solidification the initial temperature of the intrusion will be increased as discussed in the previous section.

As a numerical example, consider a 2 km thick square

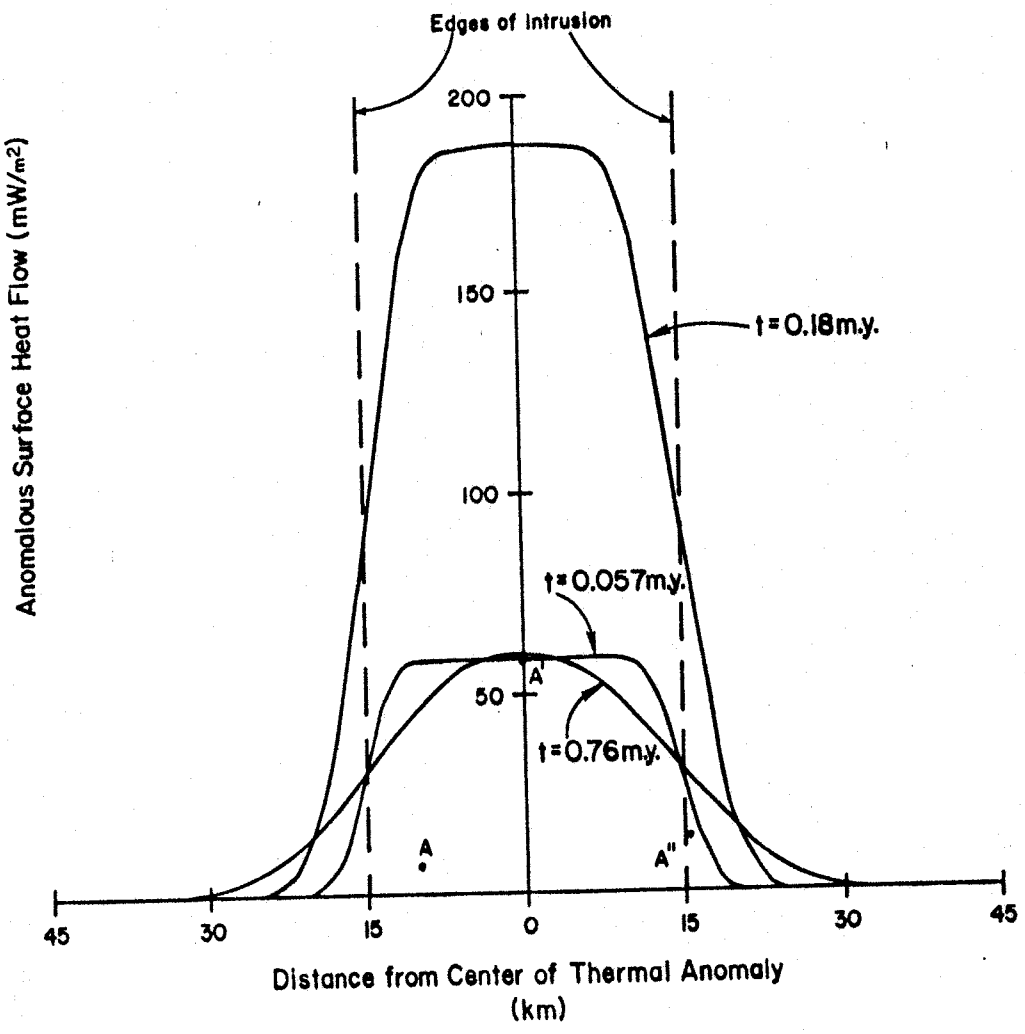

Figure 7b. Anomalous surface heat flow "Q" at several times "t" after the emplacement of a rectangular prismatic intrusion (Figure 7a). The burial depth "a" is 5 km. The length and width of the intrusion "2m" is 30 km. The thickness of the intrusion "d" = 2 km. The surface heat--flow anomaly is shown as a function of distance from the center of the intrusion along an axis of symmetry (e.g. y=0, Figure 7a). The initial anomalous temperature "Δ T" of the intrusion = 1060 °C plus 400 °C (to account for latent heat effects) = 1460 °C. The thermal conductivity of the intrusion and the country rock is 2.5 W/m°C (Chapman and Pollack, 1977). Points A, A' and A" pertain to profile in Figure 6.

prism 30 km across ("2m") which is buried at 5 km depth (Figure 7a). These dimensions approximate the intrusion inferred from gravity data near the Zuni-Bandera volcanic field (discussed above). The surface heat-flow anomaly along an axis of symmetry is shown in Figure 7b for 0.057, 0.18 and 0.76 m.y. after emplacement of the intrusion. The maximum surface heat-flow anomaly at any time is about 180 mW/m2 and occurs over the center of the intrusion about 0.18 m.y. after emplacement. Heat-flow anomalies of about 60 mW/m2 and greater occur from 0.057 to 0.76 m.y. after emplacement of the intrusion. The heat-flow data in the study area near the gravity anomaly suggest the presence of a shallow, recent intrusion. However, it is unlikely that the elevated heat flow is directly related to conduction cooling of the intrusion inferred from the gravity anomaly since the observed surface heat-flow anomaly is offset from the gravity anomaly (Figure 6). It is important to note that the effects of ground-water heat transport have not been considered. Redistribution of heat by ground-water circulation may significantly alter the shape, location and duration of the heat-flow anomaly associated with an intrusion (for example see Norton and Knight, 1977). The observed surface heat-flow anomaly is also narrower than the anomaly predicted by the heat-flow model (compare Figure 6, profile AA" and Figure 7b, note A, A' and A"). One would anticipate little if any thermal anomaly associated with an

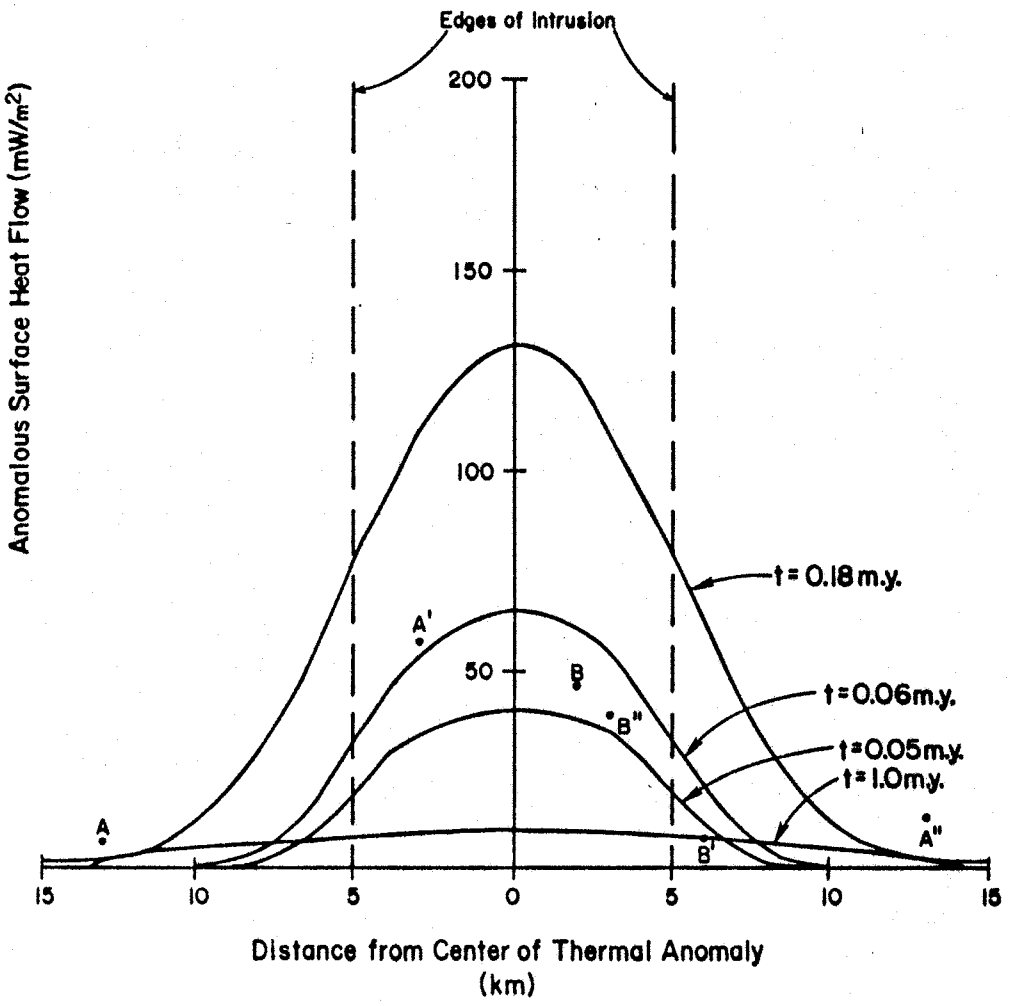

Figure 7c. Same as Figure 7b except the length and width of the intrusion "2m" is 10 km. Points A, A' and A" and B, B' and B" pertain to profiles AA" and BB" in Figure 6. Note: Since the low value of B' lies geographically between B and B", the presence of two separate intrusions is implied. The points A,A',A" and B,B',B" have been located with respect to the center of the thermal anomaly by visual estimation ot the best fit of the points to the theoretical curves.

intrusion of Laramide age (Ander and Heustis, 1982). However, a smaller source centered near Fence Lake (point A', Figure 6) should fit the observational data better. A variation of this model, one in which the width and length of the prismatic intrusion are much smaller than in the above example, is now presented.

Consider a 2 km thick square prism 10 km across ("2m") which is buried at 5 km depth (Figure 7a). The surface heat-flow anomaly along an axis of symmetry is shown in Figure 7c for several times after emplacement (equations 7 and 8). Several of the heat-flow data from the study area are also shown in Figure 7c. The heat-flow data at Cabin Spring (point A in Figure 7c, Q = 73 mW/m2), Fence Lake (point A' in Figure 7c, Q = 124 mW/m2), and Gobbler Knob (point A", Q = 79 mW/m2) lie reasonably close (considering potential measurement errors) to the heat-flow anomaly curve corresponding to 0.06 m.y. after emplacement of the intrusion (profile AA", Figure 6). Similarly, the heat-flow data at Red Hill (point B in Figure 7c, Q = 105 mW/m2), Blaine's Lake (point B', Q = 71 mW/m2), and Agua Fria (point B", Q = 112 mW/m2) lie close to the curves corresponding to the heat-flow anomaly predicted at 0.05-0.06 m.y. after emplacement of the intrusion (profile BB", Figure 6). Therefore the geographic distribution of heat-flow values in the area is generally consistent with models of recent, shallow intrusions.

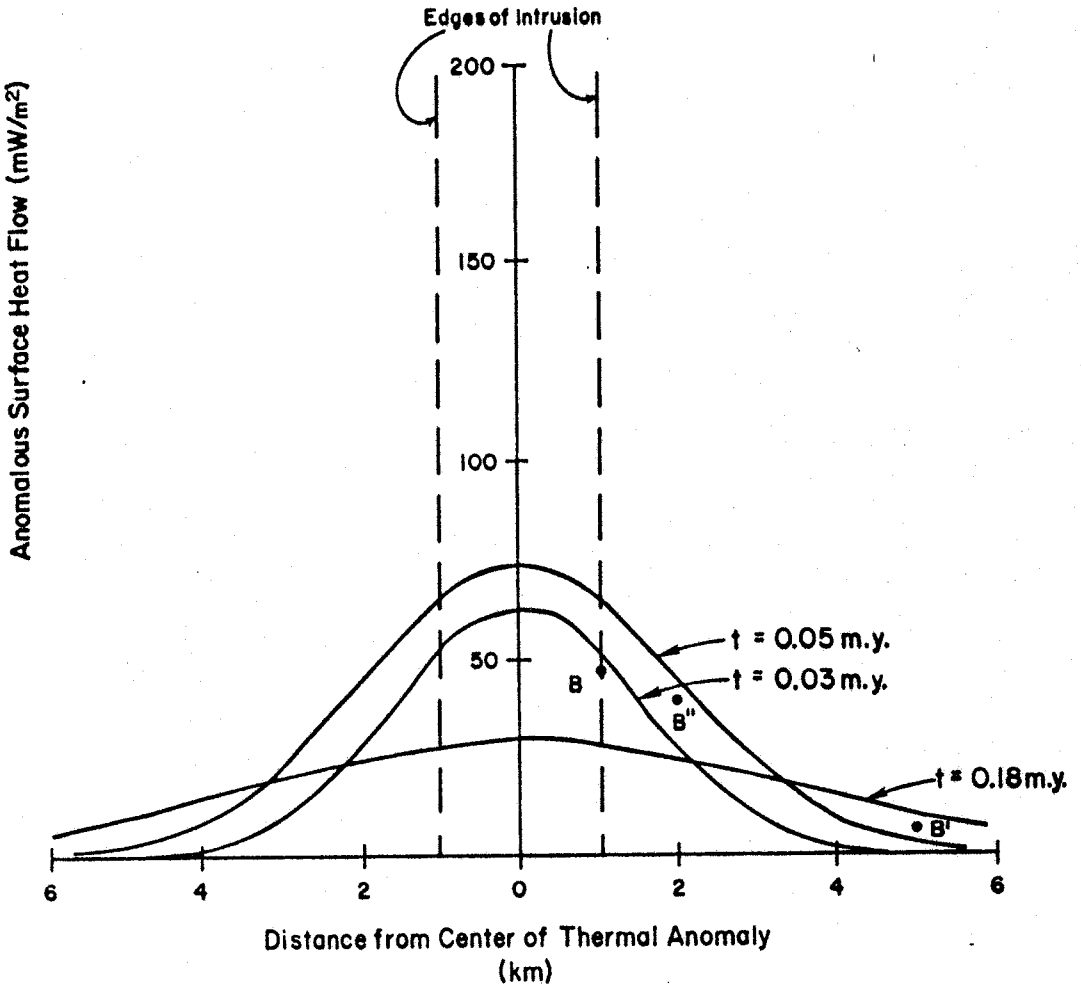

Figure 7d. Same as Figure 7c excepth the length and width of the intrusion "2m" is 2 km, thickness of the intrusion "d" is 10 km, and burial depth "a" is 3 km. The initial anomalous temperature "Δ T" is 1512 °C. Anomalous temperature is greater than for Figure 7c due to shallower burial depth. Points A, A' and A" have not been plotted since they seem to define a thermal anomaly which is broader than is expected for this case. See note in caption for Figure 7c.

The results of these models are certainly not unambiguous and similar results could be obtained from models with different prism dimensions and burial depths. For example, Figure 7d illustrates the heat-flow anomaly predicted for a narrow (width=length="2m"=2 km), thick ("d" = 10 km) intrusion buried at depth "a" = 3 km. The presence of intrusions with these dimensions and ages of about 0.03-0.05 Ma would be approximately consistent with the heat-flow anomalies at Agua Fria, Blaine's Lake and Red Hill (points B, B' and B", respectively Figure 7d).

From the above analysis it appears that much of the spatial variability of the heat-flow data may result from the presence of shallow, recent intrusions. However, it must also be kept in mind that some of the spatial variability of the heat-flow data probably results from the redistribution of heat by ground-water movement.

THERMAL CONVECTION IN A PERMEABLE LAYER

Ground water in the sedimentary section will tend to be gravitationally unstable because buoyancy forces are generated by thermal expansion of ground water due to increased temperature at depth. Thermal convection of ground water may result when buoyancy forces overcome the viscous resistance of the ground water to flow. Turcotte and Schubert (1982) present an expression to determine conditions under which thermal convection of ground water

will occur. The minimum temperature gradient across a uniform, permeable layer which will induce thermal ground--water convection is given by

$$\frac{T}{b} = \frac{\mu K Ra_{cr}}{\alpha g \rho^2 c \lambda b^2} \qquad (10)$$

where α , c , and μ are the coefficient of volumetric expansion, the specific heat, and the dynamic viscosity of the fluid, respectively (Turcotte and Schubert, 1982). The variables K, λ , and b are the thermal conductivity, the permeability and the thickness of the saturated layer. Ra_{cr} is the critical Rayleigh number for the onset of thermal convection in a layer of saturated, permeable material heated from below (Figure 8a).

Figure 8b presents the thermal gradient required for thermal convection as a function of layer thickness for shale, sandstone, and fractured rock (parameter values given in caption of Figure 8b). A temperature gradient less than 30 $^{\circ}$C/km is not likely to result in thermal ground-water convection unless fairly thick (>100 m), relatively permeable sandstones are present (Figure 8b). Lithologic logs and drill cuttings indicate numerous shale layers rather than relatively thick sandstones. Shale layers may significantly reduce equivalent vertical permeability of the sedimentary section (Freeze and Cherry, 1979). Thus the

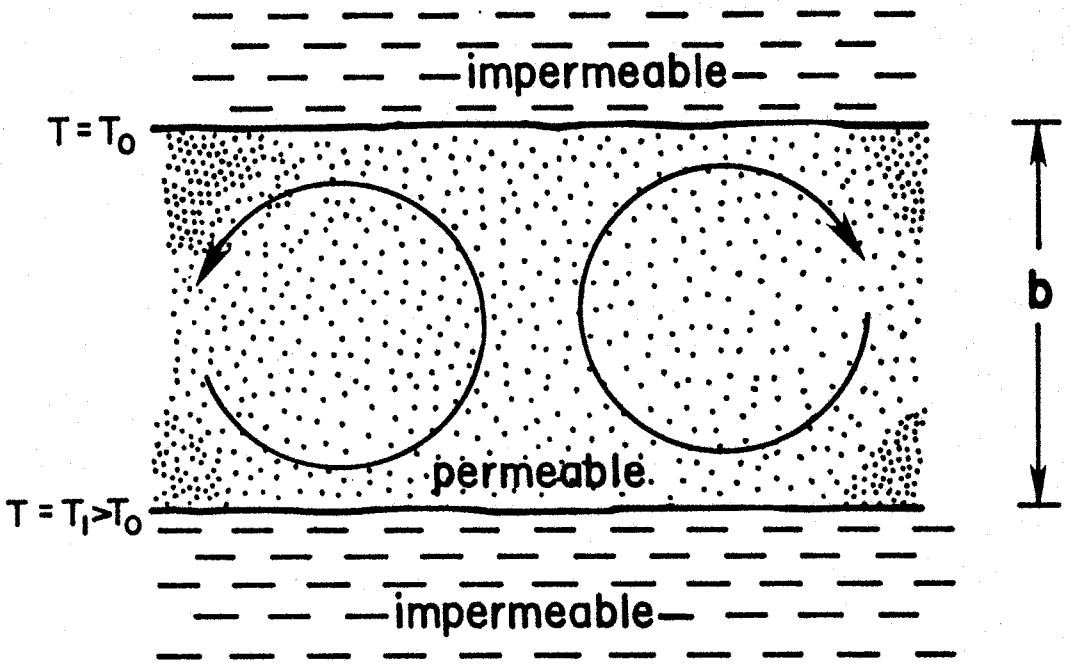

Figure 8a. Illustration of two-dimensional cellular convection in a permeable medium (after Turcotte and Schubert, 1982). Thermal convection is driven by buoyancy forces generated by heating (thermal expansion of water) at the lower boundary.

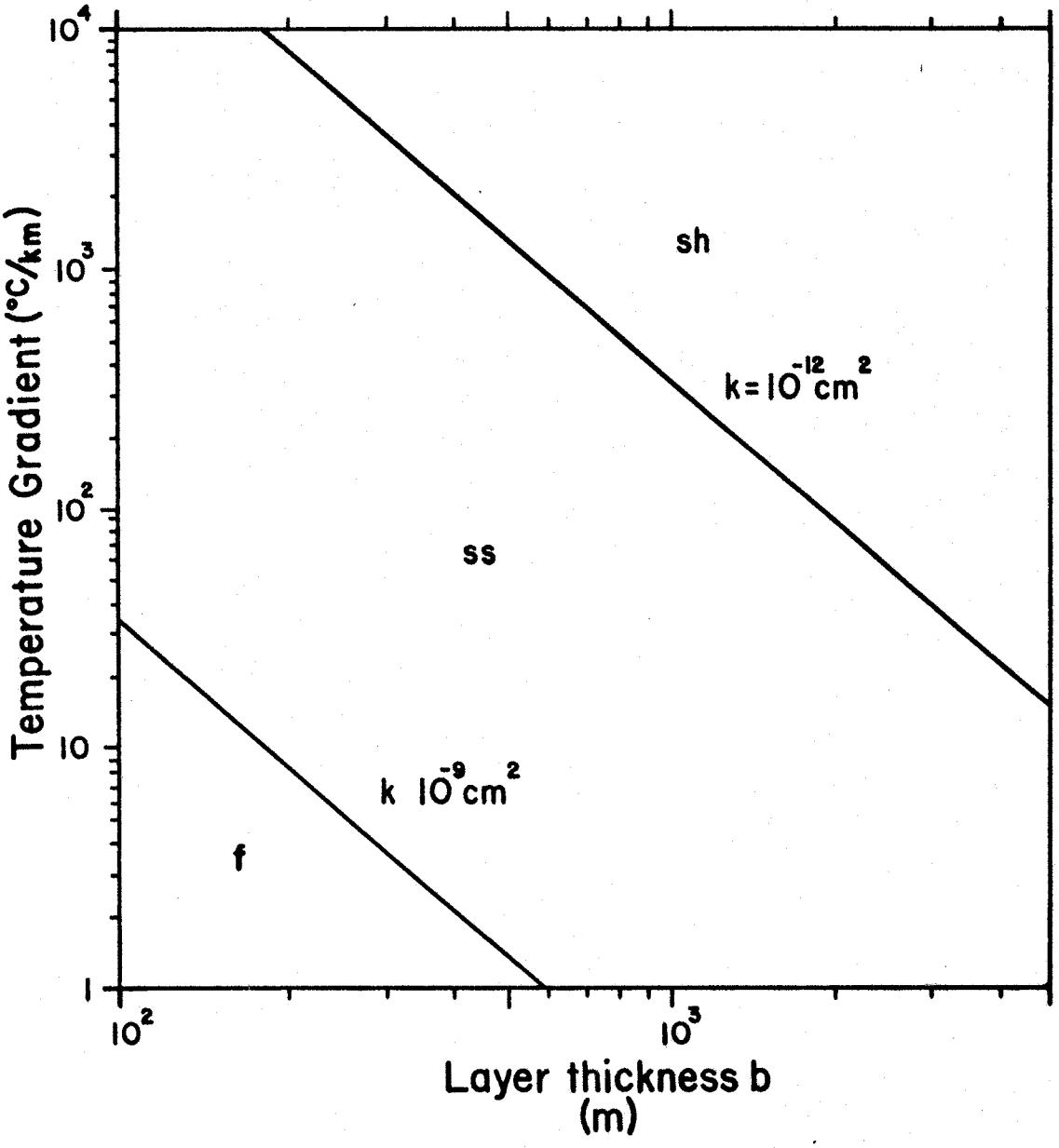

Figure 8b. Thermal gradient required for thermal convection (equation 10) as a function of layer thickness for permeability values k=10E-09 and 10E-12 cm2. These values represent the approximate upper and lower limits of permeability for sandstone (ss). Permeability values outside this range would correspond to fractured rock (f) and shale (sh; Freeze and Cherry, 1979).

likelihood of thermal convection due to the regional temperature gradient is estimated to be quite small. However, higher temperature gradients associated with magma intrusion may initiate local thermal ground-water convection (Norton and Knight, 1977). In addition, fracture zones may promote thermal ground-water convection by increasing permeability.

As discussed above, free convection (i.e. ground-water movement due to density variations) may occur in areas with high temperature gradients (see Figure 8b). However, heat transfer may also occur under forced ground-water convection (ground-water movement resulting from hydraulic forces applied to the hydrogeologic system). Forced ground-water flow systems may be influenced by topography and geology. For example, highlands are often areas of recharge while lowlands are generally areas of discharge (Freeze and Cherry, 1979). Also, the effect of variations in geology on the flow system may be considerable. Hydraulic conductivity variations (which generally coincide with lithology variations) of several orders of magnitude may occur over relatively short distances. Thus, understanding a ground--water flow system and its contribution to heat transfer may require a significant amount of data relating to recharge and discharge areas, hydraulic conductivity variations and specific discharge along flow paths.

The regional ground-water flow system for the study

area is presently not well defined. Hydrologic investigations in the study area relate to recharge and flow in shallow, very local flow systems (Summers, 1972; Stone, 1984; Stone and McGurk, 1987). Deep, regional flow systems in the study area have not been investigated due primarily to the lack of deep wells. As such, the effects of regional flow systems on the heat-flow pattern in the study area cannot presently be incorporated into the study.

Although fluid-phase transport of heat cannot be considered in this study, it is useful to note the possible or likely effects of ground-water heat transport. The role of ground-water circulation in heat transport is, perhaps, most significant where volcanic and magmatic activity is occurring. The emplacement of magma into the crust is likely to induce thermal ground-water convection; such convection may redistribute heat several kilometers away from the intruded magma in a few thousand years (Norton and Knight, 1977). Thermal ground-water convection may also occur in regions of high heat flow. Convective ground-water circulation in such a region may cause the surface heat flow to vary by an order of magitude between areas of upward and downward ground-water flow (Donaldson, 1962). Ground-water flow patterns may control regional heat-flow patterns. Recharge and discharge areas may be characterized by low and high heat flow in regions which otherwise, in the absence of ground-water flow, would exhibit a uniform, regional heat

flow (Majorowicz and Jessop, 1981; Smith and Chapman, 1983).

COAL MATURATION DATA AND ANALYSES

In the present study coal maturation data have been obtained in order to provide constraints on thermal histories proposed for the study area. The thermal maturation of coal, which is exponentially dependent on temperature but linearly dependent on time, essentially integrates through time the total heating the coal has experienced since its deposition (Waples, 1981; Appendix II).

PRESENTATION OF THE COAL MATURATION DATA

The coal maturation data used in this study are discussed below in terms of vitrinite reflectance which is often used as an indicator of thermal maturation. Vitrinite reflectance may be determined by direct measurement or may be estimated from the results of proximate analysis. Vitrinite reflectance measurement and proximate analysis are discussed in Appendix II.

Cretaceous coals are present throughout much of the study area and have been sampled at many locations for proximate analysis (Figure 9, Table 3). Proximate analyses are commonly performed on coal samples to determine the relative proportions of moisture, mineral matter, fixed carbon, and volatile matter in the coal (Appendix II). The

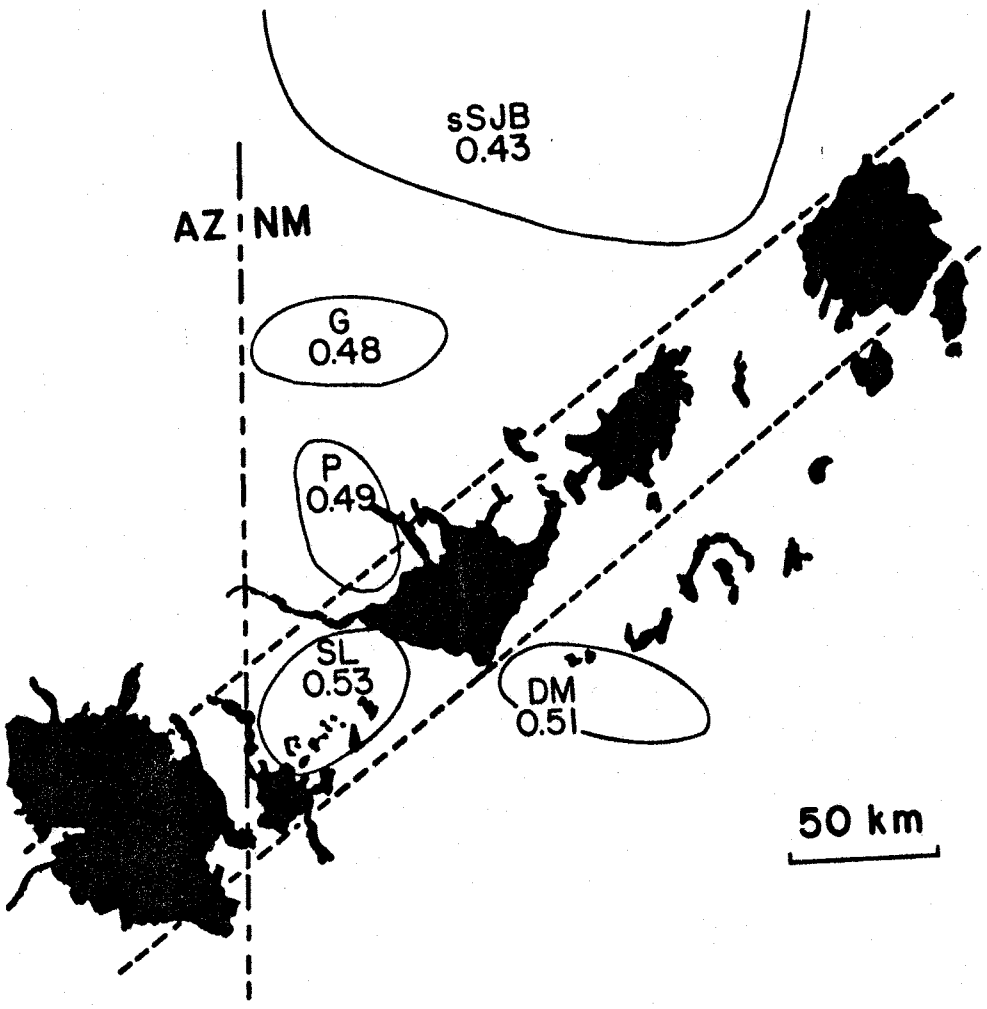

Figure 9. Map of study area showing distribution of coal maturation data. Heavy dashed line represents the Arizona New Mexico state line. Parallel dashed lines represent boundaries of the Jemez zone (Aldrich and Laughlin, 1984). Dark shaded areas represent volcanic rocks. Stippled areas represent coal maturation data regions (Table 3). Regions: SL, Salt Lake; DM, Datil Mountains; P, Pinehaven; G, Gallup; sSJB, southern San Juan Basin. Values within the coal maturation data regions are the mean vitrinite reflectance for the regions in % vitrinite reflectance (Table 3; map after Aldrich and Laughlin, 1984).

Table 3. Data groups used for variance and "F" test analyses for vitrinite reflectance data. Data are from Fieldner and others (1936), Allen and Balk (1954), Fassett and Hinds (1971), Chapin and others (1979), Frost and others (1979), Tabet (1981), Osburn (1982), Anderson and Mapel (1983), and Campbell (1984; unpublished data).

Region		N sites	N samples	R (sites) (% Ro)	R(samples) (% Ro)
I	Salt Lake	33	144	0.53±0.11	0.53±0.11
II	Datil Mtns.	18	26	0.51±0.10	0.50±0.11
III	Pinehaven	5	8	0.49±0.09	0.47±0.09
IV	Gallup	28	68	0.48±0.05	0.47±0.05
V	s. San Juan B.	17	17	0.43±0.09	0.43±0.09

R(sites) is the mean site vitrinite reflectance and standard deviation within a region. R(samples) is the mean sample vitrinite reflectance and standard deviation within a region. N sites is the number of data sites within a region. N samples is the number of data samples within a region. The Kolmogorov-Smirnov test does not lead to rejection of normality at about the 5% significance level for data regions I, II and III (Lindgren and others, 1978). The sample distributions for regions IV and V are somewhat skewed but appear to be approximately normal (Dixon and Massey, 1983).

coal maturation data summarized in Table 3, originally presented by several investigators in terms of percent volatile matter, have been converted to percent vitrinite reflectance using the correlation scale of Dow (1977; see Table 3 for data references).

Vitrinite reflectance may also be measured with a reflecting light microscope photometer (Appendix II). Measurements of vitrinite reflectance for several samples from the Salt Lake region are presented in Table 4. The average measured vitrinite reflectance in this region is about 26% less than the vitrinite reflectance estimated from proximate analysis data (estimated minus measured over estimated). However, the 0.14% difference in vitrinite reflectance obtained between the two techniques (0.39% measured vitrinite reflectance versus 0.53% estimated vitrinite reflectance) corresponds to a relatively small difference in maturation levels (see Waples, 1980).

STATISTICAL MODELS

One of the fundamental objectives of this study is to examine the spatial variability of the data in an effort to define regional trends in the present-day heat flow and the thermal history of the study area. Therefore the coal maturation data within the study area have been divided into several regional data sets for statistical analyses (Figure 9, Table 3). The average vitrinite reflectance values for

Table 4. Vitrinite reflectance measurement data. Coal samples for vitrinite relfectance measurement were provided by F. Campbell, New Mexico Bureau of Mines and Mineral Resources, Socorro. Vitrinite reflectance measurement is discussed by Stach and others (1975) and in Appendix II.

	Location (T.-R.-S.)	Depth Interval (ft)	Vitrinite Reflectance (% Ro ± st. dev.)
1.	1N-19W-8	104.0-118.0	0.37 ± 0.06 0.38 ± 0.04
2.	2N-18W-24	162.5-163.3	0.36 ± 0.04 0.37 ± 0.04
3.	2N-19W-24	155.0-165.0	0.40 ± 0.05 0.40 ± 0.06
4.	3N-16W-6	48.2-51.6	0.37 ± 0.04 0.38 ± 0.04
5.	4N-16W-31	44.0-53.0	0.37 ± 0.04 0.41 ± 0.03
6.	4N-17W-3	133.0-143.0	0.37 ± 0.04 0.37 ± 0.04
7.	4N-17W-14	134.0-143.5	0.38 ± 0.04 0.41 ± 0.04
8.	4N-17W-23	30.0-35.0	0.40 ± 0.05 0.40 ± 0.05
9.	5N-16W-30	181.0-186.5	0.41 ± 0.07 0.37 ± 0.06
10.	5N-17W-1	20.0-30.0	0.42 ± 0.05 0.42 ± 0.05

each region indicate that the coals have a relatively low thermal maturation level (low rank bituminous, Table 3; Dow, 1977).

The coal maturation data indicate a fairly uniform level of thermal maturation for the study area (Figure 9). The level of maturation in the Salt Lake region (within the volcanically active Jemez zone, Figure 9, Table 3) appears to be somewhat elevated with respect to the level of maturation in the surrounding regions (i.e. the Datil Mtns., Pinehaven, Gallup and southern San Juan Basin regions; Figure 9, Table 3). However, in the study area there does not appear to be a profound trend of increasing coal maturation toward areas of volcanic activity as is apparent northward across the San Juan Basin (see Clarkson, 1984). For example, the vitrinite reflectance across the San Juan Basin ranges from 0.40 to 1.10% compared with the vitrinite reflectance in the study area which ranges from 0.43 to 0.53%. The level of thermal maturation in the southern San Juan Basin is somewhat less than the level of maturation in the southern part of the study area (Figure 9, Table 3).

The level of maturation of the southern San Juan Basin coals (Fruitland Formation, deposited about 73 Ma; Molenaar, 1977) agrees well with values calculated from thermal models which assume a steady-state heat flow of 67 mW/m2 for various burial histories (Clarkson, 1984). The coals south of the southern San Juan Basin were deposited about 92 Ma

and have slightly higher levels of thermal maturation (Molenaar, 1977; Figure 9, Table 3). Results of thermal models (discussed later) suggest that the difference in burial times between the Fruitland Formation coals of the southern San Juan Basin and the other coals south of the southern San Juan Basin, which were deposited about 19 m.y. earlier, can account for much of the relatively small difference in thermal maturation levels between the two areas.

NESTED ANALYSIS OF VARIANCE AND F TEST

A nested analysis of variance model (Snedecor and Cochran, 1973) has been applied to compare several levels or components of variance in the vitrinite reflectance data. The levels examined are; (i) variances between vitrinite reflectance values for different samples at given sample sites, (ii) variances between vitrinite reflectance values at different sample sites within regions, and (iii) variances between vitrinite reflectance values in different regions. The results of the variance analyses are presented in Table 5 for vitrinite reflectance data groups within different regions.

The largest components of variance estimated are generally the "between samples within sites". These variance estimates correspond to standard deviations of up to approximately 0.10% vitrinite relfectance (Table 5). The

Table 5. Variance analyses for vitrinite reflectance data sets. Analyses after presentations in Snedecor and Cochran (1973). Standard deviations also presented for comparison in percent vitrinite reflectance.

Regions	d**2 d (% Ro)	w**2 w (% Ro)	r**2 r (% Ro)
I,II,III,IV,V	0.00790 (0.089)	0.00098 (0.031)	0.00139 (0.037)
I,II,III,IV	0.00790 (0.089)	0.00106 (0.033)	0.00101 (0.032)
I,II,III	0.01023 (0.101)	0.00123 (0.035)	0.00019 (0.014)
I,II	0.01044 (0.102)	0.00118 (0.034)	0.00014 (0.012)
I,III	0.01019 (0.101)	0.00132 (0.036)	0.00052 (0.023)
II,III	0.00837 (0.091)	0.00208 (0.046)	-0.00073 (NA)
III, IV	0.00088 (0.030)	0.00214 (0.046)	-0.00033 (NA)
IV,V	0.00079 (0.028)	0.00275 (0.052)	0.00052 (0.023)
I,IV	0.00787 (0.089)	0.00086 (0.029)	0.00165 (0.041)
I,V	0.01041 (0.102)	0.00085 (0.029)	0.00438 (0.066)

Region I - Salt Lake; Region II - Datil Mountains; Region III - Pinehaven; Region IV - Gallup; Region IV - southern San Juan Basin.
d**2, d - variance and standard deviation estimates "between samples within sites", standard deviation in parentheses
w**2, w - variance and standard deviation estimates "between sites within regions", standard deviation in parentheses
r**2, r - variance and standard deviation estimates "between regions", standard deviation in parentheses
NA - not applicable, standard deviation estimate not calculated since variance estimate less than zero.

"between sites within regions" and "between regions" component of variance estimates are typically much less than the "between samples within sites" variance estimates (exceptions are Group III, IV and Group IV, V, Table 5). Standard deviations for "between sites within regions" and "between regions" are less than about 0.05% vitrinite reflectance. The estimates of the components of variance contain information regarding regional differences in vitrinite reflectance. An approximate "F" test has been applied to the components of variance results to determine whether regional differences in vitrinite reflectance exist.

The approximate "F" test which has been applied to the vitrinite reflectance data is a test of the hypothesis that the "between regions" variance is equal to zero. An approximate F-random variable can be constructed based upon the results of the nested analyses of variance (Graybill, 1961; Reiter and others, 1985). Results of the approximate "F" tests are presented in Table 6 and include the calculated "F" ratio with two separate degrees of freedom and the resultant "P" values. The "P" values are significance levels, with small "P" values indicating that the hypothesis of no-differences ("between regions" variance equal to zero) is unlikely. In other words, small "P" values support the hypothesis that statistically significant differences between the data groups of different regions exist (Reiter

Table 6. "F" test analyses for various vitrinite reflectance regions. Analyses after Graybill (1961) and Dixon and Massey (1983).

Regions	degrees of freedom	F	P
I,II,III,IV,V	4, 67	6.113	P < 0.01
I,II,III,IV	3, 53	4.966	P < 0.01
I,II,III	2, 62	1.403	0.25 ≤ P < 0.50
I,II	1, 46	1.421	0.10 < P < 0.25
I, III	1, 70	1.600	0.10 < P < 0.25
II, III	1, 16	0.2564	0.50 < P < 0.75
III, IV	1, 32	0.0721	0.75 < P < 0.90
IV, V	1, 45	3.716	0.05 < P < 0.10
I, IV	1, 22	12.15	P < 0.01
I, V	1, 80	11.83	P < 0.01

Region I - Salt Lake; Region II - Datil Mtns.; Region III - Pinehaven; Region IV - Gallup; Region V - southern San Juan Basin.
Degrees of freedom are approximated (Graybill, 1961; Reiter and others, 1985). F is the "F" value used in the statistical test. P values are discussed in the text; the smaller the P value the more confidence one may have that the difference in means of the various regions is not due to chance alone and thus is real.

and others, 1985).

Based upon vitrinite reflectance data, statistically significant differences between some of the various regions exist (Table 6). Perhaps the most significant difference is between the Salt Lake region and the southern San Juan Basin and Gallup vitrinite reflectance data regions. "F" test analyses which group the Salt Lake region and the southern San Juan Basin, and the Salt Lake region and Gallup region, indicate that the difference in means between the Salt Lake region and the latter two regions is probably not due to chance alone (regions I, IV and I, V; Table 6). The average vitrinite reflectance for the Salt Lake region data appears to be somewhat higher than the mean in the adjacent regions, the Datil Mountains and Pinehaven regions. However, the data in the Datil Mountains and Pinehaven regions do not seem to exhibit a statistically significant difference in mean maturation levels. Similar results in differentiating regions were obtained by applying the students's t-test to the sample site maturation values, however, the t-test does not nest the components of variance (Table 7).

The practical significance of statistical differences is now considered since for large enough numbers of samples even very slight differences may be detected as statistically significant (Lindgren and others, 1978). Vitrinite reflectance measurements of a coal seam sample generally

Table 7. "t" test analyses for various vitrinite reflectance regions. Analyses after Dixon and Massey (1983).

Regions	degrees of freedom	t	P
I, II	168	1.331	0.10 < P < 0.20
I, III	150	1.363	0.10 < P < 0.20
II, III	32	0.545	0.40 < P < 0.60
III, IV	74	0.354	0.60 < P < 0.80
V, IV	83	2.375	0.02 < P < 0.05
I, IV	210	4.378	P < 0.01
I, V	159	3.602	P < 0.01

Region I - Salt Lake; Region II - Datil Mtns.; Region III - Pinehaven; Region IV - Gallup; Region V - southern San Juan Basin.
t is the "t" value used in the statistical test (Dixon and Massey, 1983).

yield a normal distribution about the mean vitrinite reflectance with a standard deviation of data of about 0.10% vitrinite reflectance (Stach and others, 1975). Similar standard deviations of the data are inferred from the "between samples within site" variance estimates in Table 5 (estimated standard deviation "d" between samples within sites, 0.028 to 0.101% vitrinite reflectance) which in all cases are much greater than the "between regions" variance estimates. In addition, within the sub-bituminous coal rank region vitrinite reflectance increases relatively slowly as the volatile matter content decreases (volatile matter content has been used to estimate vitrinite reflectance). Low rank bituminous coals demonstrate a large amount of variability in volatile matter content (Figure 10; Stach and others, 1975; Dow, 1977). An estimate of the variability of vitrinite reflectance as a function of volatile matter content can be obtained from Figure 10. Vitrinite reflectance has a range of about 0.25% reflectance at any given volatile matter content for low rank bituminous coals (vitrinite reflectance < 0.75%, Figure 10). Thus the range of vitrinite reflectance (for a given value of volatile matter content) is about an order of magnitude greater than the standard deviation attributed to regional differences (in Table 5). The large numbers of vitrinite reflectance data used in the variance analyses may be able to identify differences between the regional mean reflectances.

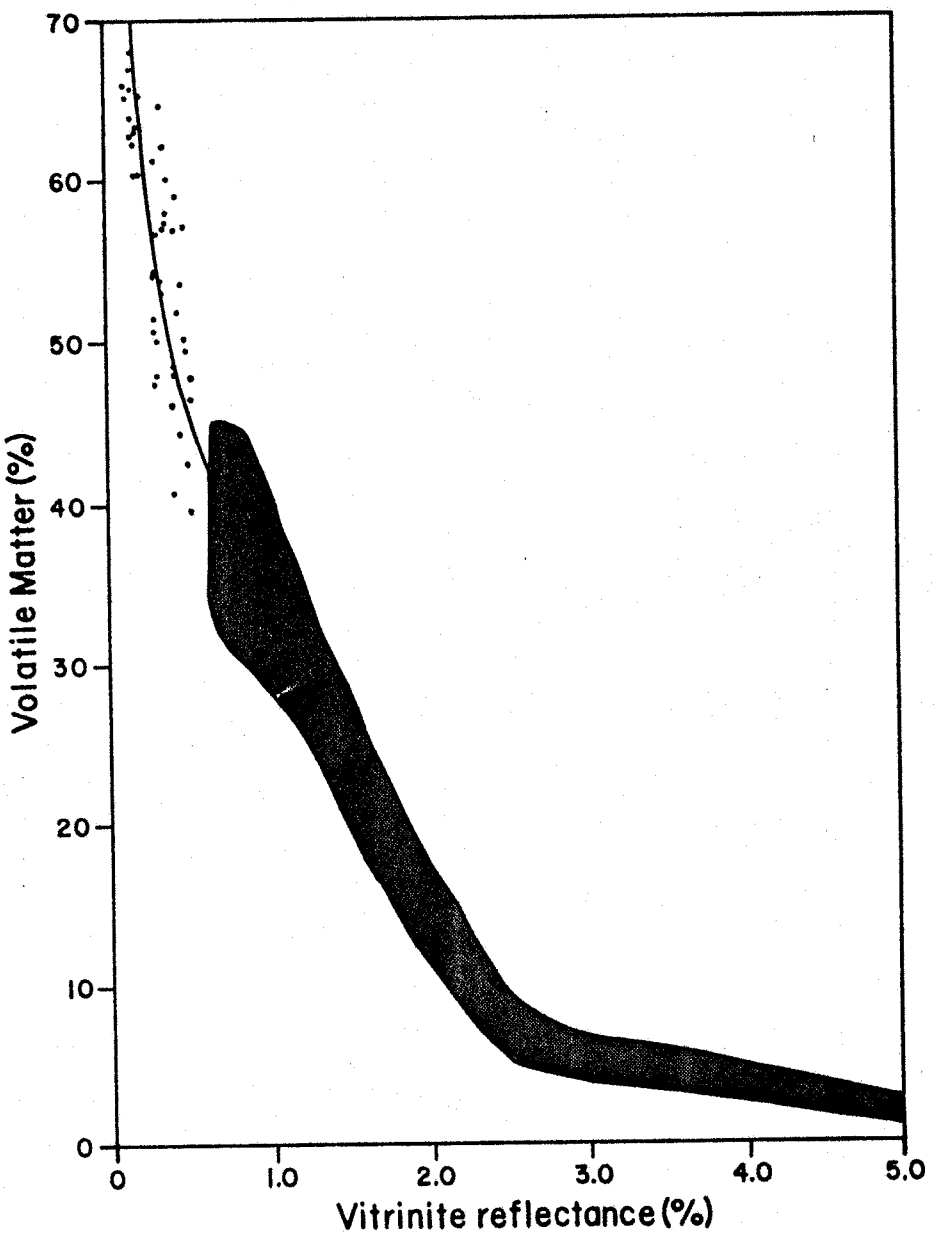

Figure 10. Relationship between volatile matter and vitrinite reflectance (Stach and others, 1975).

However, the differences may be small enough to be geologically indistinguishable. Thus, while differences in the mean levels of maturation for some of the various regions within the study area may be statistically significant, the practical significance of the difference between means may be slight or perhaps questionable.

GEOTHERMAL MODELS

Several geothermal models have been applied to the coal maturation data. The geothermal models incorporate surface temperature variations due to paleoclimate and uplift of the CP, with models of the burial history of the coals in the study area. Burial histories are loosely constrained by present sediment thicknesses, sediment ages, erosional unconformities, and estimated rates of deposition/erosion. The Time-Temperature Index of maturation (TTI) method has been used to calculate maturation levels for the various geothermal models (Waples, 1980; Clarkson, 1984; Appendix II). The calculated values of vitrinite reflectance are then compared to observed levels of thermal maturation. Analyses of coal maturation data, when combined with heat-flow data and volcanic age dates, help define the post late-Cretaceous thermal history of the area and constrain tectonic models for the late Cenozoic evolution of the southern Plateau boundary.

STEADY-STATE UNIFORM HEAT FLOW

The level of maturation of the Fruitland Formation coals in the southern San Juan Basin may be closely matched by thermal models which use a generalized San Juan Basin geologic history with a steady-state heat flow (Clarkson, 1984). Because of the proximity of the southern San Juan Basin to the northern part of the study area and because the heat-flow data suggest the background heat flow for the study area may be similar to or perhaps somewhat greater than the heat flow for the southern San Juan Basin, the generalized steady-state thermal history model of Clarkson (1984) has been extended to predict coal maturation levels for the study area.

Clarkson (1984) presents a burial history for the Fruitland Formation coals in the southern San Juan Basin which, when combined with a steady-state thermal model, yields calculated levels of maturation in good agreement with observed values. The thermal model assumes steady--state surface heat flow of 67 mW/m2 which is the approximate average of measurements of the present-day heat flow in the southern San Juan Basin (Clarkson, 1984). Coal maturation levels are calculated from the temperature history of the coal which is a function of the thermal gradient, burial depth and ground surface temperature. Because coal maturation is also a function of time, burial depth and surface temperature must be estimated for the time period commencing

with the deposition of the coal and ending with the present. Clarkson (1984) has estimated burial depth, ground surface elevation and sea level temperature for the San Juan Basin over the past 73 m.y., i.e. since the deposition of the Fruitland Formation coals. The estimated histories for thermal gradient, burial depth and surface temperature are sufficient to calculate coal maturation levels. The thermal model presented by Clarkson (1984) is modified here to predict coal maturation levels in the study area.

Coal in the present study area is located within upper Cretaceous sediments which have been deposited approximately 95 to 89 Ma (Molenaar, 1977; Hook, 1983; Campbell and Roybal, 1984). Present burial depths of coals in the study area are generally less than burial depths of Fruitland Formation coals in the southern San Juan Basin (see references given in Table 3). Therefore, modification of the thermal model presented by Clarkson (1984) of the southern San Juan Basin for use in the present study area requires extending the model history from about 72 Ma to about 92 Ma and decreasing the present-day depth of burial (Molenaar, 1977; Figures 11 and 12, model I). Transient temperature effects, for example due to sedimentation (Appendix I), are not incorporated into the present model. The coal temperature at a given time is approximated by multiplying the steady-state temperature gradient by the burial depth of the coal and adding the surface temperature.

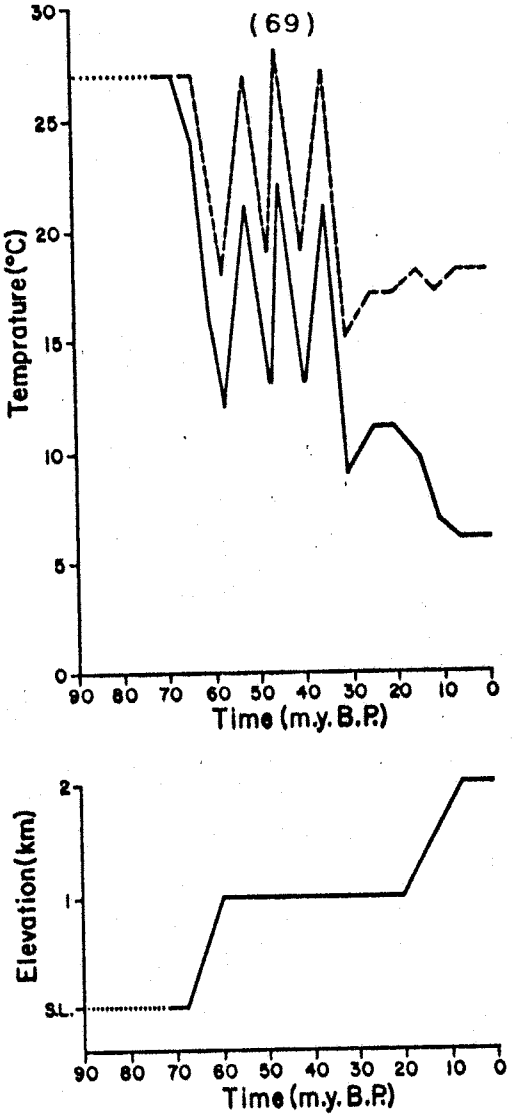

Figure 11.
Top. Estimate of average paleotemperature in the study area for the last 92 m.y. (solid line; after Clarkson, 1984). The average paleotemperature in the study area was estimated from the estimated average paleotemperature at sea level in the study area (dashed line) and with a -6 ^{o}C/km atmospheric gradient correction for uplift of the Colorado Plateau. Dotted line (92-72 Ma) is extrapolated for this study (see Clarkson, 1984).

Bottom. Estimated ground-surface elevation of Colorado Plateau used to estimate effects of Plateau uplift on paleotemperatures (after Clarkson, 1984). Plateau uplift estimated to occur about 70 to 60 Ma (Damon in Bird, 1979) and after 24 Ma (Luchitta, 1972; McKee and McKee, 1972; Chapin and Seager, 1975). Fossil flora data from the Rio Grande rift suggest regional uplift occurred after about 14 Ma (Axelrod and Bailey, 1976). Mountain building in the southern Rocky Mountains area (east of the study area) began 17 to 12 Ma and culminated between 7 and 4 Ma (Eaton, 1976).

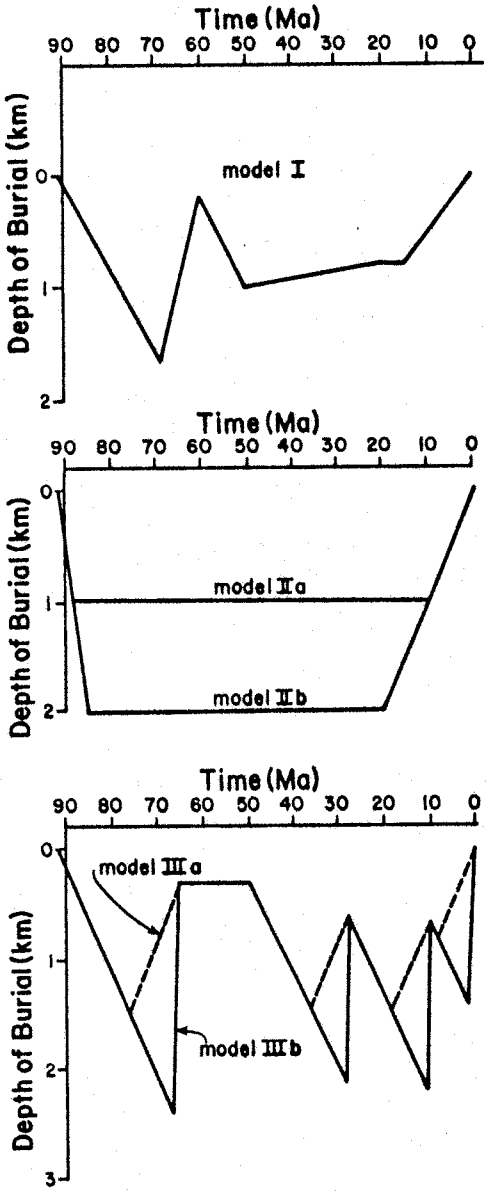

Figure 12.

Top. Model I, burial history for coals in the study area (modified, see p.68, from burial history for the Fruitland Formation coals in the southern San Juan Basin, Clarkson, 1984).
Middle. Models IIa and IIb, burial histories for coals in the study area modified (see p. 71) from general San Juan Basin burial histories (after Clarkson, 1984).
Bottom. Models IIIa and IIIb, burial histories for coals in the study area interpreted from the stratigraphic record and estimates of sedimentation/denudation rates (see text; Guilinger, 1982).

The level of maturation predicted by the modified burial history (model I, Figure 12) is about 0.47% vitrinite reflectance and agrees well with the observed values for the coals in the Pinehaven and Gallup regions (Table 3). Somewhat higher temperatures (discussion below), perhaps due to deeper burial depths or higher heat flow, are required to match the observed coal maturation levels in the Salt Lake and Datil Mountains regions (Table 3, Figure 9).

Hypothetical thermal models are now considered in order to illustrate the effect of burial depth on the level of coal maturation. The general models consist of coal deposition 92 Ma and rapid burial followed by a rather constant depth of burial at 1 or 2 km (Figure 12, models IIa and IIb). Late Tertiary-Recent erosion occurred regionally including much of the study area (Molenaar, 1977). This erosional event has been incorporated into models IIa and IIb (Figure 12). Erosion, beginning about 20 Ma, reduces the depth of the coal burial to present-day depths (Figure 12). These general models, with 1 or 2 km burial depths, result in calculated values of vitrinite reflectance of 0.46 or 0.63%, respectively. Average values of vitrinite reflectance for the coal regions in the study area south of the San Juan Basin range from 0.47 to 0.53% (Table 3). If model II is, in the first order, appropriate for the study area, a coal burial depth slightly greater than 1 km would be appropriate.

A third set of hypothetical burial models is illustrated in Figure 12 (models IIIa and IIIb). Deposition in the Salt Lake region since late Cretaceous time (~92 Ma) has been interrupted by periods of weathering and erosion (Guilinger, 1982). Models IIIa and IIIb were constructed using estimates of the sedimentation rate (10 cm/1000 y, after Reiter and others, 1986) and the denudation rate (10 and 100 cm/1000 y, models IIIa and IIIb, respectively; after Leopold and others, 1964). The estimate of the sedimentation rate is from the Albuquerque Basin (syn-rift, ~ 30-0 Ma) and are, thus, probably greater than the actual sedimentation rates in the study area (Reiter and others, 1986). The estimates of the denudation rates used in model IIIa and IIIb are also somewhat high (Leopold and others, 1964). Relatively high sedimentation and denudation rates require the coal to be buried at greater depths and experience higher temperatures than lower rates (for example compare models IIIa and IIIb, Figure 12). Therefore higher sedimentation and denudation rates will generate higher maturation levels. These models (models IIIa and IIIb, Figure 12) using denudation rates of 10 and 100 cm/1000 y predict vitrinite reflectance values of 0.45 and 0.57%, respectively. Thus, these model results compare well with the observed levels of thermal maturation (Table 3). Comparison between model IIIa and model IIIb results (Table 8) indicates that the level of coal maturation may not be very

Table 8. Summary of calculated levels of coal maturation in % vitrinite reflectance for several burial history models and heat flows, Q. The burial history models I, II and III are discussed in the text and illustrated in Figure 12.

Model	Q = 59 mW/m2	Q = 67 mW/m2	Q = 75 mW/m2
I	0.44	0.47	0.51
IIA	0.44	0.46	0.50
IIB	0.62	0.68	0.82
IIIA	0.43	0.45	0.50
IIIB	0.53	0.57	0.66

sensitive to an order of magnitude change in erosion rate. Sedimentation and erosion rates in the study area may be somewhat lower than the estimates used in the models. For example, Cather and others (1987) calculate deposition rates of 3.2 to 17.7 cm/1000 y for the Datil Group (volcanic tuffs) in the western Gallinas Mountains east of the present study area (compare to 10 cm/1000y used in model IIIa). Measured rates of deep-sea clay accumulation range from less than 1 cm/1000 y to greater than 10 cm/1000 y (Gilluly and others, 1975). The hypothetical burial histories IIa, b and IIIa, b are limiting case examples which illustrate the model sensitivity to variations in burial history. Detailed stratigraphic studies yielding burial histories more representative of the study area would be most useful.

The results presented above for models I, II and III suggest that the relatively small differences in the level of maturation between the various regions within the study area could easily result from differences in the burial histories of the regions. In each of the above models the level of maturation was calculated assuming a steady-state heat flow of 67 mW/m2. Because the regional heat flow for the study area is somewhat uncertain, the level of maturation has also been calculated for the burial histories presented above with the regional heat flow Q = 59 and 75 mW/m2. The results of these calculations are summarized in

Table 8 along with the results for the models described above where the regional heat flow Q = 67 mW/m2.

Comparison of the observed levels of maturation with the levels of maturation calculated above for the various burial histories and regional heat flows (Tables 3 and 8, respectively) allows some first order conclusions to be made. In order for the calculated level of maturation to agree with the observed values (0.47 to 0.53% vitrinite reflectance) certain combinations of burial history and regional heat flow must be present. For example, a relatively shallow burial history (average burial depth $\lesssim$ 1-1.5 km, models I, IIa and IIIa, Figure 12) requires the regional heat flow to be greater than the present average heat flow for the interior CP (i.e. $\gtrsim$ 65 mW/m2). Alternatively, relatively deep burial histories (average burial depth > 1.5 km, models IIb and IIIb, Figure 12) imply the regional heat flow has been similar to that of the Plateau interior, i.e. 58 to 65 mW/m2. It must be kept in mind, however, that a steady-state regional heat flow was assumed for the analyses. Magmatic activity, which may locally increase heat flow for periods of time shorter than the burial history of the coal, is now considered.

TRANSIENT HEAT-FLOW EFFECTS ON COAL MATURATION

In the previous section the effects of various burial histories on coal maturation levels were investigated for

regions with steady heat flow. Magmatic intrusion may, however, temporarily increase heat flow and thus may affect levels of coal maturation. Therefore the effects of transient heat-flow events will now be examined.

Consider the transient temperature anomaly associated with the emplacement of an extensive sill (Figure 5a). The mathematical treatment of this problem has been discussed previously in this manuscript (equation 7). The thermal effect of sill intrusion on coal maturation will depend on coal burial depth, roof thickness (depth to sill, "a" in Figure 5a), and sill thickness. The anomalous temperature experienced by coal buried at 1 and 2 km depth is illustrated as a function of time after sill emplacement in Figures 13a and 13b, respectively. The curves A through E represent the anomalous temperatures (at 1 and 2 km depth, Figures 13a and 13b) resulting from sills of various thickness intruded at depths of 2 to 5 km. The temperature anomaly resulting from sill emplacement may be combined with the coal burial history to illustrate the effect of the intrusion on coal maturation levels.

As a simple exercise, consider two examples of coals buried at depths of 1 or 2 km for the last 92 m.y. Such a burial history is a first order approximation of the various burial histories previously presented for the study area (Figure 12). The level of thermal maturation has been calculated for this simple burial history with and without

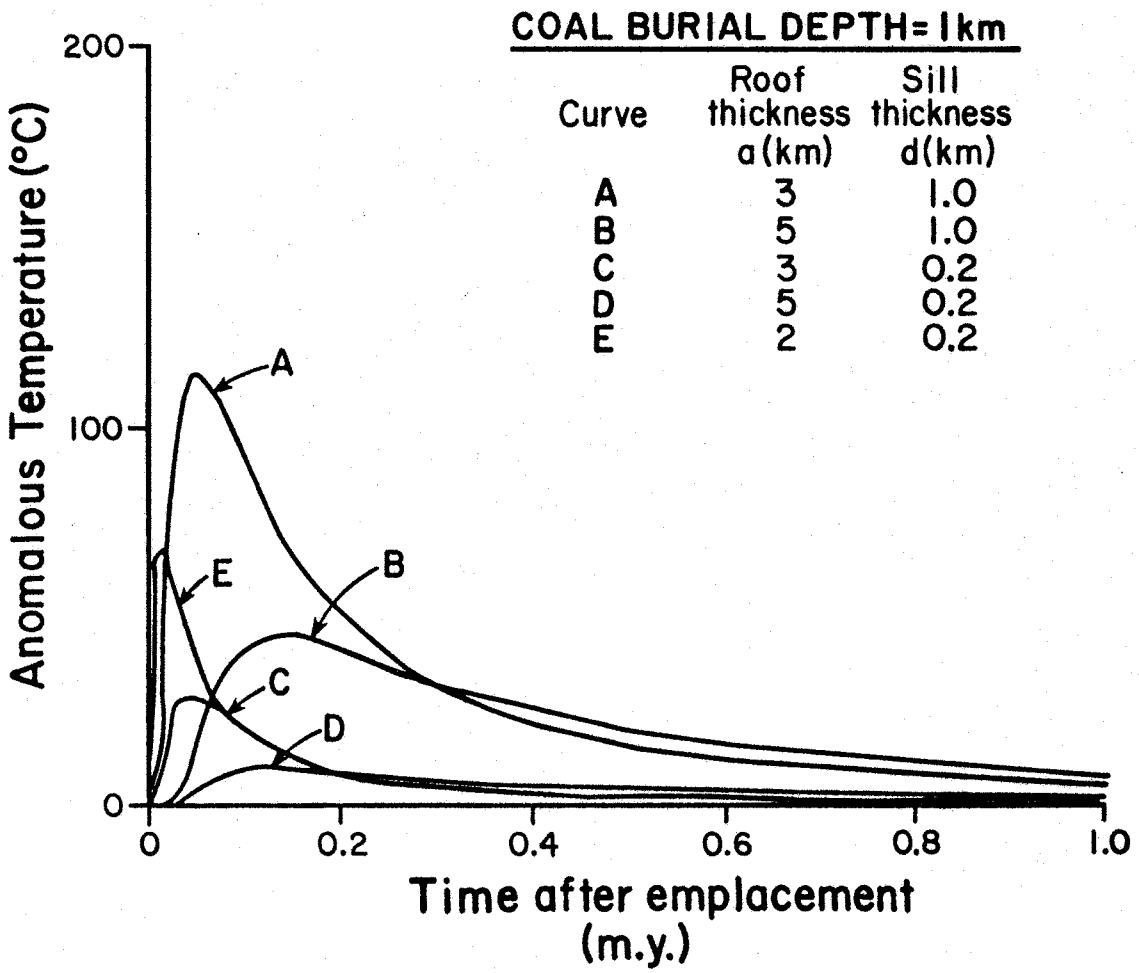

Figure 13a. Anomalous temperature of coal as a function of time "t" after sill emplacement. Burial depth of coal is 1 km.

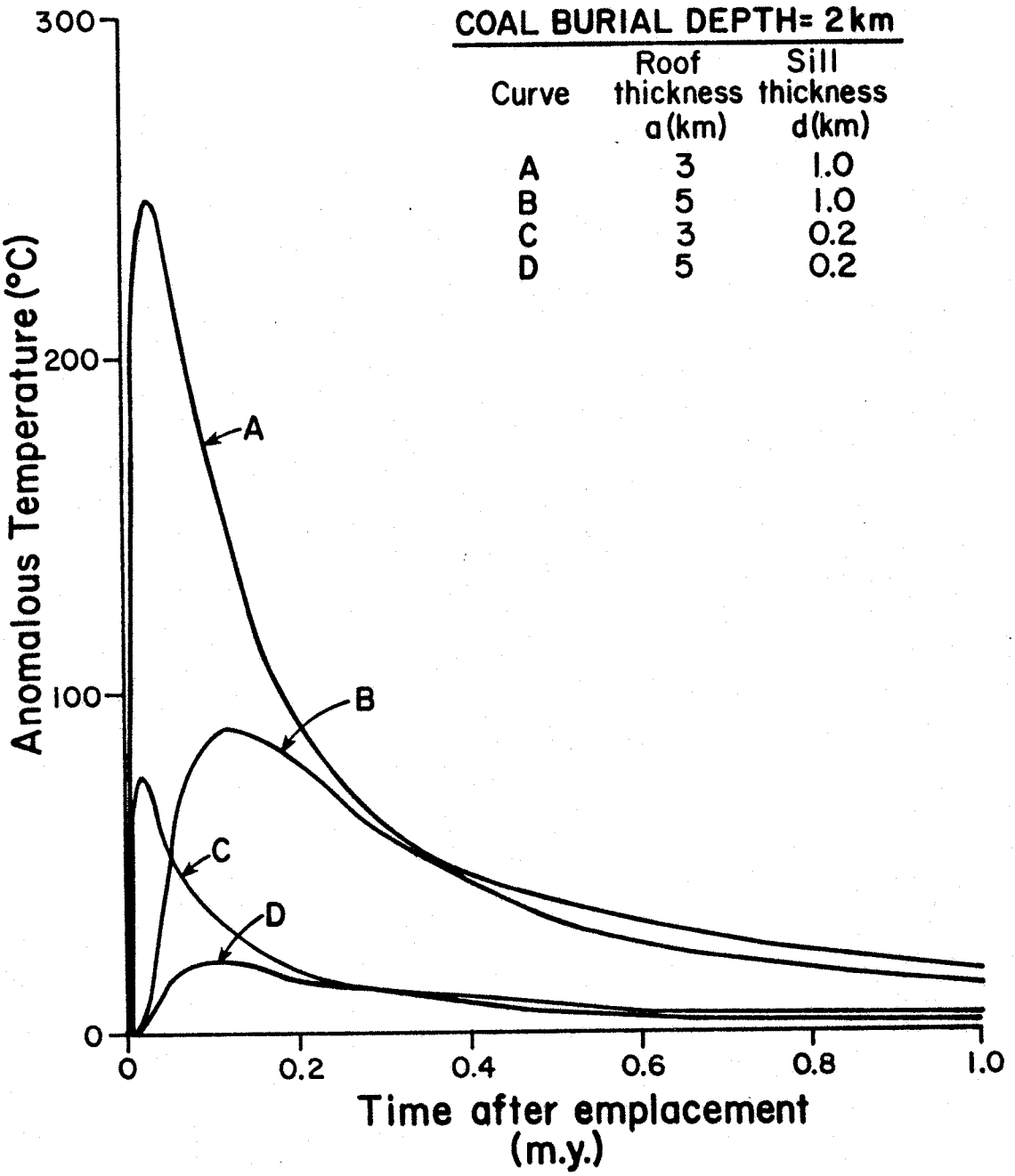

Figure 13b. Anomalous temperature of coal as a function of time "t" after sill emplacement. Burial depth of coal is 2 km.

emplacement of the sills modeled in Figures 13a and 13b (background temperature assumed to be 41 °C and 67 °C at 1 and 2 km depth, respectively, Table 9). The results presented in Table 9 reflect the influence of sill emplacement on coal maturation. For comparison, the expected level of maturation without sill intrusion is also presented in Table 9. Anomalous coal temperatures, which remain elevated for a period of time sufficient to increase maturation levels, are associated with relatively thick, shallow sills (Table 9, Figures 13a and 13b).

The pattern of volcanic activity and the spatial variability of heat-flow data in the study area suggest that magmatic activity in the study area may presently occur as shallow, local intrusions rather than areally extensive sills. Due to lateral cooling, the influence of a local intrusion (for example, the rectangular prismatic intrusion illustrated in Figure 7a) has been presented earlier in this manuscript (equation 8). The effects of a local intrusion on coal maturation were calculated for a prismatic intrusion of width 1 or 5 km ("2m" in Figure 7a). The intrusion thicknesses and depths modeled are the same as in the sill emplacement models in Table 9 (0.2 and 1 km thick, 2, 3 and 5 km depth). The results presented in Table 10 are the maximum expected maturation levels since they have been calculated for coals which lie above the center of the intrusion (i.e. where the temperature anomaly will be the

Table 9. Estimated levels of thermal maturation of coal resulting from emplacement of an extensive sill (Figure 5a). Values are in % vitrinite reflectance. Thermal models A through E are discussed in the text and illustrated in Figures 13a and 13b.

Model	Roof Thickness a (km)	Sill Thickness d(km)	% Vitrinite Reflectance Coal Burial Depth 1km	2km
A	3.0	1.0	0.50	>5.0
B	5.0	1.0	0.41	0.62
C	3.0	0.2	0.41	0.56
D	5.0	0.2	0.40	0.55
E	2.0	0.2	0.41	NA
Without Sill Emplacement			0.40	0.55

greatest, Lachenbruch and others, 1976).

Due to lateral cooling, rectangular prismatic intrusions, i.e. intrusions of limited areal extent, will have a diminished effect on coal maturation levels as compared to areally extensive sills of comparable thickness and emplacement depths. For example, consider the maturation level of two coal seams (buried at depths of 1 and 2 km) overlying a 1 km thick sill which is emplaced at a depth of 3 km (model A, Table 9). Sill emplacement increases the maturation level of the coal from 0.40 or 0.55% vitrinite reflectance to 0.50 or > 5.0% vitrinite reflectance (coal burial depth 1 or 2 km, respectively, model A, Table 9). Intrusions with the same thickness (1km) and emplacement depth (3 km) but having limited areal extent, for example with a width of 1 or 5 km (width = "2m" in Figure 7a, models A1 or A2, Table 11), will increase the maturation level of the coal from 0.40 or 0.55% vitrinite reflectance to only 0.55 or 2.02% vitrinite reflectance, respectively (for coal buried at 2 km depth). The maturation levels of coals buried at 1 km depth will not be significantly affected by the emplacement of such local intrusions (1 km thick, < 5 km wide, emplaced at 3 km depth, Table 10).

The thermal analyses presented above illustrate the potential influence of magmatic intrusions on coal maturation levels. The results seem to suggest that coal maturation levels will record mainly the emplacement of

Table 10. Estimated levels of thermal maturation of coal over the center of a shallow rectangular intrusion (Figure 6a). Values are in % vitrinite reflectance. Models A through E correspond to models A through E in Table 9 (for comparison between emplacement of an extensive sill and a rectangular prismatic intrusion, Figures 5a and 7a, respectively).

Model	Width 2m (km)	Roof Thickness a(km)	Intrusion Thickness d(km)	Coal Burial Depth 1 km	2km
A1	1.0	3.0	1.0	0.40	0.55
A2	5.0	3.0	1.0	0.41	2.02
B1	1.0	5.0	1.0	0.40	0.55
B2	5.0	5.0	1.0	0.40	0.55
C1	1.0	3.0	0.2	0.40	0.55
C2	5.0	3.0	0.2	0.40	0.55
D1	1.0	5.0	0.2	0.40	0.55
D2	5.0	5.0	0.2	0.40	0.55
E1	1.0	2.0	0.2	0.40	NA
E2	5.0	2.0	0.2	0.41	NA
Without Intrusion				0.40	0.55

relatively shallow, thick intrusions. Relatively shallow intrusions are better able to increase the temperature of the coal and intrusions that are relatively thick are able to maintain the elevated temperatures for longer periods of time. Due to lateral cooling, local intrusions (as compared to areally extensive sills) are much less effective in raising the level of thermal maturation of coals. Coal maturation data indicate a relatively low level of thermal maturation with little variability across the study area (Table 3). The lack of anomalously high maturation values in the study area suggests that the effect of transient heat sources on coal maturation is minimal which, via the discussion, does not preclude their existence. The slightly higher % vitrinite reflectance values in the Salt Lake region, as compared with the Pinedale or Datil Mountains regions (0.53% versus 0.49 or 0.51%) is interesting because it is of this small order of increase in % vitrinite reflectance that might be expected from intrusive activity.

DISCUSSION

Heat-flow data in west-central New Mexico, on the southern boundary of the Colorado Plateau, exhibit a complex heat-flow pattern which does not appear to have a straightforward correlation to recent volcanism (Table 1, Figure 2). Sites with relatively high heat flow (>90 mW/m2) are often located near sites with significantly lower heat flow (<70 mW/m2). Although high heat-flow sites are located near centers of recent volcanism along the portion of the Jemez lineament within the study area, high heat-flow values also occur in the northern part of the study area away from recent volcanic activity (Figure 2).

K-Ar data have been obtained from volcanic centers located along the Jemez lineament between the White Mountains-Springerville and Zuni-Bandera volcanic fields (Minier and others, 1987). The data suggest volcanic activity during latest Miocene and Pleistocene times, approximately 6.7 and 1.0 Ma (Table 2). Volcanism may have occurred as late as 0.0229 Ma at Zuni Salt Lake (Bradbury, 1966). Pliocene and Pleistocene ages have also been reported for the White Mountains-Springerville and Zuni-Bandera volcanic fields (<4Ma, Callender and others, 1983; Aubele and others, 1986).

The Jemez lineament does not seem to be clearly

associated with a regional heat-flow anomaly (as, for example, the heat-flow anomaly associated with the San Juan volcanic field; Figure 1; Reiter and Mansure, 1983). Low to intermediate heat-flow values (<70 mW/m2) are located within the volcanically active Jemez zone (Figures 1 and 2). From the data, the heat-flow pattern in the study area may be described as local areas of elevated heat flow superimposed on a regionally intermediate background heat flow. The background heat flow appears to be similar to the average heat flow of the interior Colorado Plateau and southern San Juan Basin. This heat-flow pattern would be consistent with the emplacement of relatively shallow, recent intrusions of limited areal extent. Results of first-order heat conduction analyses suggest that the heat-flow anomalies observed in the study area may result from intrusions as shallow as 3 to 5 km which were emplaced during Quaternary time (< 1 Ma).

Many of the heat-flow data have been measured at relatively shallow depths and therefore may be perturbed by ground-water circulation. However, a few deep heat-flow estimates in the study area, which are less likely to be perturbed by ground-water circulation than are shallow data, support the hypothesis that the background or regional heat flow is similar to the intermediate values observed in the interior Colorado Plateau and specifically the southern San Juan Basin (Table 1).

Ground-water circulation may increase heat flow by

transporting deep thermal waters to shallow depths. Similarly, vertically downward ground-water movement may decrease the temperature gradient at shallower depths (Bredehoeft and Papadopulos, 1965). A correction has been applied to the heat-flow data to account for heat transported by vertical ground-water movement within the zone of measurement (after Mansure and Reiter, 1979). The heat-flow correction for ground-water movement may be quite large, up to 100 mW/m2. However, the specific discharges calculated from the correction are not inconsistent with the limited amount of available hydrologic data (see p. 17). The correction, however, cannot account for heat transport beneath the zone of measurement.

Thermal ground-water convection may be induced by buoyancy forces resulting from the thermal expansion of water. Thermal convection requires high temperature gradients and high permeability (Figure 8b). High temperature gradients could be induced by intruding magmas while high permeabilities may be present in fracture zones. It is likely that thermal convection would occur in the study area only in the presence of magma intrusions and high permeability zones. For example, thermal springs (22 °C versus mean annual air temperature of 12 °C; Levitte and Gambill, 1980) are present at the north end of the Atarque monocline (A on Figure 15) where permeability is, perhaps, locally increased due to fracturing. The thermal springs may also

reflect convection induced by high temperature gradients resulting from the emplacement of magma. Geochemical data obtained from thermal waters in the study area suggest that these waters have not circulated to great depths (Levitte and Gambill, 1980).

The coal maturation data indicate a uniform and relatively low level of maturation across the study area. The level of coal maturation in the study area is somewhat greater than maturation levels for the younger Fruitland Formation coals in the southern San Juan Basin (0.53 vs. 0.43, Figure 9). Much of this relatively small difference in maturation levels can be explained by the difference in coal burial times between the southern San Juan Basin and the study area (i.e. the coals in the study area have been buried about 20 m.y. longer than the Fruitland Formation coals in the San Juan Basin). Although there do not appear to be any profound regional trends in coal maturation across the study area, results of statistical analyses suggest that there are some differences between the average level of coal maturation levels for the various regions within the study area (Tables 5 and 6). For example, coal maturation levels in the Salt Lake coal field (within the volcanically active Jemez zone) are slightly elevated with respect to the level of coal maturation in the neighboring regions (Table 3). In general however, the Jemez lineament does not appear to be associated with an obvious or profound increase of coal

maturation levels as is apparent going northward across the San Juan Basin approaching the thermal source beneath the San Juan Mountains volcanic field (Clarkson, 1984).

Coal maturation levels have been predicted for the study area using estimates of the coal thermal burial histories. The calculated levels of maturation are consistent with observed maturation levels when a thermal/-burial model appropriate for the southern San Juan Basin is applied to the study area (e.g. Clarkson, 1984). The interpretation of coal maturation levels contains considerable ambiguity with respect to thermal and burial histories. A given maturation level may result from a number of different thermal/burial models.

Several of the coal maturation models considered in this study assume a relatively shallow ($\lesssim$1 km) burial history for the coal. In order for the maturation models to accurately predict the observed levels of coal maturation, the regional heat flow must be greater than the average heat flow for the interior Colorado Plateau (i.e. > 58-65 mW/m2, if the coals were buried at about 1 km). However, other thermal maturation models, which incorporate deeper burial histories (1 to 2 km), suggest that the regional heat flow in the study area is comparable to that observed in the interior Colorado Plateau. These models did not consider transient heat-flow effects such as may result from magmatic intrusion (discussed below).

The results of heat conduction analyses suggest that many of the observed heat-flow anomalies in the study area may be the result of shallow, recent intrusions. Therefore additional models have been considered to examine the effect of magmatic intrusions on coal maturation levels. The model results suggest that only relatively shallow, thick intrusions which can maintain elevated coal temperatures for significant time periods are likely to affect the coal maturation levels (Figure 12; Tables 9 and 10). The observed levels of coal maturation indicate a relatively low, uniform level of thermal maturation across the study area. This observation suggests that relatively shallow, thick magmatic intrusions have not been emplaced in the study area. Deeper or thinner intrusions which can not significantly affect coal maturation levels, but which can temporarily increase heat flow, may be present and may be indicated by the heat-flow data if they are sufficiently recent. The very slight level of increased level of coal maturation in the Salt Lake region is what might be expected from repeated emplacement of numerous, small, thin intrusions; however, other explanations are possible.

Geophysical data indicate that crustal and or lithospheric thinning may be occurring on the northwest periphery of the Colorado Plateau (Bodell and Chapman, 1982; Eggleston and Reiter, 1984). Other studies also suggest that portions of the Plateau boundary may be migrating towards the Plateau

interior (Keller and others, 1979; Thompson and Zoback, 1979). Some of the characteristic features of crustal and lithospheric thinning such as volcanism, high heat flow and faulting, are observed in the study area (Callender and others, 1983). However, unlike the northwestern periphery of the Plateau, low to intermediate heat-flow values characteristic of the Plateau's thermal interior are observed in the present study area (see Eggleston and Reiter, 1984). Of course the heat-flow data in the study area are relatively shallow and a number of deeper data would be most desirable. The complex distribution of heat-flow values in the study area suggests that the anomalous, high values result from shallow, recent intrusions or ground-water movement. Possible implications of the low to intermediate background heat flow on crustal and or lithospheric thinning models, as compared to the northwestern periphery of the CP, may be considered. If a regional thinning event is occurring under the study area, then initiation of the event occurred later than in the northwestern periphery of the Plateau. Alternatively, thinning may be occurring at a slower rate and or greater depth along the southern Colorado Plateau.

Other investigators hypothesize that the Jemez lineament is a zone of weakness which has been leaking magma to the surface (Chapin and others, 1978). A change in the orientation of the regional stress regime is believed to

have increased the extension across the Jemez lineament beginning about 7 Ma allowing magmas to leak to the surface (Aldrich and Laughlin, 1984). The K-Ar dates are consistent with this hypothesis (Table 2). The spatial variability of heat flow along the Jemez lineament within the study area, i.e. the presence of low to intermediate heat-flow values, along with high heat-flow values, at sites near Pleistocene volcanic rocks may be consistent with the hypothesis that the Jemez lineament is acting as a zone of crustal weakness. Periodic intrusion of magma at various locations could result in local areas of high heat flow with a lower background flux. Magma intrusion along the Jemez lineament does not account for heat-flow anomalies away from the lineament towards the interior of the Colorado Plateau, where high heat-flow values are observed near intermediate values suggesting relatively shallow depths to the heat source. A model which may help to explain high heat-flow anomalies away from the Jemez lineament is now discussed.

Monoclines are perhaps the most characteristic structural feature of the Colorado Plateau (Kelley, 1955). A model to describe the development of monoclines on the CP has been presented by Davis (1978). The monoclines appear to be related to movement on high-angle faults in the Precambrian basement. During Laramide time (about 80 to 40 Ma) the Colorado Plateau experienced regional southwest--northeast compression which resulted in reverse movement

along the high-angle basement faults. The monoclines are thought to be upper crustal expressions of near-vertical movement along reactivated fault zones (Davis, 1978). Observations of monoclines in the Grand Canyon region, and laboratory models, support the hypothesis that monoclines result from high-angle movements along reactivated faults of Precambrian age (Davis, 1978).

Davis (1978) has constructed a map of inferred basement fault zones for the CP by applying criteria obtained from his laboratory model to the monocline fold pattern of the Plateau. The laboratory model consists of a pine board, cut into blocks along steeply dipping planes ("high-angle faults"), which is overlain by a layer of clay ("sediments"). Horizontal compression applied to the pine board causes deformation in the overlying clay layer through high-angle reverse movement along the saw cuts in the pine board (Davis, 1978). By comparing the experimental monocline fold pattern in the clay layer to the array of saw cuts in the pine board, Davis (1978) identified several relationships which may exist between monoclines and basement fractures in the CP. These relationships or criteria include aligned end-points of monocline segments, aligned monocline segments, abrupt bends in the traces of individual monoclines, and branching-converging monoclines. Figure 14 illustrates the spatial relationships between the monoclines (solid lines) and inferred basement fracture

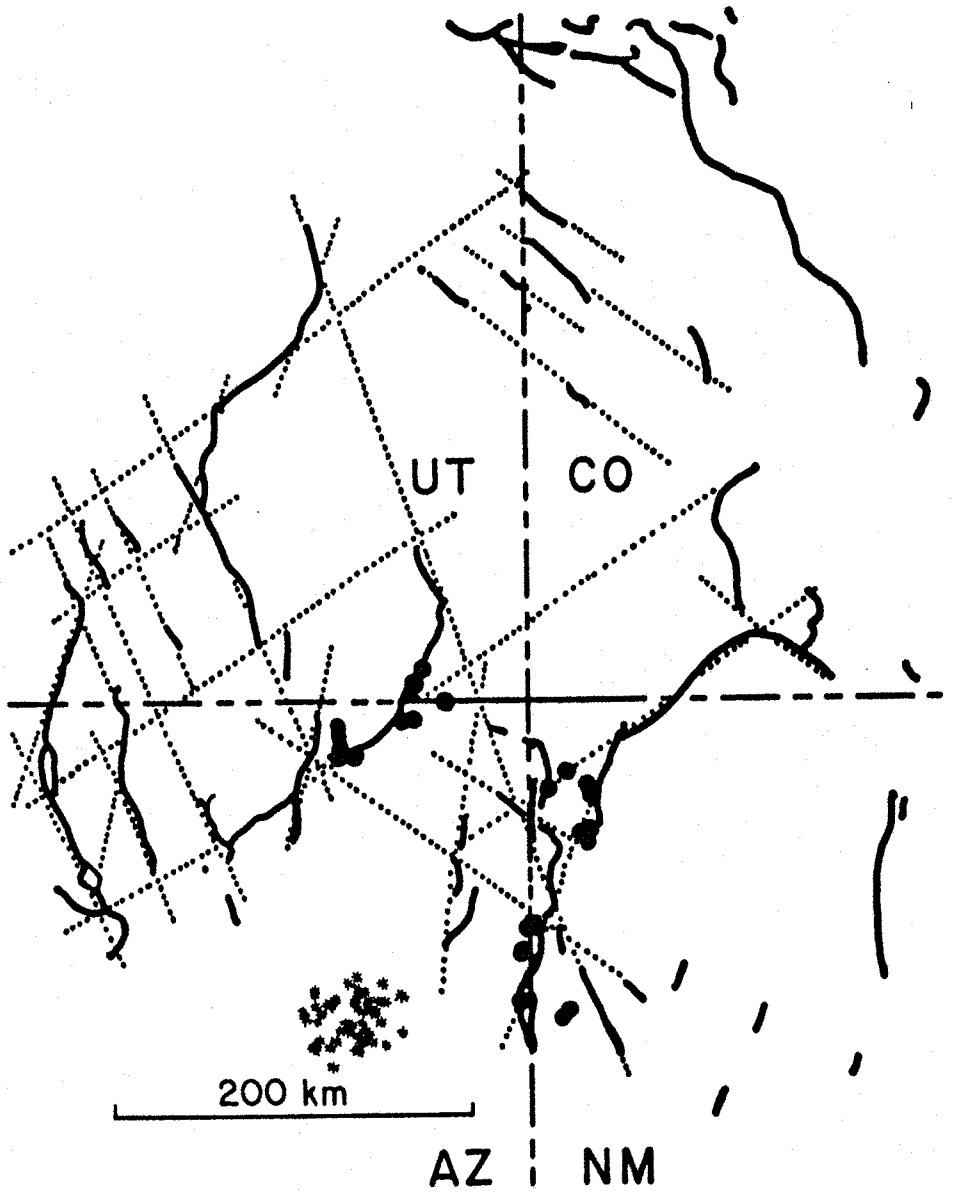

Figure 14. Map of the Four Corners area of the Colorado Plateau. The dark, curved lines represent monoclines; the dotted lines represent the basement fracture system inferred from the monocline pattern. Large dots represent intrusive rocks. The asterisks indicate the location of the Hopi Buttes volcanic field. (Naeser, 1971; Davis, 1978).

system (dotted lines) for the Colorado Plateau(Davis,1978).

The location of Oligocene dikes and diatremes in the Four Corners area have been superimposed on the map of the inferred basement fracture system (Figure 14). Note that the volcanic centers are often located on or near inferred basement fault zones or the intersection of two inferred basement fractures. This observation suggest that the basement fracture system may have acted as a zone of weakness and therefore localized magma emplacement. Zones of weakness may also provide pathways for enhanced groundwater circulation. It is interesting to note that the northeast trend of many of the inferred basement fractures is similar to the northeast trend of the Jemez lineament.

Three monoclines (Atarque, Gallestina, and Nutria; A, G and N in Figure 15) are present in the study area (Anderson, 1982, 1983; Anderson and Mapel, 1983). Based on the aligned end-points of monocline segments Anderson (1986) has inferred the presence of basement fractures in the study area (Figure 15; see Davis, 1978). The northeast trend of the basement fractures inferred by Anderson (1986) is similar (approximately parallel) to the northeast trend of the Jemez lineament and similar to the trend of many of the inferred basement fractures for other areas of the Colorado Plateau (Davis, 1978). Changes in the regional dip of sediments across the inferred basement fractures are also observed.

Figure 15. Monoclines, faults and inferred basement fractures in the study area. Inferred basement fractures labeled WD, T and N are from Davis (1978); inferred basement fractures labeled A, G, J, and O are from Anderson (1982, 1983, 1986). M indicates the location of another basement fracture zone inferred by the relatively high heat-flow values along the trend. Monocline and fault pattern is from Wilson and others (1969) and Baldridge and others (1983). The star east of Zuni indicates the location of an intrusion (see Anderson, 1986). See Figure 2 for a description of the remaining symbols.

The fracture zones, inferred to exist near Zuni (Anderson, 1986; Figure 15) may be acting as zones of crustal weakness. For example, an intrusion, located east of Zuni, may have intruded along one of the basement fractures (Figure 15; Anderson, 1986). Also, deformation resulting from movement along the fracture zone may be associated with locally increased permeability. A thermal spring is located at the north end of the Atarque monocline (A in Figure 15) at the intersection of two inferred basement fracture zones (Levitte and Gambill, 1980). It seems then that the basement fracture zones may be influencing both magma emplacement and ground-water circulation. High heat-flow values located nearby may reflect the presence of recent, shallow intrusions or thermal waters (e.g. the high heat-flow values, 108 and 124 MW/m2, east and and southeast of Zuni, New Mexico, Figure 15). Similar structural controls of magma emplacement and ground-water circulation in the Socorro area are described by Chapin and others (1978).

Sites with high heat flow, located in other parts of the study area where recent volcanic activity is not indicated, may also reflect the presence of additional basement fracture zones. For example, consider the heat--flow sites located north of Springerville (sites with values of 86, 116 and 149 mW/m2, Figure 15). These sites are located approximately along the extension of the southern-

most basement fracture zone inferred by Anderson (1986, O in Figure 15). Farther north are two basement fracture zones, trending north to north-northeast, inferred by Davis (1978; WD and T in Figure 15). Sites with high heat flow are also located near or along the extension of these inferred fracture zones (sites with values of 94, 109 and 159 mW/m2).

High heat flow observed in the southern part of the study area may reflect the presence of a basement fracture zone which trends northeast from the Springerville area (M in Figure 15). The zone of high heat flow (8 of 12 sites > 90 mW/m2) is located in, and is approximately parallel to, the Jemez lineament. The zone of high heat flow is also parallel to other inferred basement fracture zones to the north (i.e. O and J in Figure 15). It is interesting to note that low to intermediate heat flows may also be located on or near the inferred basement fracture zones. For example, intermediate heat flows are observed along the northeast-trending fracture zone inferred to exist near Springerville and Quemado or for example along the northwest-trending fracture zone associated with the Nutria monocline (M and N in Figure 15). With ground-water movement enhanced along these fractures, heat flow may well be expected to be increased or decreased (due to upward or downward ground-water flow and heat transport) relative to the regional heat flow.

A histogram of the heat-flow data in the study area is presented in Figure 16. The distribution of data is somewhat skewed with high heat-flow data generally having greater deviations from the mean than the low heat-flow data. Many of the high heat-flow data are located within 5 km of inferred basement fracture zones (74% or 17 of 23 of the values $\geq$ 90 mW/m2; Figure 16). Heat-flow data with values less than 90 mW/m2 indicate a decreased percentage of sites located within 5 km of inferred basement fracture zones (25% or 10 of 40 of the values less than 90 mW/m2). A similar observation is made if the data within 5 km of the southernmost inferred fracture zone are not included in the calculation (see Figure 16). This observation suggests that most of the high heat-flow data are associated with the inferred basement fractures and may reflect enhanced magma emplacement and/or ground-water circulation. The greatest number of heat-flow values occur between 60 and 70 mW/m2 which allows us to suggest a regional or background heat flow of about 65 mW/m2.

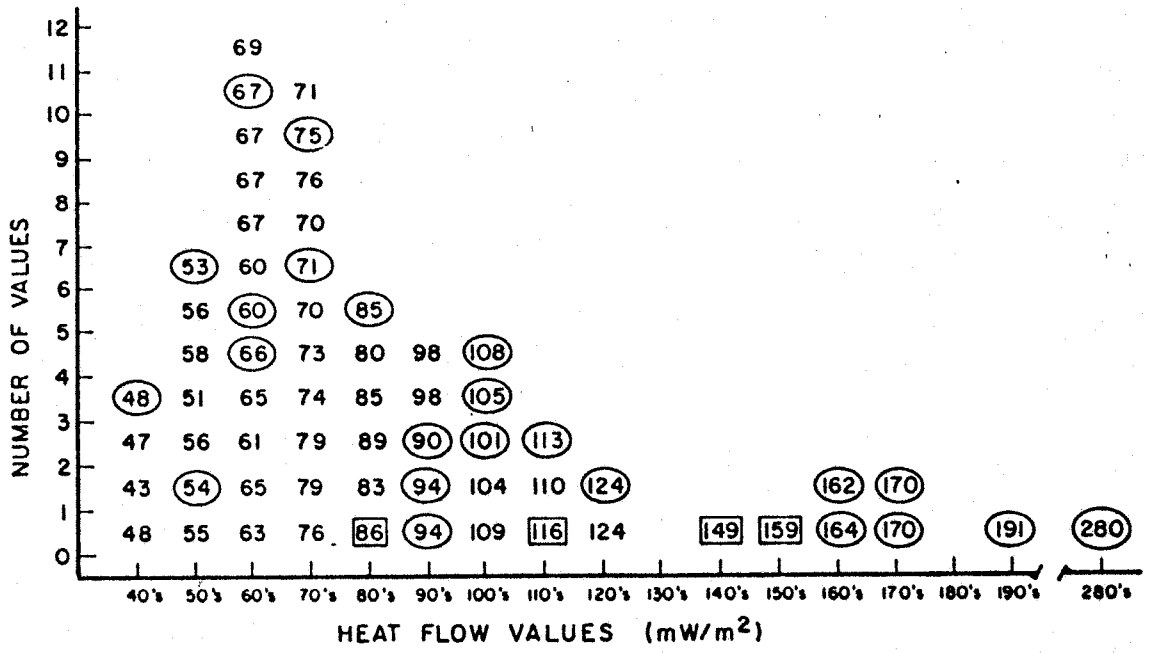

Figure 16. Histogram of heat-flow values in the study area. Circled heat-flow values are located within 5 km of inferred basement fractures (see Figure 15). Heat-flow values in squares are located within 5 km of an extension of basement fracture. 17 of the 23 values $\geq$ 90 mW/m2 (74%) and 10 of the 40 values < 90 mW/m2 (25%) are located within 5 km of an inferred basement fracture. Excluding the data within 5 km of the southernmost inferred fracture zone, 10 of the 16 values $\geq$ 90 mW/m2 (63%) and 6 of the 36 values < 90 mW/m2 (17%) are located within 5 km of an inferred basement fracture zone. Excluding the southernmost fracture zone but including all of the data in the study area (Figure 15), 10 of 23 of the values $\geq$ 90 mW/m2 (43%) and 6 of the 40 values < 90 mW/m2 (15%) are located within 5 km of an inferred basement fracture.

CONCLUSIONS

New heat-flow data on the southern periphery of the Colorado Plateau demonstrate considerable spatial variability which is not related to recent volcanism in a straightforward manner. Sites with relatively high heat flow (>90 mWm2) are located within the Jemez zone, where new K-Ar dates suggest volcanic activity during Pliocene and Pleistocene time. High heat-flow sites are also present outside the Jemez zone away from recent volcanism. Similarly, sites with low to intermediate heat flow (<70 mW/m2) are located both in proximity to, and away from, areas of recent volcanic activity. Results of heat conduction analyses, which have been applied to the heat-flow data, suggest the presence of relatively recent (<1 Ma), shallow intrusions. The heat-flow data are, however, relatively shallow and thus may be perturbed by ground-water movement within and beneath the zone of heat-flow measurement. Corrections which account for heat transport by vertical water movement within the zone of heat-flow measurement indicate that the magnitude of ground-water advection of heat may be considerable.

Coal maturation data indicate relatively small spatial variations in thermal history which may result from differences in coal burial histories across the study area. The slightly increased level of coal maturation observed

in the Salt Lake coal field (along the Jemez lineament) would be anticipated from small intrusions, however, any maturation modeling would be sensitive to a number of other parameters and would therefore be most ambiguous. The observed level of regional maturation may be predicted by thermal models which assume a steady-state heat flow similar to that reported for the interior Colorado Plateau (< 65 mW/m2) if the average coal burial depth is between 1 and 2 km. Shallower coal burial history models (about 1 km) require somewhat greater heat flows (67 to 75 mW/m2) to predict coal maturation levels.

Two general hypotheses have been proposed to describe the tectonic evolution of the southeastern boundary of the Colorado Plateau. One hypothesis suggests that the geophysical boundary of the Plateau is migrating toward the Plateau interior as a result of crustal/lithospheric thinning, for example as is thought to be occurring along the northwestern Plateau boundary. Another hypothesis, however, suggests that much of the volcanic activity along the southeastern Plateau boundary reflects the presence of a pre-existing zone of weakness in the lithosphere, the Jemez lineament, which has leaked magma to the surface. Several observations derived from this study tend to favor the latter hypothesis. First, profound regional trends in heat flow are not observed in the study area (although deeper heat-flow data are surely needed). The data present a

heat-flow pattern consisting of local anomalies of relatively high heat flow superimposed on a regional low to intermediate heat-flow setting, rather than a gradual increase of heat flow from the Plateau interior across the transition zone to the Rio Grande rift/Basin and Range Province. Sites with relatively high heat flow located towards the Plateau interior and away from recent volcanic activity may reflect magma intrusion and/or ground-water movement along crustal zones of weakness associated with Laramide deformation (monoclines). Second, the lack of profound regional trends in coal maturation across the study area suggests that any post-Cretaceous thermal events which may be associated with the southern Plateau boundary or Jemez lineament have been initiated relatively recently and/or are occurring at relatively great depths; or the thermal events are in the form of relatively small, widely spaced intrusions.

APPENDIX I

HEAT FLOW

Despite its small magnitude at the earth's surface, terrestrial heat flow is an important reflection of the various tectonic phenomena in the earth. Many geologic processes such as mountain building and volcanism, as well as the distribution of mineral and energy resources, are directly related to geothermal processes which operate within and below the earth's crust. The consideration of terrestrial heat-flow is necessary to obtain a better understanding of thermal phenomena in the earth's interior. Heat-flow measurements are made by obtaining the product of the temperature gradient and the appropriate rock thermal conductivity. Since they are obtained in the very uppermost portion of the earth's crust, heat-flow data are essentially boundary values, and as such will relate to the thermal processes operating within and below the earth's crust.

The flow of heat per unit time per unit area at a point in a medium is proportional to the temperature gradient at that point. This basic relation for conductive heat transport is Fourier's Law which in one dimension is of the form

$$Q = -K \, (dT/dx) \qquad (I-1)$$

where Q is the heat flow per unit time per unit area at a point in a medium of thermal conductivity K due to a temperature gradient dT/dx. Thus a heat-flow value represents the determination of two separate quantities, the temperature gradient and the thermal conductivity. Processes which affect the thermal conductivity or the temperature gradient therefore affect the heat-flow determination. Some of these processes and their associated effects are discussed below.

Two separate measurements, the temperature gradient and the corresponding thermal conductivity of the rocks below the surface, are necessary to calculate the heat flow at a particular location. The temperature gradient (the rate of temperature change with depth) is obtained by recording temperatures as a temperature probe is lowered down a drillhole. Due to the high cost of drilling, temperature gradients are usually measured in previously existing wells such as those drilled for petroleum or mineral exploration. The thermal conductivity is measured in the laboratory, ideally on rock samples obtained from the well in which the thermal gradient has been measured. The product of the thermal gradient and the thermal conductivity is the heat flow at a particular location.

Ground-water Perturbations

Most of the heat-flow data presented in this study may

be considered shallow data (temperature gradients measured to < 750 m depth) and as such are more likely to be influenced by near surface heat-flow perturbations than are deeper data. Perhaps the strongest perturbation of heat flow is that which is introduced by ground-water movement (e.g. Donaldson, 1962; Mansure and Reiter, 1979; Majorowicz and Jessop, 1981). It has been suggested that, due primarily to generally decreasing permeability with depth (Magara, 1980), deeper heat-flow data are less likely to be influenced by ground-water movement than are shallow data (Reiter and others, 1979; Reiter and Mansure, 1983). Although shallow data sets generally show greater variance than deep data sets, a number of shallow data may provide a mean value of heat flow which has regional significance and is in reasonable agreement with deep data (Reiter and Mansure, 1983; Chapman and others, 1984).

The transport of heat by ground-water movement has been discussed by Stallman (1963), Philip and De Vries (1957) and De Vries (1958). Bredehoeft and Papadopulos (1965) have presented a method for estimating the rate of steady, vertical ground-water movement from temperature data. This method has been used to estimate vertical ground-water in the vadose and saturated zones (Sorey, 1971; Boyle and Saleem, 1979; Sammis and others, 1982).

Heat-Flow Estimates

Estimates of terrestrial heat flow may also be made by estimating the temperature gradient and the thermal conduc-

tivity at a site (Reiter and Tovar, 1982; Eggleston and Reiter, 1984). Heat-flow estimates are typically based upon temperature gradients estimated from petroleum botton-hole temperature data. Reiter and Tovar (1982) discuss the uncertainties associated with temperature gradient and thermal conductivity estimates. Statistical analyses of heat-flow estimates and measurements indicate that the mean of estimates and the mean of deep measurements in the northern Colorado Plateau are in close agreement. This observation suggests that carefully calculated heat-flow estimates may provide reasonable heat-flow values (Reiter and others, 1985). Two petroleum drillholes are present in the study area and have been used to estimate heat flow (Table 1).

Sedimentation/Erosion Effect

The sedimentary history of the study area since late Cretaceous time consists of periods of deposition, weathering and erosion. Major unconformities occur at the base of the Baca Formation, at the base of the Fence Lake Formation and at the base of the Bidahochi Formation (Campbell, 1981; Chamberlin, 1981; Guilinger, 1982). A thick weathered zone was formed during the Paleocene (Chamberlin, 1981; Guilinger, 1982). Periods of deposition include Eocene (Baca Formation; Cather and Johnson, 1984), early Oligocene (volcaniclastic Spears Formation; Chapin and others, 1978), Miocene (Fence Lake Formation, Guilinger, 1982), and

Pliocene (Bidahochi Formation; Anderson and Frost, 1982). Pliocene-Pleistocene volcanic rocks are also found in the study area (Bradbury, 1966; Laughlin and others, 1979; Callender and others, 1983).

The processes of sedimentation and erosion can disturb the near-surface temperatures in the earth's crust. The subsurface temperatures in an area undergoing sedimentation or erosion may be calculated by solving the one-dimensional, transient diffusion equation for a radioactive, semi-infinite solid which moves along the x axis at velocity U. Given an initial temperature distribution Vo+ax with the surface x=0 being maintained at temperature V1+bt for time t>0, Carslaw and Jaeger (1959, p. 388) show that the solution is

$$
\begin{aligned}
v = {} & V_o + ax + (kAt/K) - aUt + \\
& + \frac{1}{2}(V_1 - V_o)\left\{\operatorname{erf}\frac{x - Ut}{2(kt)^{1/2}} + e^{Ux/k}\operatorname{erfc}\frac{x + Ut}{2(kt)^{1/2}}\right\} + \\
& + \frac{1}{2U}\left(b + aU - \frac{kA}{K}\right)\left\{(x + Ut)e^{Ux/k}\operatorname{erfc}\frac{x + Ut}{2(kt)^{1/2}} + (Ut - x)\operatorname{erfc}\frac{x - Ut}{2(kt)^{1/2}}\right\}
\end{aligned}
\qquad (I-2)
$$

where A is the heat generated per unit time per unit volume of the material by radioactive processes, k and K are the thermal diffusivity and the thermal conductivity, respectively, of the material, and erfc is the complementary error function. U>0 is the sedimentation rate; U<0 corresponds to the rate of erosion.

Although the Cenozoic sedimentation/erosion history in the study area is complex, the magnitude of the temperature

disturbance caused by sedimentation and erosion may be estimated by using the solution of Carslaw and Jaeger (1959) discussed above. Estimating the sedimentation rate (Table 2 in Reiter and others, 1986) and the erosion rate (Tables 3-1 and 3-2 in Leopold and others, 1964), the disturbance to the temperature gradient by sedimentation and erosion is calculated to be a few percent of the regional temperature gradient. Even a rapid sedimentation rate for a prolonged period of time disturbs the temperature gradient only 2-14 % (Rio Grande rift, Reiter and others, 1986).

Annual/Diurnal Effect

Diurnal and seasonal variation of the ground surface temperature may affect temperatures below the surface. The temperature disturbance due to periodic heating of a semi--infinite half-space presented by Carslaw and Jaeger (1959, p. 65) is

$$v = A \exp(-kx) \cos(wt-kx) \qquad (I-3)$$

where the periodic temperature variation is Acos(wt) at the ground surface x=0, A and f are the amplitude and frequency, respectively, of the surface temperature variation, $w = 2\pi f$, x is depth, k is $w/2K$, and K is the thermal diffusivity of the material. In a material with thermal diffusivity K=0.01 cm2/s the temperature disturbance decreases to 1.0 - 0.1 %

of the amplitude of the surface temperature variation at 15 - 22 m depth respectively. The subsurface temperature disturbance due to diurnal temperature variations decreases much more rapidly with depth than does the annual disturbance since the diurnal variation has a much higher frequency than the annual variation. Most of the temperature measurements have been made at depths greater than 25 m and thus should not be significantly affected by diurnal or annual ground surface temperature variations.

Climate Effect

Birch (1948) estimates the effects of Pleistoce climatic variations upon geothermal gradients. The solution for the effect of surface temperature upon the internal temperature of a semi-infinite conducting solid is combined with schematic paleoclimatic histories in order to estimate the subsurface temperature disturbance. The temperature disturbance v at depth x is given as

$$V = A_1\left[1 - \mathrm{erf}\left(x/\sqrt{4ka_1}\right)\right] + A_2\left[\mathrm{erf}\left(x/\sqrt{4ka_1}\right) - \mathrm{erf}\left(x/\sqrt{4ka_2}\right)\right] + \ldots. + A_n\left[\mathrm{erf}\left(x/\sqrt{4ka_{n-1}}\right) - \mathrm{erf}\left(x/\sqrt{4kt}\right)\right] \qquad (I\text{-}4)$$

where k is the thermal diffusivity of the uniform medium, Ai is the average constant temperature for the time period ai until ai-1, and erf is the error function (Birch, 1948). The analyses by Birch (1948) suggest that the climatic

correction to the geothermal gradient may never exceed 3 °C/km with a still smaller maximum correction more probable.

Clauser (1984) presents results of calculation of climatic corrections for non-periodic surface temperature variations with average periods intermediate between those associated with ice ages and that of annual variation. The algorithm presented by Clauser (1984) obtains a solution by means of the Laplace transform, the surface thermal history fo the last several hundred years, and a numerical Fourier transformation. The temperature gradient disturbance decreases exponentially with depth to less than 3°C/km at about 50-70 m depth and to less than 0.3°C/km by 100 m depth.

Topography Effect

In the absence of topography and convective heat-transfer processes, the conductive thermal regime is essentially one-dimensional, i.e. the isotherms are horizontal planes. Topography, however, may warp the isotherms into three--dimensional surfaces. This lateral variation of temperature at depth is caused in part by the three-dimensional geometry of a thermal boundary (the ground surface) and in part by the decrease of air temperature with increased elevation (the atmospheric temperature gradient). Analyses of the effect of topography on subsurface temperatures are presented by Lees (1910), Jeffreys (1938) and Birch (1950). The subsurface isotherms generally parallel the topography near

the surface becoming horizontal planes at greater depths.

Due to irregular topography and lateral variation of thermal conductivity, the three-dimensional mathematical treatment of the topographic disturbance of subsurface temperatures may become exceedingly complex. A simplified, two-dimensional analysis may provide a reasonable model for features such as mountain ranges. Lees (1910) obtains the following solution for the two-dimensional diffusion equation with radiogenic heat production for an infinitely long mountain range symmetric about the z axis with z=0 at the foot of the range:

$$V = V_o + gz - \frac{wz^2}{2k} + A\,\frac{z + a}{x^2 + (z + a)^2} \qquad \text{(I-5)}$$

where v is the temperature at depth z, Vo is the surface temperature at the foot of the range, K is the thermal conductivity of the material and A is the heat generated per unit time per unit volume of material due to radioactive processes. A and a are constants determined from the atmospheric temperature gradient and the dimensions of the mountain range. The temperature disturbance is greatest at the crest of the mountain range and decreases both with depth and with horizontal distance from the center of the mountain range.

The topography in the study area is typically gentle.

Lees' (1910) model has been used to estimate the possible topographic effect on temperature gradients in the southern part of the study area, specifically, in the area of Santa Rita Mesa and Largo Creek. The areal extent of Santa Rita Mesa lends itself to a two-dimensional approximation while the relief between Santa Rita Mesa and Largo Creek suggests that the greatest topographic temperature disturbance in the region would be likely to occur at the edge of the mesa. The calculations show that a gradient measured at the edge of the mesa would be lowered by approximately 10% of the regional gradient while a gradient measured near the foot of the mesa would be lowered by about 1 % due to topographic effects. Since the maximum topographic effect is small and the topographic effect rapidly decreases away from the mesa edge, the disturbance of temperature gradients by topography is considered to be negligible, < 1 % because none of the data are located near the edge of the mesa.

Thermal Conductivity Anisotropy and Refraction Effects

Anisotropy may occur at the microscopic scale due to mineral orientation, at a regional scale due to layering of sedimentary formations of unequal thermal conductivity, and at an intermediate scale due to laminae within the rock which are usually related to the attitude of the bedding planes. The anisotropy in thermal conductivity for many rocks is only 10 or 20 % (Sass and others, 1971) however some rocks, such as shales, may demonstrate considerable

anisotropy (up to 40%, Reiter and Mansure, 1983).

In many cases rock core from drillholes are not available for thermal conductivity measurement but rather the measurement of thermal conductivity must be made on drill cuttings, small irregularly-shaped fragments recovered from the circulating drilling fluid. The measurement technique for fragment samples is discussed below (Sass and others, 1971). Reiter and Mansure (1983) consider the effect that ansisotropy within the rock fragments has on the thermal conductivity when measured using the fragment technique described by Sass and others (1971). In addition, Reiter and Mansure (1983) present a method for determining an anisotropy correction for fragment measurements. The fragment thermal conductivity is corrected to the value of vertical thermal conductivity (i.e. parallel to the direction of heat flow) which is generally perpendicular to bedding planes (Reiter and Mansure, 1983). Solid core samples oriented horizontally and vertically are usually not available for anisotropy measurement.

On a regional scale the effect of thermal conductivity ansisotropy will vary in magnitude depending upon the complexity of geological structure. In areas with horizontal sedimentary layering the effects of anisotropy will be relatively minor since the flow of heat will be generally perpendicular to the layered structure. However in areas with relatively simple geologic structures, an anticline for example, refraction of heat flow may result due to region-

ally anisotropic thermal conductivity. Reiter (1969) presents several examples of the effect anisotropy and geologic structure may have upon the geotherm.

Thermal Conductivity

Thermal conductivity may be determined from Fourier's Law, a basic relation for conductive heat transport. The one-dimensional form of Fourier's Law of heat conduction is given by equation I-1. Thus the thermal conductivity may be given by

$$K = -Q/(dT/dx) \qquad (I-6)$$

Reiter and Hartman (1971) present a steady-state absolute method for determining the thermal conductivity of a rock specimen by measuring Q and dT/dx in equation (I-6). A known flux of heat is put in contact with the specimen and the resulting temperature gradient across the specimen is determined with thermocouples (Figure I-1). Insulation surrounding the heater and specimen creates an essentially one-dimensional thermal regime in which heat flows downward through the specimen into the heat sink, i.e. the aluminum block. Reiter and Hartman (1971) calculate an absoluted accuracy of $\pm$ 4 % for this technique.

Often the rock samples available for thermal conductivity measurement are not solid core from which whole-rock specimens may be taken but rather are drill cuttings, small

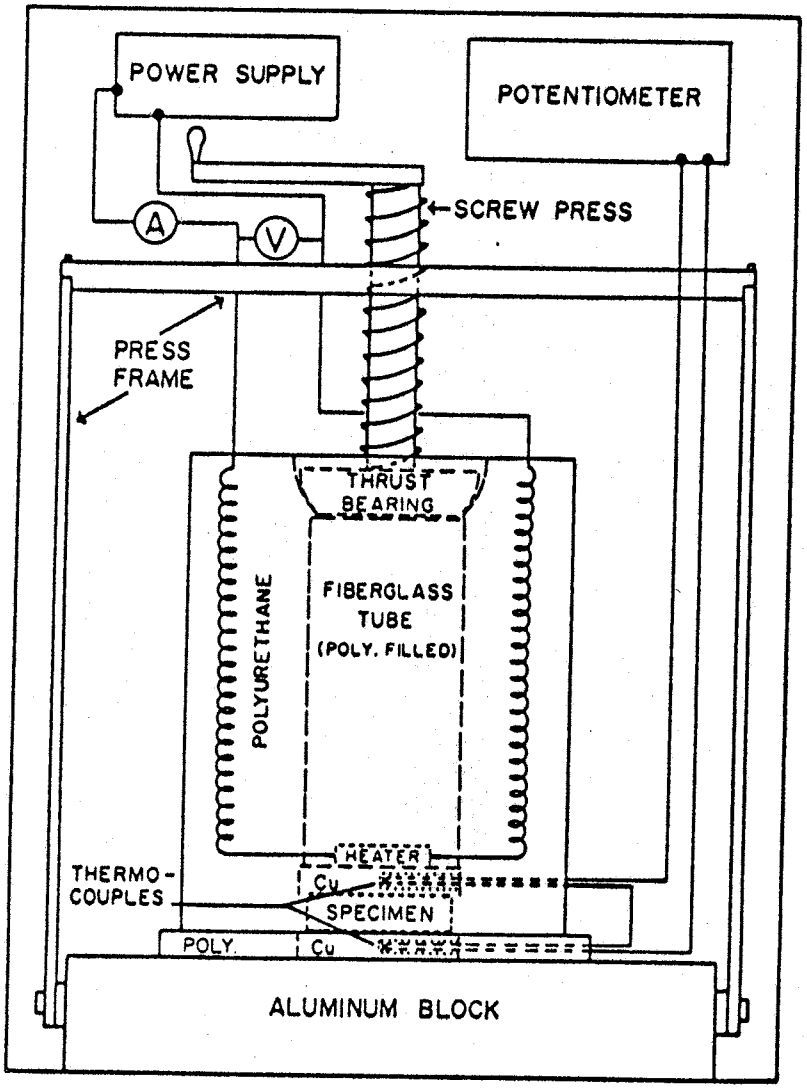

Figure I-1. Schematic diagram illustrating the thermal conductivity measurement apparatus (from Reiter and Hartman, 1971).

irregularly-shaped rock fragments of various sizes. Sass and others (1971) present a technique for estimating whole-rock conductivities from mixtures of rock fragments and water. The procedure consists of packing a plastic cylindrical cell having copper end plates with rock fragments and then vacuum-flooding the cell with distilled water (Figure I-2). The composite thermal conductivity of the plastic cell may be determined following the method of Reiter and Hartman (1971) and, by means of an interpretive model, the mean conductivity of the rock fragments may then be deduced.

Sass and others (1971) model the composite thermal resistance of the plastic cell containing the rock and water aggregate as the thermal resistance of the rock/water aggregate and the plastic cell wall in parallel. Thus, the thermal conductivity of the rock/water aggregate is

$$K_a = \left(\frac{D^2}{d^2}\right) K_c - \left(\frac{D^2-d^2}{d^2}\right) K_p \qquad \text{(I-7)}$$

where Kc is the measured thermal conductivity of the plastic cell containing the rock/water aggregate, Kp is the thermal conductivity of the plastic cell wall, and, D and d are, respectively,

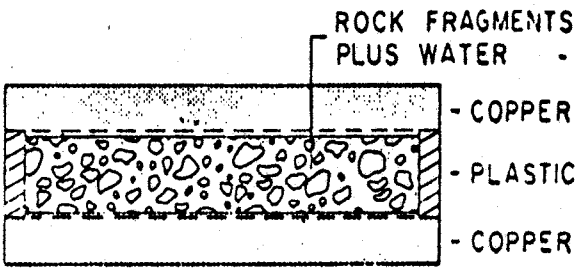

Figure I-2. Diagram of the thermal conductivity cell, side view (from Sass and others, 1971).

the outer and inner diameters of the plastic cell wall. The effective thermal conductivity of the rock/water aggregate may be related to the thermal conductivity of the solid rock, Kr, and the thermal conductivity of the water, Kw, by

$$K_a = K_r^{\,1-\phi} K_w^{\,\phi} \qquad \text{(I-8)}$$

where ϕ is the total volume fraction of water in the packed cell (includes both inter- and intra-fragment porosity; Woodside and Messmer, 1961). Substitution of equation I-8 into I-7 yields the solid rock thermal conductivity

$$K_r = K_w \left(\frac{D^2}{d^2} \frac{K_c}{K_w} - \frac{D^2-d^2}{d^2} \frac{K_p}{K_w} \right) \frac{1}{1-\phi} \qquad \text{(I-9)}$$

The in-situ thermal conductivity (i.e. the thermal conductivity of the rock with in-situ porosity ϕ_o of the porous rock Kpr may be related to the solid rock (negligble porosity) thermal conductivity by

$$K_{pr} = K_w^{\,\phi_o} K_r^{\,1-\phi_o} \qquad \text{(I-10)}$$

which, when combined with equation I-9, yields

$$K_{pr} = K_w\left(\frac{D^2}{d^2}\frac{K_c}{K_w} - \frac{D^2-d^2}{d^2}\frac{K_p}{K_w}\right)\left(\frac{1-\phi_o}{1-\phi}\right) \quad \text{(I-11)}$$

The in-situ porosity of the porous rock may be determined from density logs or density bottle measurement.

Thermal conductivity measurements are made in the laboratory at about 20°C under a pressure not greater than about 1 MPa; however, in this study the rocks may experience in-situ temperatures and pressures ranging from 15 to 25°C and 1 to 10 MPa, with both temperature and pressure increasing with depth. Thermal conductivity decreases about 0.2% per °C increase in temperature but increases about 0.1 % per MPa increase in pressure (sandstone, Clark, 1966). Errors between in-situ thermal conductivity and that measured in the lab due to opposing temperature and pressure effects are estimated to be about 1 %. This is less than the reproducibility of measurements which would be about $\pm$ 4 % (Reiter and Hartman, 1971).

Temperature Gradient

The temperature gradient is obtained by measuring temperature at many depths in a borehole. Measurements are made by lowering a thermistor (a resistor, the resistance of which varies with temperature in a known manner) down the borehole, stopping at depth and measuring the thermistor equilibrium resistance with a Mueller bridge, a type of Wheatstone bridge. Although of low resistivity, the

conductors leading from the bridge down the borehole to the thermistor may, due to their long length, act as additional resistors in series in two arms of the Wheatstone bridge. The Mueller bridge essentially allows these conductors to be interchanged and thus cancel potential systematic errors that might be introduced by conductors of unequal resistance as would be the case in a standard Wheatstone bridge (Roy and others, 1968). The measured resistances are then converted to temperature by means of tables provided by the thermistor manufacturer (e.g., Fenwal, 1978).

Errors in the measured temperature gradient may be due to the measuring equipment or due to the temperature disturbance associated with drilling. Errors due to the measuring equipment include such factors as stretching of the cable which carries the conductors and thermistor down the borehole, and inaccuracies of the thermistor probe and Mueller bridge. Shearer (1979) reports that errors of < 1 % are introduced by inaccuracies of the electrical equipment while stretching of the conductor cable introduces a systematic error of < 3 %.

The temperature disturbance induced by the circulation of fluids in the borehole during drilling may be quite profound, and is a function of rock properties (e.g. porosity and thermal conductivity), fluid properties (e.g.-temperature and pressure), duration of circulation, and time elapsed between cessation of circulation and temperature measurement. Experimental and theoretical studies suggest

that the temperature disturbance due to drilling decays exponentially with time and is negligible after a time which is a function of the parameters listed above (about 10 to 20 times the total drilling time; Lachenbruch and Brewer, 1959; Jaeger, 1961; Reiter and Tovar, 1982; Drury, 1984).

APPENDIX II

COAL MATURATION

The formation of coal begins with the deposition of organic material in peat-forming swamps which may be found in a wide range of sedimentary environments. Controls on peat formation and coal deposition as well as depositional models of coal bearing sequences are discussed by Ward (1984). The primary constituents of coal (an almost entirely organic substance) are called macerals and are analogous to minerals in rocks (Van Krevelen, 1961). Vitrinite, coalified woody tissues derived from stems, roots and vascular tissues of leaves, is a maceral of coal which in many cases comprises more than 70-80 % of any given coal bed or coal seam (Ting, 1982).

In proximate analysis, the amounts of moisture, volatile matter, ash and fixed carbon in a coal sample are measured. Moisture and volatile matter contents are determined by weight loss after heating the sample at specified temperatures and times; the ash content represents the inorganic material left behind when all the combustible substances have been burned off (Berkowitz, 1979). The fixed carbon content is indirectly determined as the difference between 100 % and the sum of the percentage moisture, volatile matter and ash contents (normalized

by the weight of the sample; Berkowitz, 1979).

Thermal maturation occurs during burial and heating of organic material. Continued heating of organic material increases coal rank and, in some cases, may generate oil and gas (Waples, 1981). As coal rank (thermal maturity) increases there is a progressive decrease in volatile matter and moisture content and a corresponding increase in the fixed carbon content (Ting, 1982).

There are several characteristics of hydrocarbons which may be used as indicators of thermal maturation. For example, vitrinite reflectance is an optical characteristic of coal which is often used as a thermal maturation indicator. Vitrinite reflectance is the only maturity measurement which increases in a rather uniform manner (exponentially) with thermal maturity and is not affected by kerogen composition. In addition, vitrinite reflectance may be used over the entire coal rank range from lignite to anthracite (Dow, 1977; Heroux and others, 1979).

Vitrinite reflectance is usually measured with a reflecting light microscope photometer which is calibrated with glass standards (Ward, 1984). The measurement procedure consists of measuring, with a microscope photometer, the percentage of light of a specified frequency that is reflected by vitrinite particles in a polished coal sample. The vitrinite reflectance measurement is calibrated by comparison with the amount of light reflected by a glass standard of known reflectance. The vitrinite reflectance

reported for a sample is the average of measurements made on 100 or more vitrinite particles in that sample (Ting, 1982). The accuracy of the sample measurement depends on the number of individual particle measurements per sample. The standard deviation of the mean of 100 individual measurements made on a sample is about 0.02% vitrinite reflectance (Stach and others, 1975); vitrinite reflectance values for most coals range from 0.2 to 2.5 % (Ting, 1982). A detailed discussion of vitrinite reflectance measurement is given by Stach and others (1975).

With increasing thermal maturation coal becomes more aromatic (in aromatic hydrocarbons the carbon atoms are connected in a planar ring structure, Brown and Lemay, 1977) which gives rise to increased reflectivity; the fixed carbon content of coal also increases with thermal maturation (Ting, 1982). The variation of vitrinite reflectance with rank (dry, ash-free fixed carbon content), based upon a large number of measurements, defines a characteristic curve (Stach and others, 1975; Berkowitz, 1979). The correlation between vitrinite reflectance and fixed carbon content is useful in that it allows proximate analysis data, which are much more common than vitrinite reflectance data, to be used in coal maturation studies.

Waples (1980, 1981) discusses the theory and application of Lopatin's method to coal maturation studies. Lopatin's Time-Temperature Index of thermal maturity (TTI) method is based upon chemical reaction rate theory which

states that the temperature dependence of maturity is exponential and that the time dependence of thermal maturity is linear. The time-temperature index of maturity is

$$TTI = \sum_{n} r^{n} \Delta t_{n} \qquad \text{(II-1)}$$

where Δt_n is the time (in m.y.) spent by the sediment in the nth 10°C temperature interval. In equation II-1 the parameter r is taken to be 2.0 which yields good empirical results and is supported by the Arrhenius equation which states that chemical reaction rates approximately double for every 10 °C increase in temperature. The resultant time--temperature index of maturation has been correlated to vitrinite reflectance (Waples, 1980, 1981). Clarkson (1984) also discusses the TTI method and presents a modified TTI method which uses numerical methods to integrate over complex temperature histories

$$TTI = \int 2^{[T(^{\circ}C)-105]/10}\, dt \qquad \text{(II-2)}$$

where T(°C) is the temperature of the coal at time t.

APPENDIX III

THERMAL CONDUCTIVITY AND TEMPERATURE DATA

The thermal conductivity and temperature data used to obtain heat-flow measurements and estimates in this study are presented in this appendix. The data presented for each well include:

1. well name
2. location - North latitude and West longitude in decimal degrees
3. depth to water, if known
4. thermal conductivity distribution with depth, measured or estimated whole rock thermal conduct ivity and porosity
5. temperature distribution with depth, tabulated and plotted

The temperature data for wells designated by "Los Alamos No." are from Levitte and Gambill (1980).

Agua Fria 1N-19W-3-2
lat. 34.34
long. 108.82
depth to water: 79-87 m

Thermal Conductivity data

depth interval (feet)	rock type	Kr (W/mK)	porosity
90-100	sh	2.34	.24
110-150	ss	4.40	.24
150-180	sh	2.34	.18
180-200	sh/ss	2.84	.18
200-225	ss	4.40	.24
225-255	sh	2.34	.15
255-261	ss	4.40	.18
261-265	sh	2.34	.12
265-273	ss	4.40	.21
273-280	sh	2.34	.12
280-281	coal	0.36	.03
281-283	sh	2.34	.21
283-284	coal	0.36	.03
284-287	sh	2.34	.12
287-288	coal	0.36	.03
288-290	sh	2.34	.18
290-293	ss	4.40	.21
293-294	coal	0.36	.03
294-357	ss	4.40	.21

Kr - average value
porosity - from density log
coal - Kr and porosity, average of measurements

Temperature Gradient data

depth (m)	temperature (degrees C)
8.78	15.954
10.78	15.118
12.81	14.693
14.86	14.498
16.78	14.343
18.73	14.194
20.73	14.103
22.70	14.049
24.78	13.992
26.70	13.999
28.83	14.018
30.78	14.033
32.78	14.064

date logged: 18 July 1984
tool: 4k ohm

34.88	14.092
36.70	14.170
38.81	14.202
40.75	14.253
42.78	14.328
44.75	14.379
46.83	14.427
48.73	14.509
50.78	14.565
52.73	14.653
54.75	14.705
56.75	14.774
58.78	14.830
60.68	14.883
62.78	14.969
64.70	15.053
66.78	15.143
68.73	15.242
70.86	15.333
72.78	15.387
74.68	15.499
76.75	15.548
78.81	15.433
80.78	15.653
82.78	16.026
84.78	16.120
86.86	16.185

date logged: 18 July 1984
tool: 100k ohm

88.48	16.124
93.44	16.282
98.55	16.578
103.63	16.925
108.64	17.131

AGUA FRIA 1N 19W 3

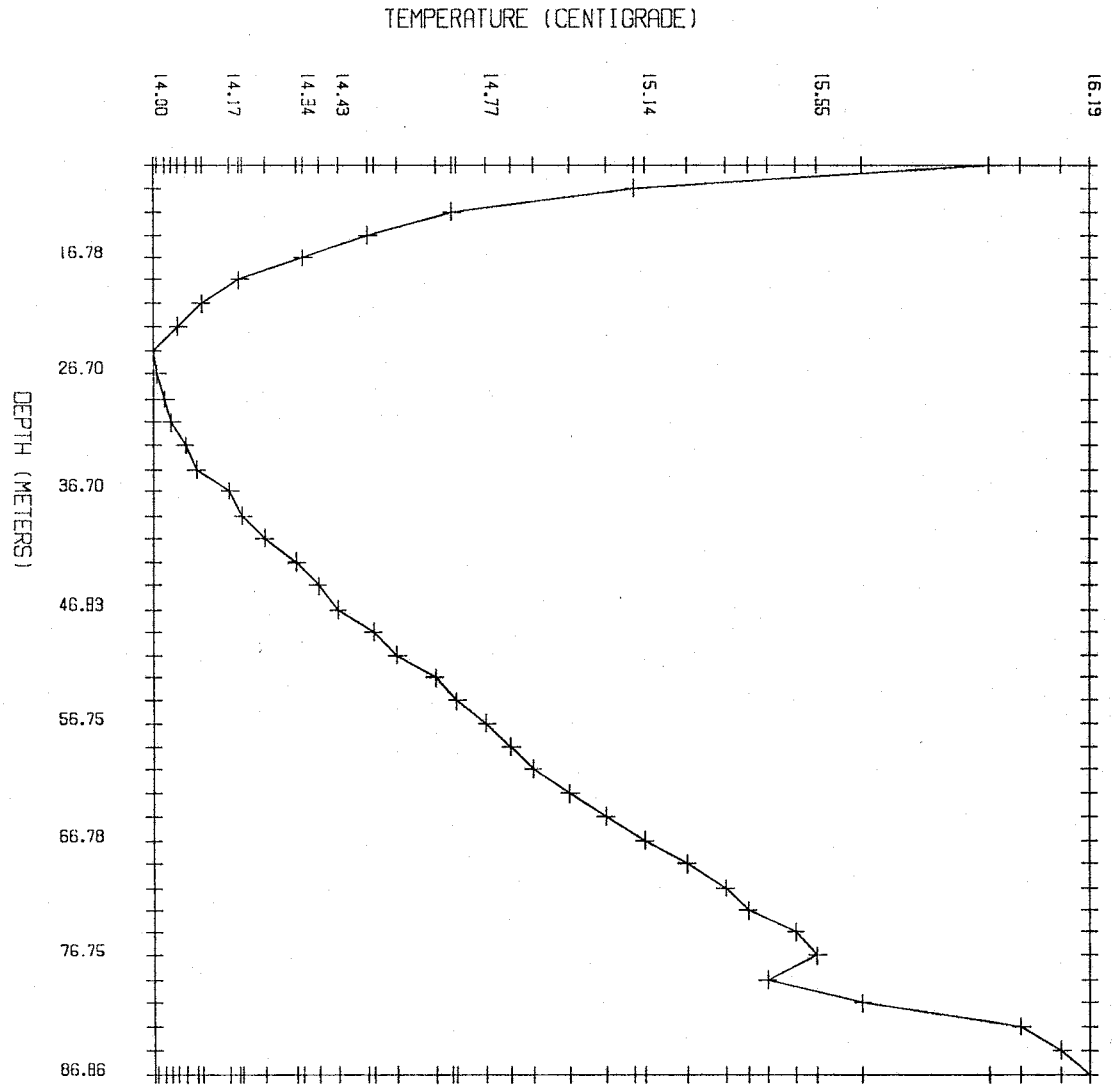

AGUA FRIA 1N 19W 3

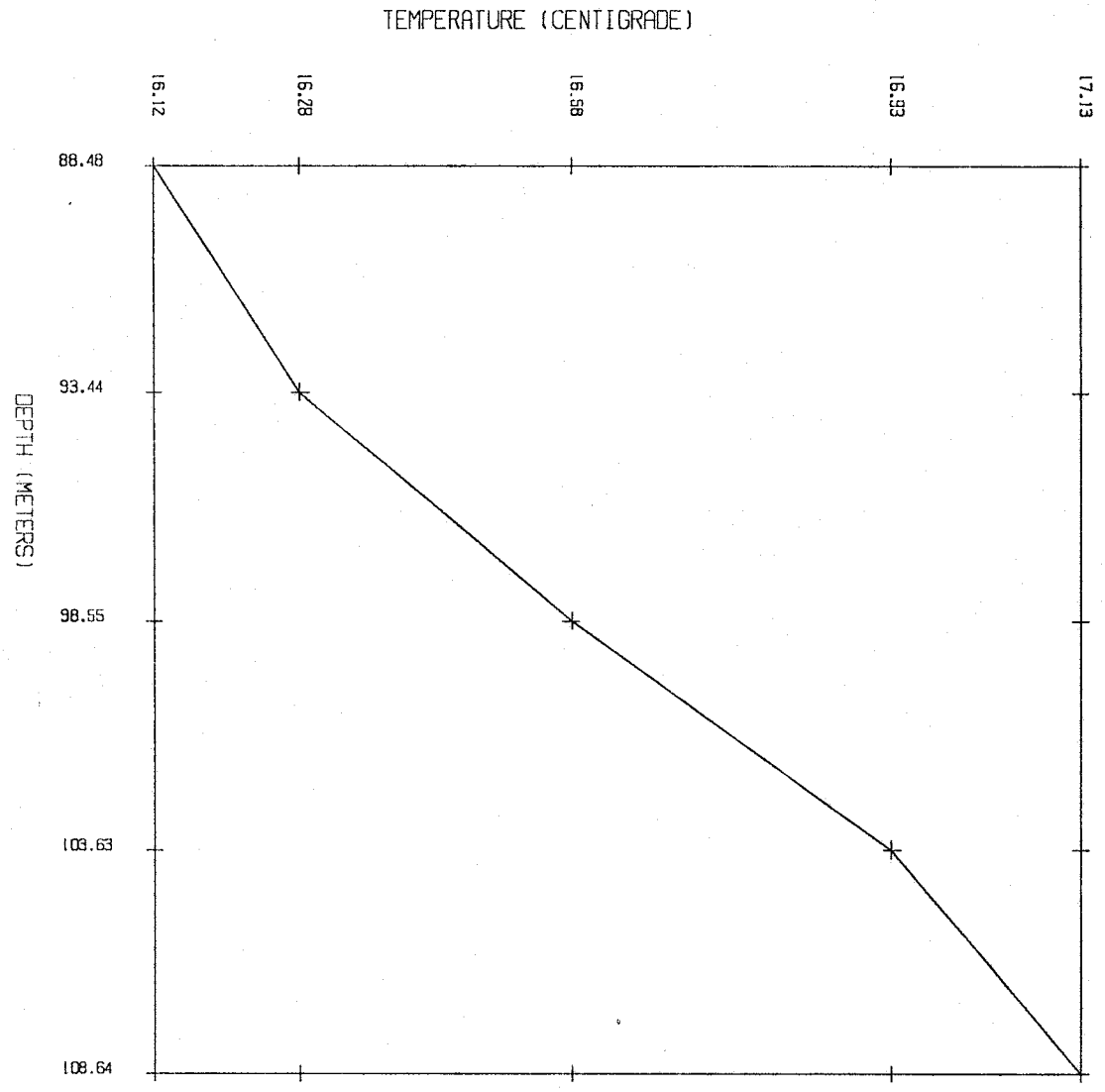

Blaine's Lake 1N-19W-13
lat. 34.31
long. 108.79
depth to water: 351 f

Thermal Conductivity data

depth interval (feet)	rock type	Kr (W/mk)	porosity
30- 40	sh/ss	2.05	.27
40- 53	sh	2.24	.21
53- 75	sh	2.21	.21
75- 95	sh	2.13	.21
95-110	ss	4.04	.21
110-125	ss/sh	2.96	.21
125-139	ss	3.60	.27
139-160	sh	2.15	.21
160-165	sh/ss	2.70	.18
165-178	sh/ss	2.52	.18
178-186	ss	4.56	.24
186-206	sh/ss	3.36	.18
206-230	sh	2.22	.21
230-251	sh	2.59	.18
251-259	sh/ss	2.81	.18
259-278	sh	2.15	.18
278-300	sh	2.10	.18
300-325	sh/ss	3.15	.15
325-351	ss/sh	3.48	.18
351-357	ss/sh	4.58	.24
357-373	sh/ss	2.73	.18
373-384	sh/ss	2.47	.15
384-401	ss	3.59	.24
401-408	sh/ss	2.83	.12
408-424	ss	4.43	.24
424-433	sh/ss	2.13	.15
434-448	sh	2.30	.24
448-485	sh	2.04	.18
485-521	sh	2.23	.15
521-541	sh	2.19	.15
541-576	sh	2.24	.18
576-589	sh	1.92	.24
589-600	sh	2.44	.15
600-619	sh/ss	2.34	.21
619-630	sh/ss	2.33	.21
630-655	sh/ss	3.02	.21

Kr - measured value
porosity - from density log

Temperature Gradient data

depth (m)	temperature (degrees C)

date logged: 10 July 1984
tool: 4k ohm

8.57	12.718
12.55	13.090
16.60	13.292
20.57	13.497
24.60	13.706
28.57	13.891
32.68	14.021
36.65	14.178
40.63	14.304
44.63	14.502
48.65	14.669
52.60	14.847
56.57	14.993
60.68	15.135
64.60	15.412
68.68	15.611
72.60	15.792
76.57	15.950
80.60	16.081
84.60	16.210
88.60	16.493
92.63	16.655
96.60	16.828
100.60	16.970
104.65	17.086
108.60	17.321

date logged: 10 July 1984
tool: 100k ohm

113.58	17.350
118.44	17.449
123.47	17.577
128.68	17.673
133.66	17.855
138.46	18.058
143.51	18.247
148.55	18.498
153.60	18.769
158.63	18.921
163.76	19.134
168.69	19.376
173.66	19.623
178.76	19.861
183.75	20.077
188.72	20.269
193.93	20.436
198.89	20.542

BLAINE'S LAKE 1N 19W 13

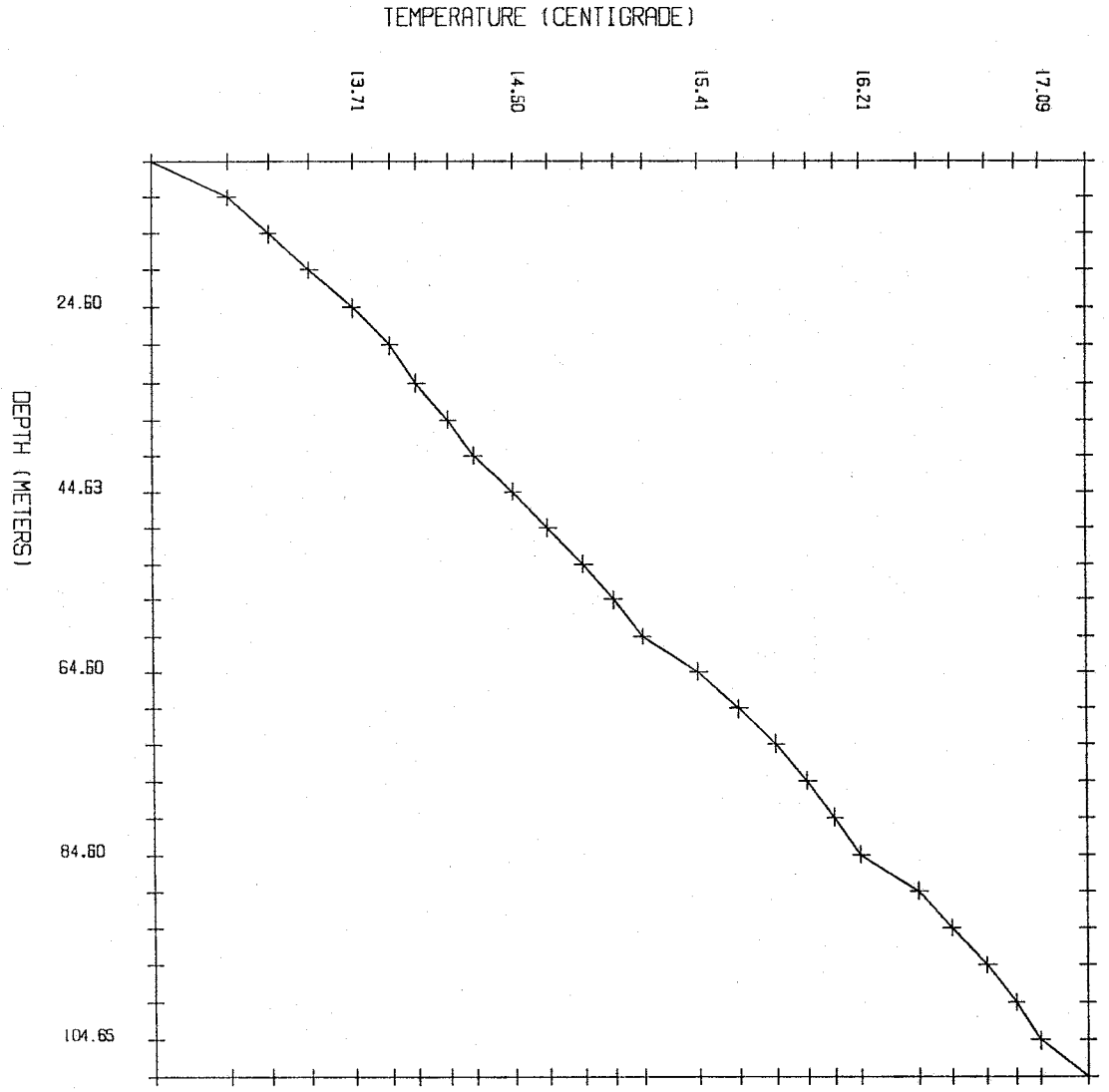

BLAINE'S LAKE IN 19W 13

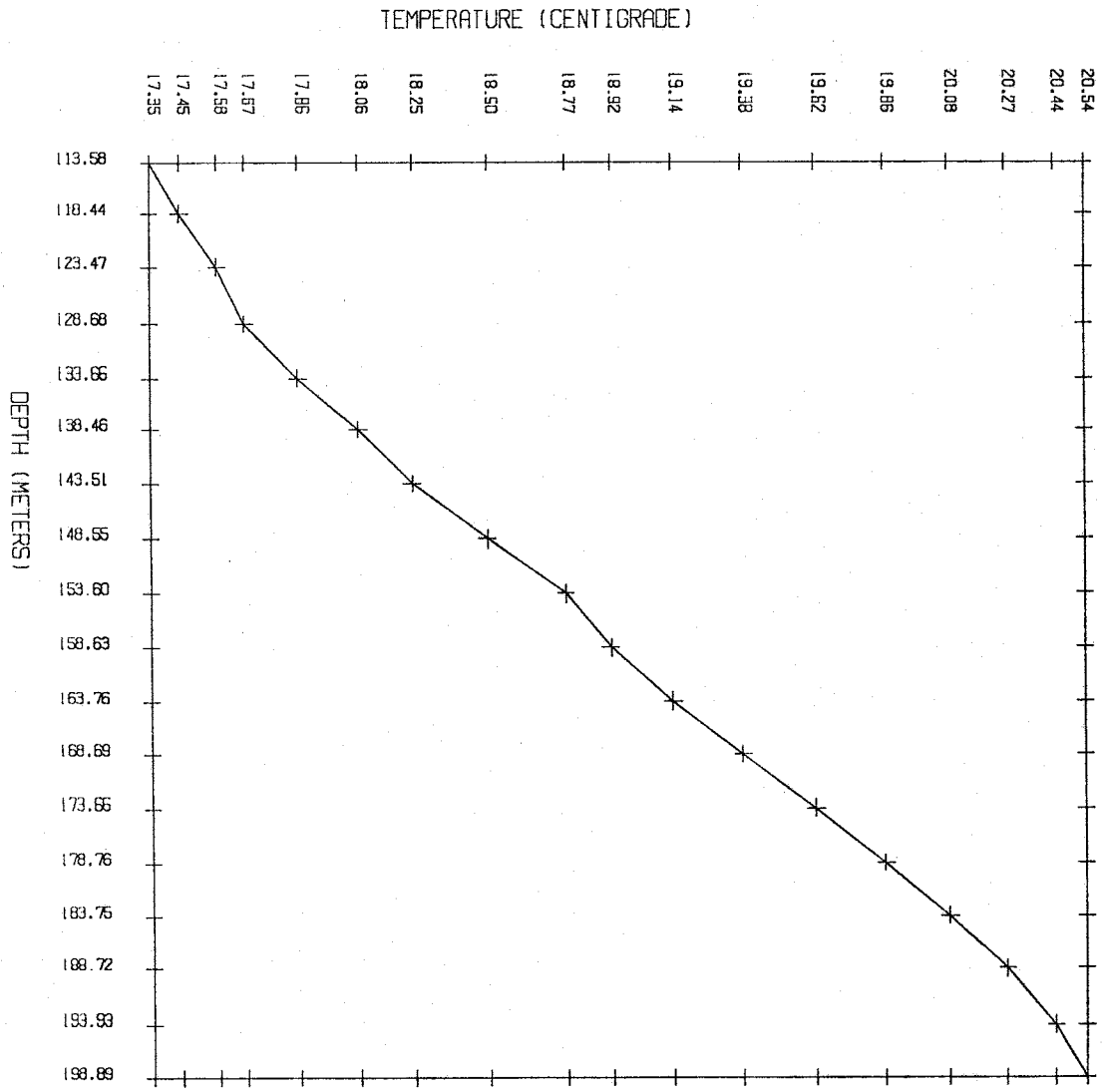

Cabin Spring 5N-18W-28
lat. 34.63
long. 108.73
depth to water: 50-55 m

Thermal Conductivity data

depth interval (feet)	rock type	Kr (W/mK)	porosity
30- 50	sh/ss	2.27	.19
50- 70	sh/ss	2.04	.19
70- 75	sh	2.32	.18
75- 95	sh	2.92	.19
95-100	ss/sh	4.03	.19
100-115	ss/sh	4.03	.19
115-120	sh	2.30	.19
120-135	sh	2.30	.19
135-140	sh	2.46	.18
140-145	sh/ss	2.72	.19
145-155	sh/ss	2.72	.19
155-175	sh	2.91	.18
175-190	sh	3.28	.18
190-210	sh/ss	2.89	.19
215-225	sh/ss	2.56	.19

Kr - measured from < 0.5 mi. ENE of well
porosity - average values

Temperature Gradient data

depth (m)	temperature (degrees C)
8.50	11.604
10.35	11.701
12.45	11.841
14.48	11.957
16.30	12.024
18.37	12.102
20.43	12.184
22.40	12.241
24.27	12.342
26.30	12.450
28.30	12.546
30.35	12.619
32.40	12.670
34.35	12.722
36.43	12.791
38.48	12.846
40.37	12.902

date logged: 19 July 1984
tool: 4k ohm

42.40	12.950
44.43	13.004
46.35	13.097
48.48	13.097

date logged: 19 July 1984
tool: 100k ohm

52.96	13.129
57.83	13.274
62.82	13.502
67.84	13.625

CABIN SPRING 5N 18W 28

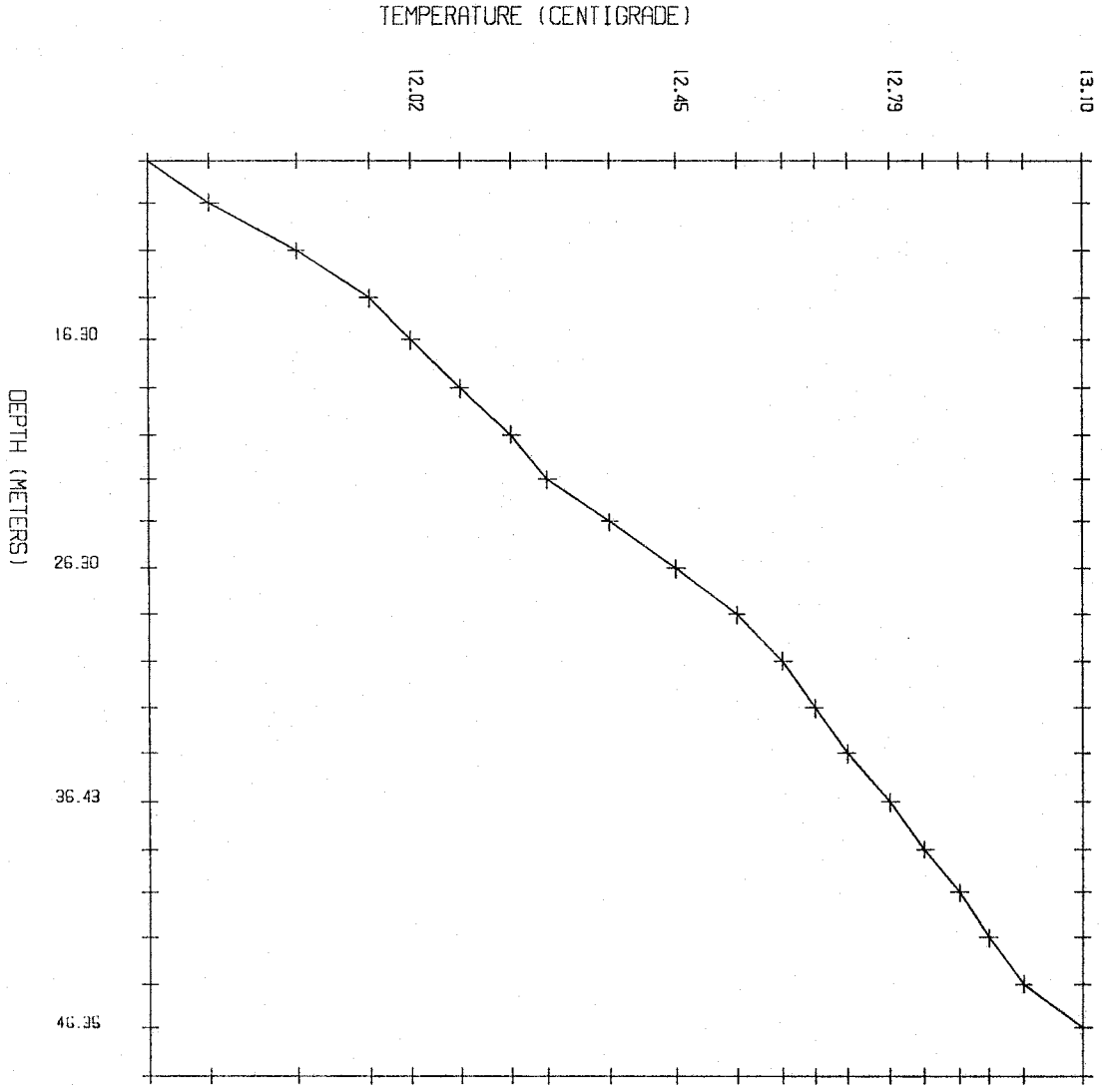

CABIN SPRING 5N 18W 28

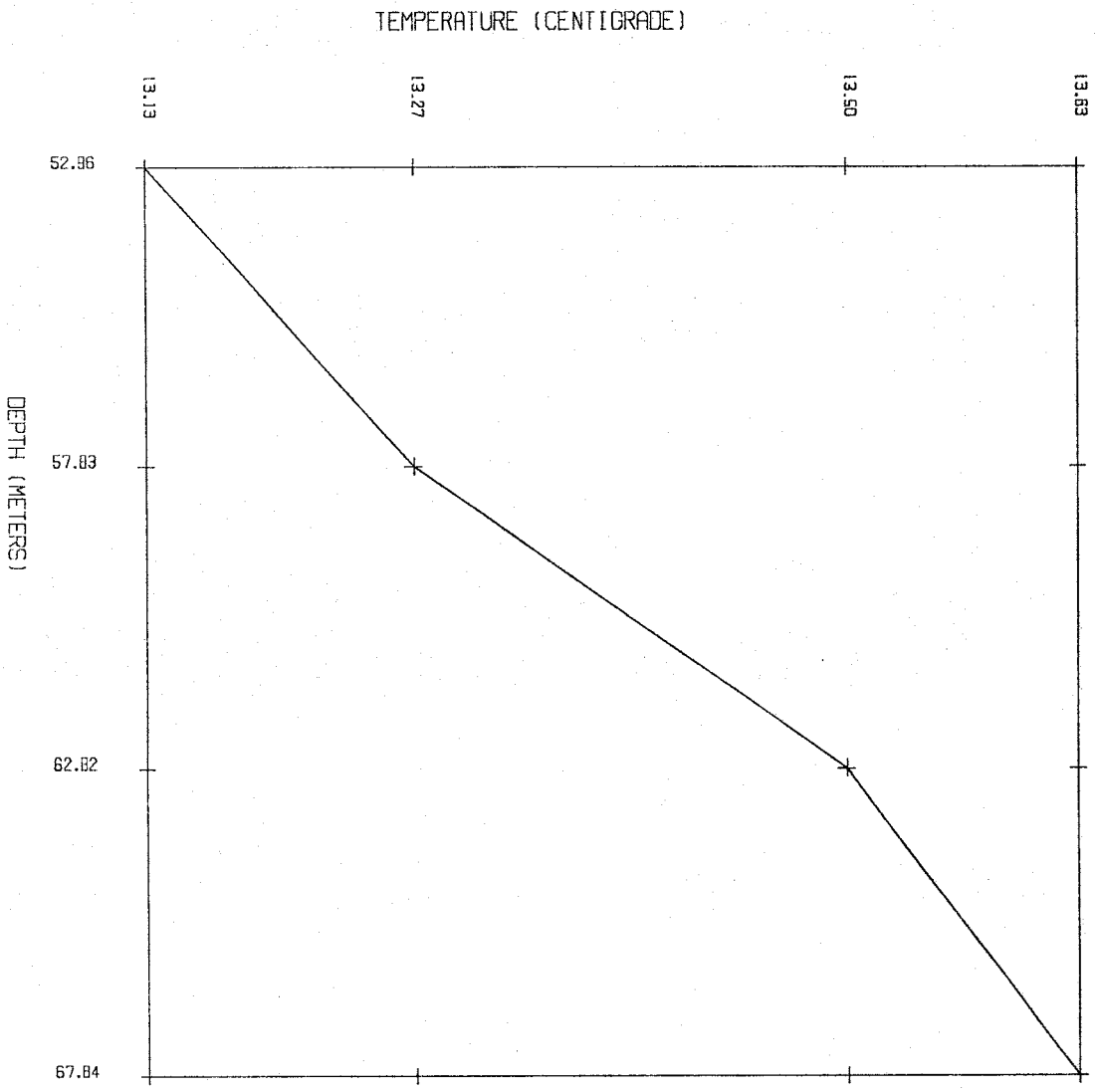

Cerro Prieto 1 4N-17W-23
lat. 34.56
long. 108.59
depth to water: >35 m

Thermal Conductivity data

depth interval (feet)	rock type	Kr (W/mK)	porosity
35- 40	sh	2.56	.17
45- 50	ss	4.37	.13
50- 55	ss	4.23	.19
55- 60	ss	4.30	.19
60- 65	ss	4.71	.19
65- 70	ss	4.54	.21
70- 75	ss	4.52	.21
75- 80	ss	3.77	.13
80- 85	sh	3.31	.11
85- 90	sh/ss	2.46	.09
95-100	sh/ss	3.06	.11
100-105	sh/ss	3.03	.09
110-115	sh/coal	1.89	.09

Kr - measured values
porosity - from density log

Temperature Gradient data

depth (m)	temperature (degrees C)
8.98	12.356
11.00	12.883
12.95	12.883
14.92	12.902
16.95	12.920
18.95	12.924
20.90	12.991
22.98	13.023
24.98	13.071
26.87	13.109
28.95	13.311
30.90	13.322
32.98	13.440
34.95	13.526

date logged: 01 August 1984
tool: 4k ohm

CERRO PRIETO 1 4N 17W 23

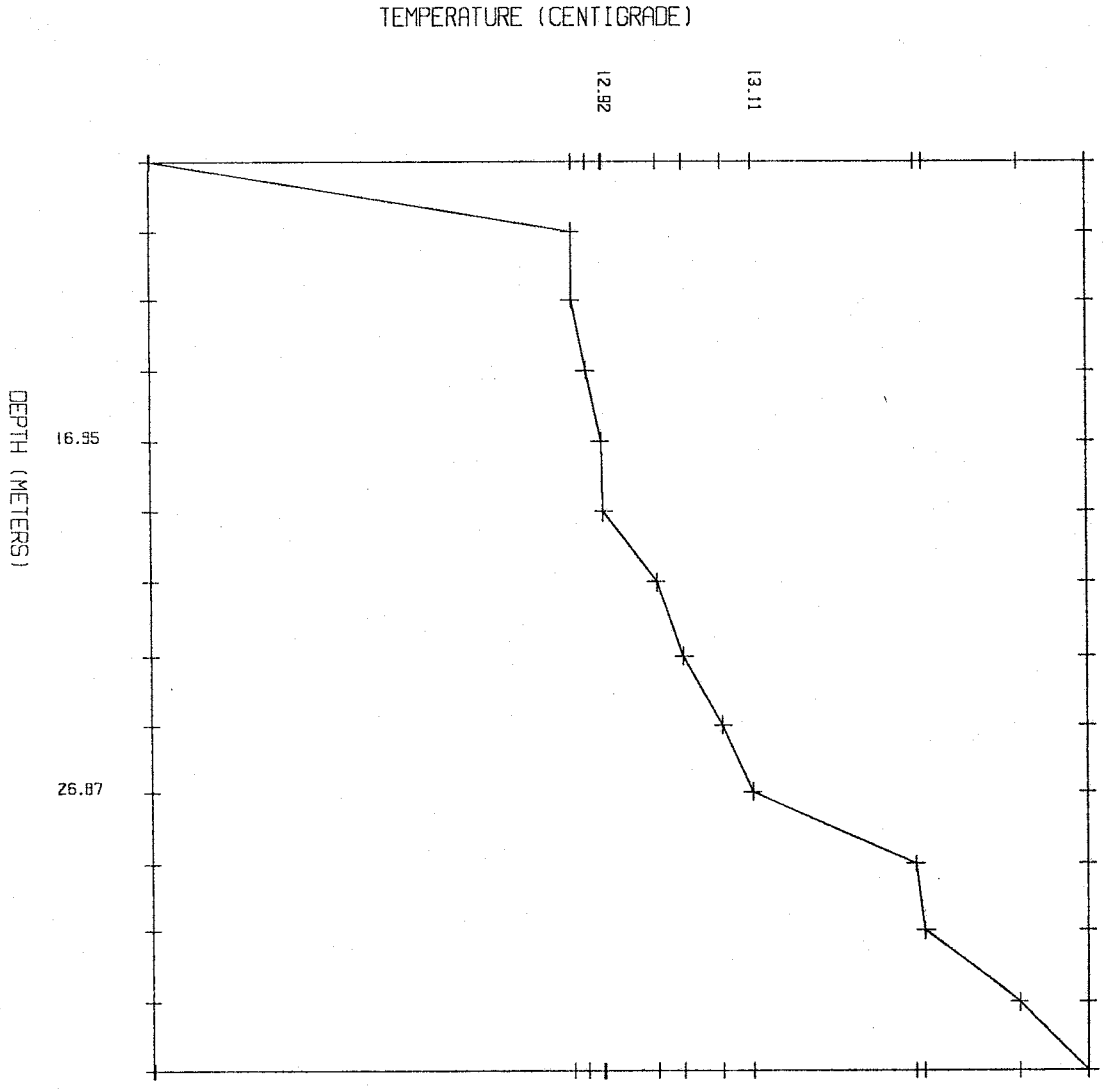

Cerro Prieto 2 4N-17W-14
lat. 34.57
long. 108.59
depth to water: >39 m

Thermal Conductivity data

depth interval (feet)	rock type	Kr (W/mK)	porosity
30- 35	ss	5.23	.23
35- 41	ss/sh	2.75	.19
41- 46	sh/ss	1.89	.19
46- 53	sh/ss	2.43	.19
53- 73	sh/ss	2.60	.19
73- 86	sh/ss	2.72	.19
86- 92	ss	3.72	.23
92-110	sh	2.05	.18
110-115	sh/coal	1.81	.19
115-120	sh/ss	3.12	.19
120-130	sh/ss	2.57	.19

Kr - measured values
porosity - average values

Temperature Gradient data

depth (m)	temperature (degrees C)
date logged: 01 August 1984	
tool: 4k ohm	
9.00	13.281
10.97	13.273
12.97	13.481
14.97	13.583
17.03	13.637
19.00	13.637
20.97	13.633
23.00	13.644
25.00	13.652
26.97	13.690
29.00	13.702
30.92	13.713
32.97	13.732
35.00	13.771
37.00	13.794
38.97	13.844

CERRO PRIETO 2 4N 17W 14

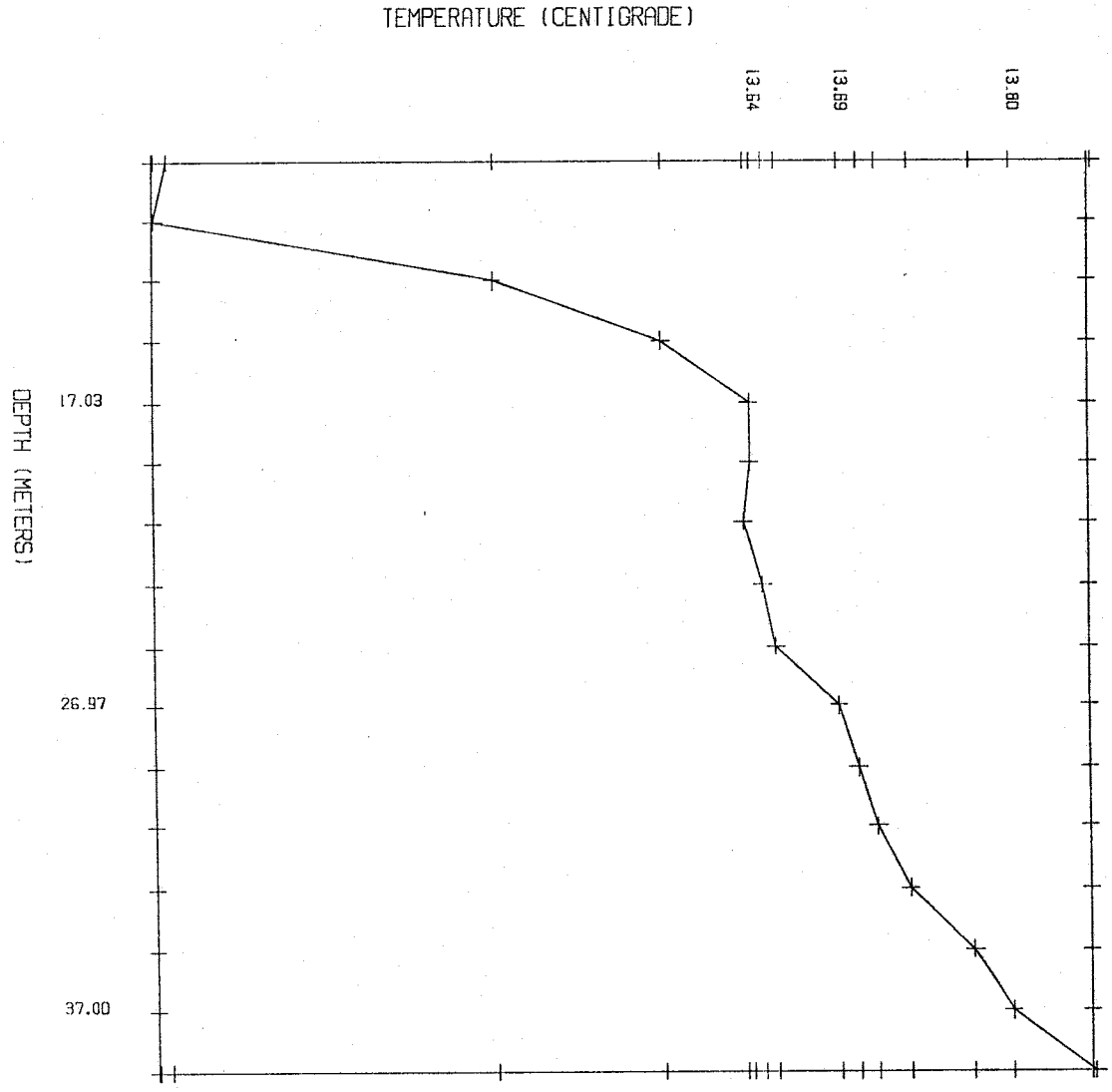

Cimmaron Mesa 1N-19W-8-2
lat. 34.32
long. 108.85
depth to water: 108 f

Thermal Conductivity data

depth interval (feet)	rock type	Kr (W/mK)	porosity
45- 57	ss	3.48	.27
57- 63	sh/ss	2.01	.21
63- 83	sh/ss	2.95	.21
83- 96	ss	6.70	.27
96-108	ss/sh	4.24	.21
108-111	coal	0.37	.03
111-118	sh	2.87	.18
118-129	ss/sh	2.76	.27
129-144	sh	2.12	.15
144-158	sh	2.37	.15
158-170	sh	2.25	.15

Kr - measured
porosity - from density log
coal - Kr and porosity, average of measurements

Temperature Gradient data

depth (m)	temperature (degrees C)
date logged: 16 September 1983	
tool: 4k ohm	
19.85	15.159
29.87	14.758
34.87	14.689
39.92	14.758
44.95	14.899
49.95	15.073
date logged: 06 April 1984	
tool: 4k ohm	
9.00	13.652
11.05	13.648
12.90	13.675
14.85	13.721
16.87	13.779
18.85	13.864
20.90	13.957
22.87	14.037
24.92	14.107
27.00	14.162

28.97	14.202
30.87	14.253
32.87	14.332
34.82	14.455
37.00	14.505
38.80	14.609
40.92	14.665
42.92	14.717
45.03	14.766
47.00	14.855
48.80	14.891
51.00	14.928

CIMMARON MESA 1N 19W 8

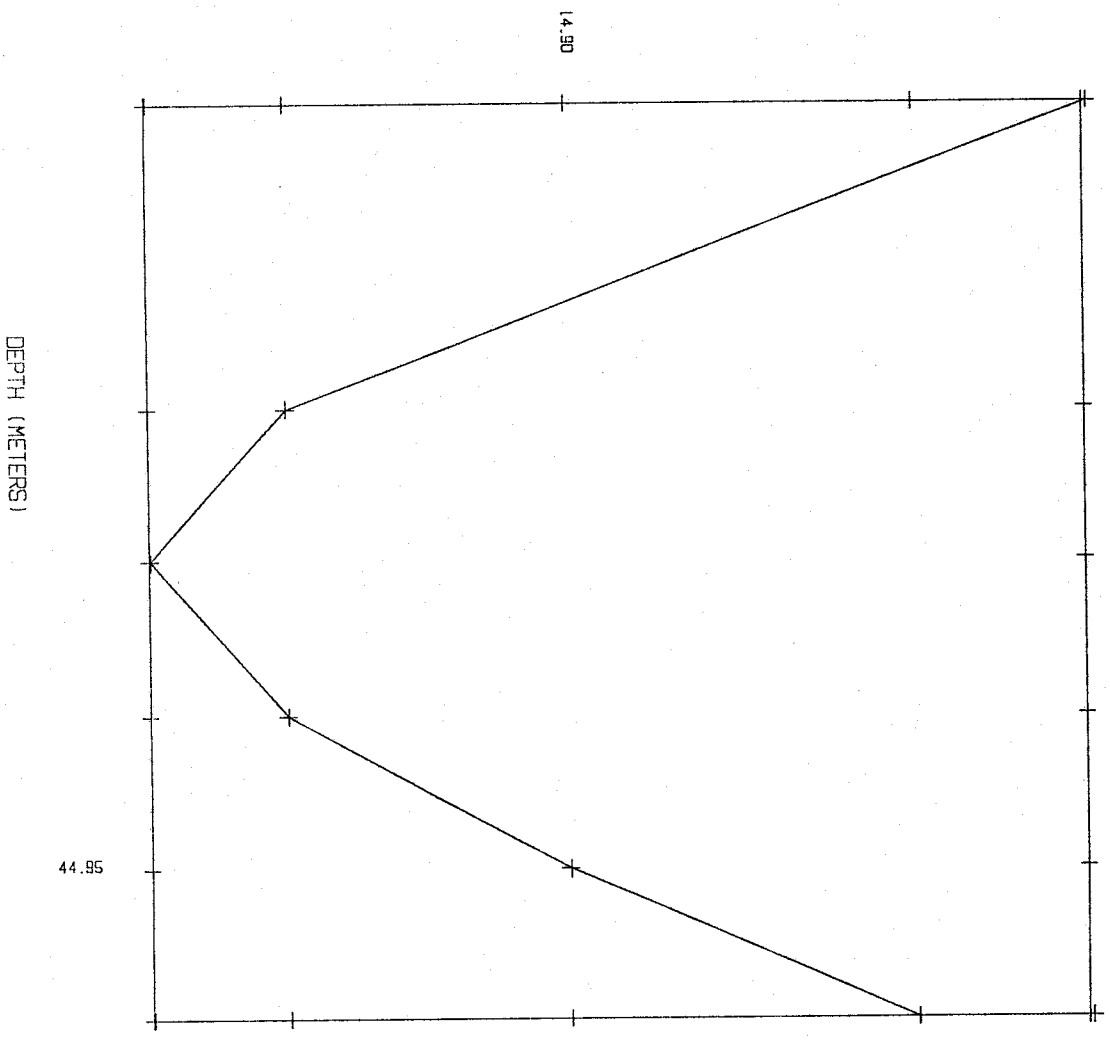

CIMMARON MESA 1N 19W 8

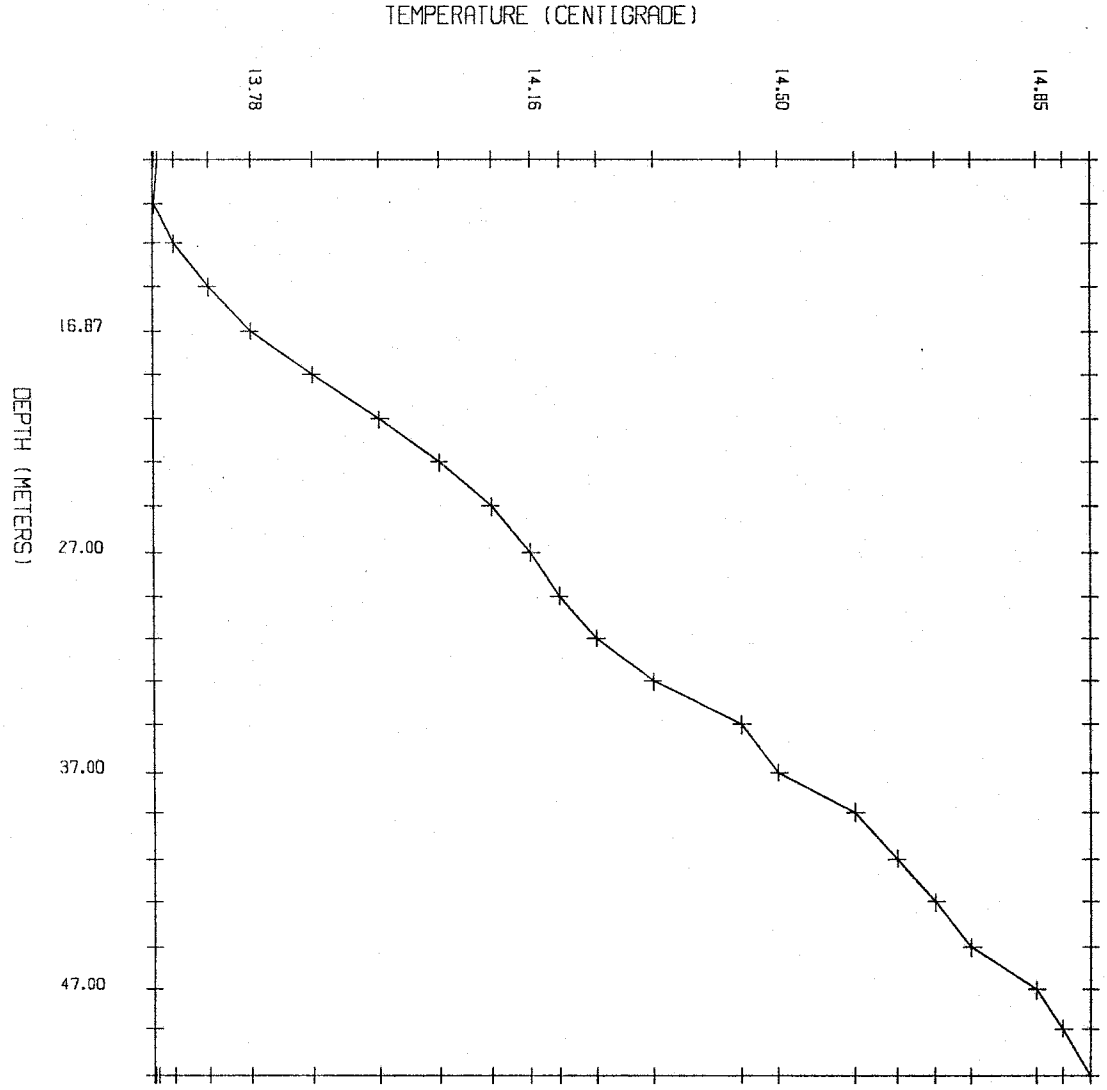

Fence Lake 5N-17W-15
lat. 34.66
long. 108.62
depth to water: 45-50 m

Thermal Conductivity data

depth interval (feet)	rock type	Kr (W/mK)	porosity
160-173	ss	4.40	.195
173-195	sh/ss	2.89	.195
195-203	sh	2.34	.180
203-213	sh/ss	2.89	.170
213-223	ss	4.40	.225
223-236	sh/ss	2.89	.180
236-246	sh	2.34	.195

Kr - average values
porosity - from density log

Temperature Gradient data

depth (m)	temperature (degrees C)
date logged: 18 August 1983	
tool: 100k ohm	
50.00	12.814
55.20	12.903
59.94	13.062
65.05	13.180
70.15	13.392
74.87	13.574

FENCE LAKE 5N 17W 15

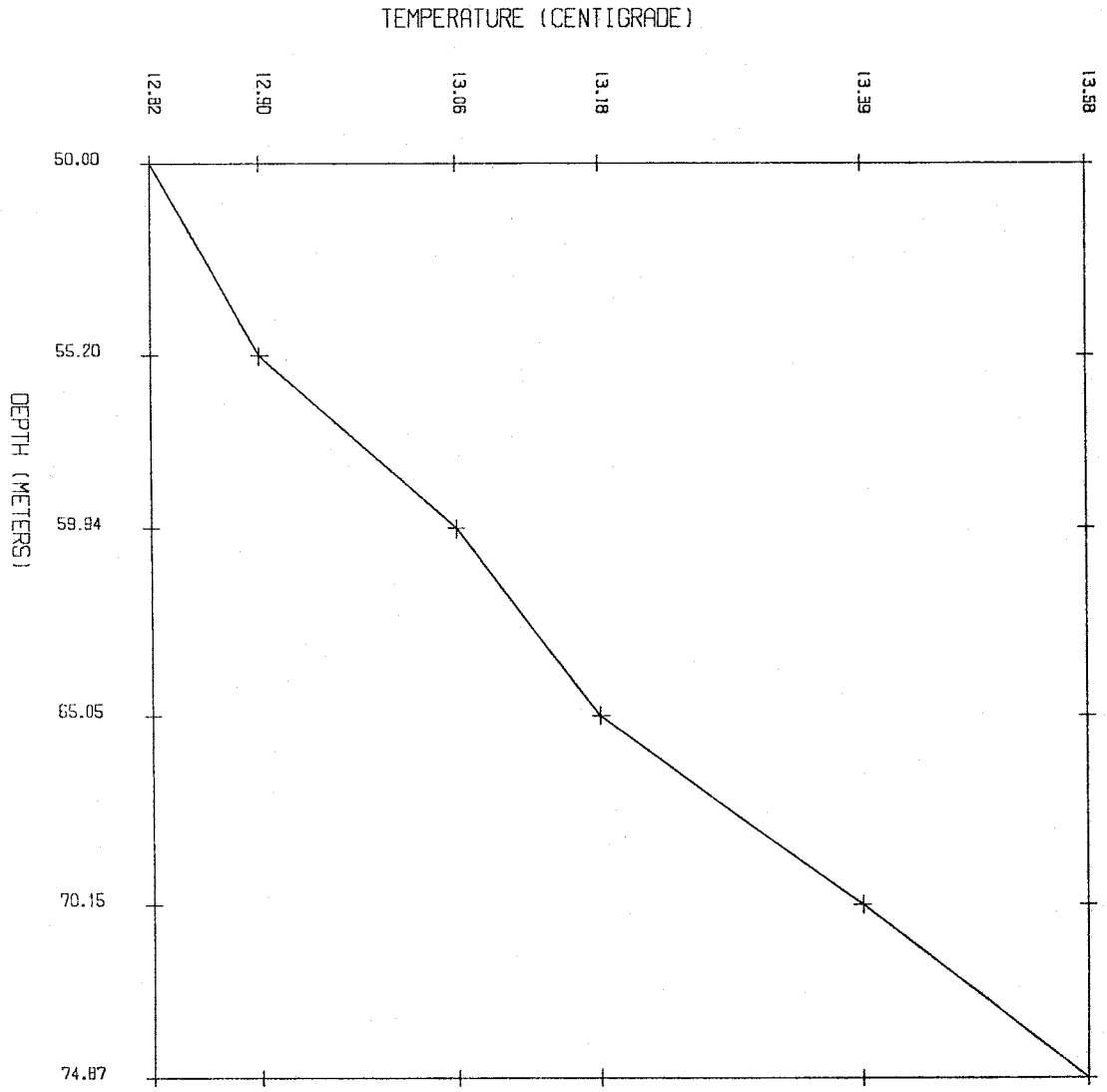

Garcia Lake 4N-16W-31
lat. 34.53
long. 108.55
depth to water: 26m

Thermal Conductivity data

depth interval (feet)	rock type	Kr (W/mK)	porosity
90-100	ss	3.73	.21
100-110	sh/ss	2.44	.18
110-115	ss	4.30	.18
115-125	ss	4.54	.24
125-135	ss	4.98	.24
135-140	ss	5.95	.24

Kr - measured values
porosity - from density log

Temperature Gradient data

depth (m)	temperature (degrees C)
date logged: 15 August 1984	
tool: 4k ohm	
9.00	13.251
10.92	13.307
12.94	13.537
14.92	13.895
16.92	14.347
18.95	14.209
20.98	14.162
22.98	14.162
24.92	14.162
26.92	14.162
28.96	14.068
30.98	14.068
32.92	14.107
date logged: 15 August 1984	
tool: 100k ohm	
28.10	13.909
30.67	13.895
33.21	13.920
35.71	13.970
38.25	14.008
40.74	14.058
43.26	14.096

GARCIA LAKE 4N 16W 31

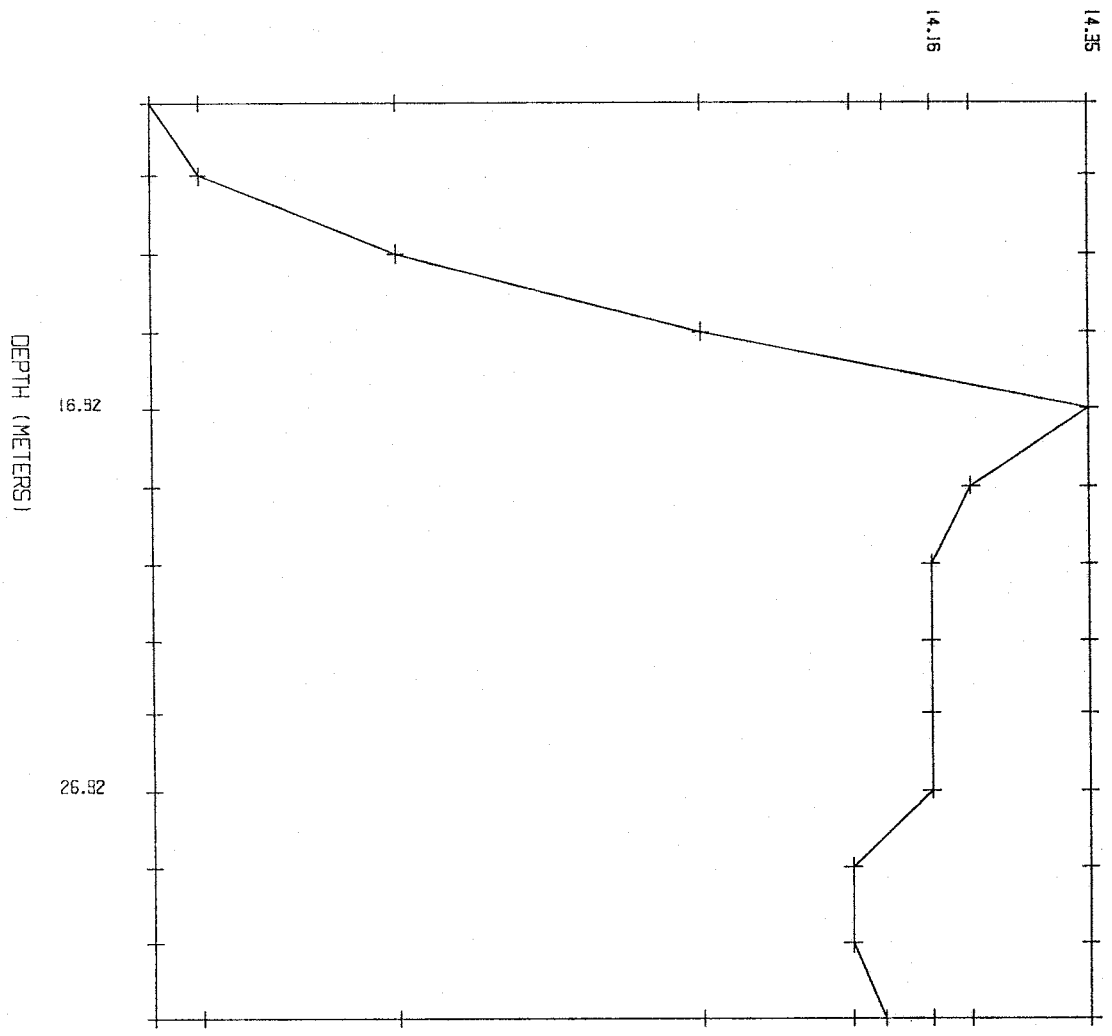

GARCIA LAKE 4N 16W 31

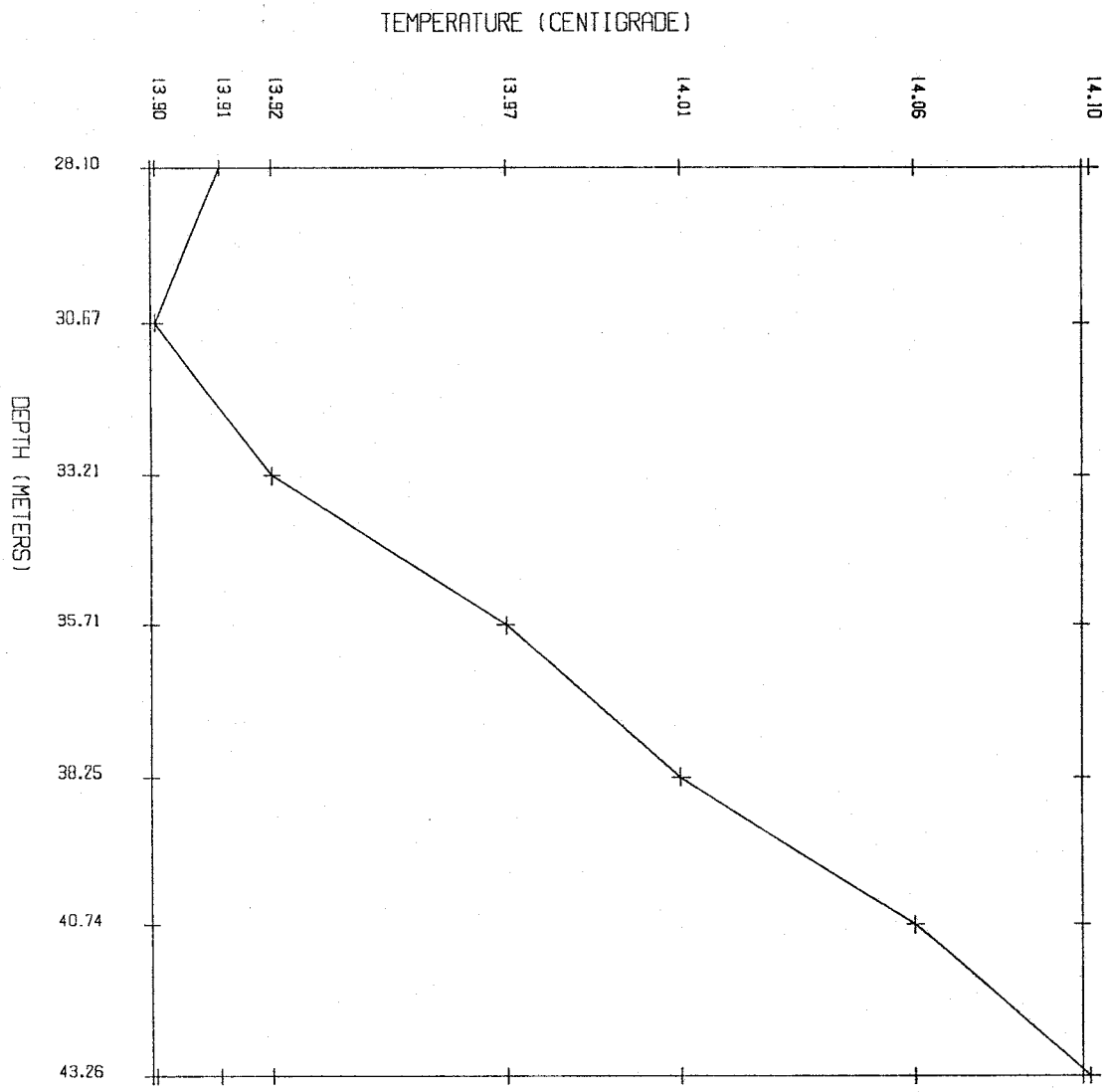

Gobbler Knob 5N-15W-30
lat. 34.63
long. 108.45
depth to water: approx. 130m

Thermal Conductivity data

depth interval (feet)	rock type	Kr (W/mK)	porosity
35- 85	ss	4.40	.23
85-125	sh/ss	2.89	.19
125-155	ss	4.40	.23
155-175	sh/ss	2.89	.19
175-195	ss	4.40	.23
195-215	sh/ss	2.89	.19
215-225	ss	4.40	.23
225-235	sh/ss	2.89	.19
235-290	ss	4.40	.23
290-300	sh	2.34	.18
300-335	sh/ss	2.89	.19
335-385	sh	2.34	.18
385-395	ss	4.40	.23
395-415	sh	2.34	.18
415-440	ss	4.40	.23
440-475	sh	2.34	.18
475-490	ss	4.40	.23
490-515	sh/ss	2.89	.19
515-535	ss	4.40	.23
535-565	sh/ss	2.89	.18
565-600	ss	4.40	.23
600-655	sh/ss	2.89	.19
655-670	sh	2.34	.18
670-725	sh/ss	2.89	.19
725-755	sh	2.34	.18

Kr - average values
porosity - average values
lithology - from well at 5N-16W-23

Temperature Gradient data

depth (m)	temperature (degrees C)
date logged: 23 August 1983	
tool: 100k ohm	
29.79	12.466
39.70	12.569
49.88	12.781
59.70	13.085
69.83	13.298
80.05	13.643

89.75	14.010
99.67	14.372
109.60	14.683
129.88	15.338
139.83	15.560
149.83	15.940
160.00	16.335
170.05	16.457
179.55	16.743
190.05	17.079
199.90	17.313
209.75	17.934
219.72	18.367
229.60	18.767

GOBBLER KNOB 5N 15W 3C

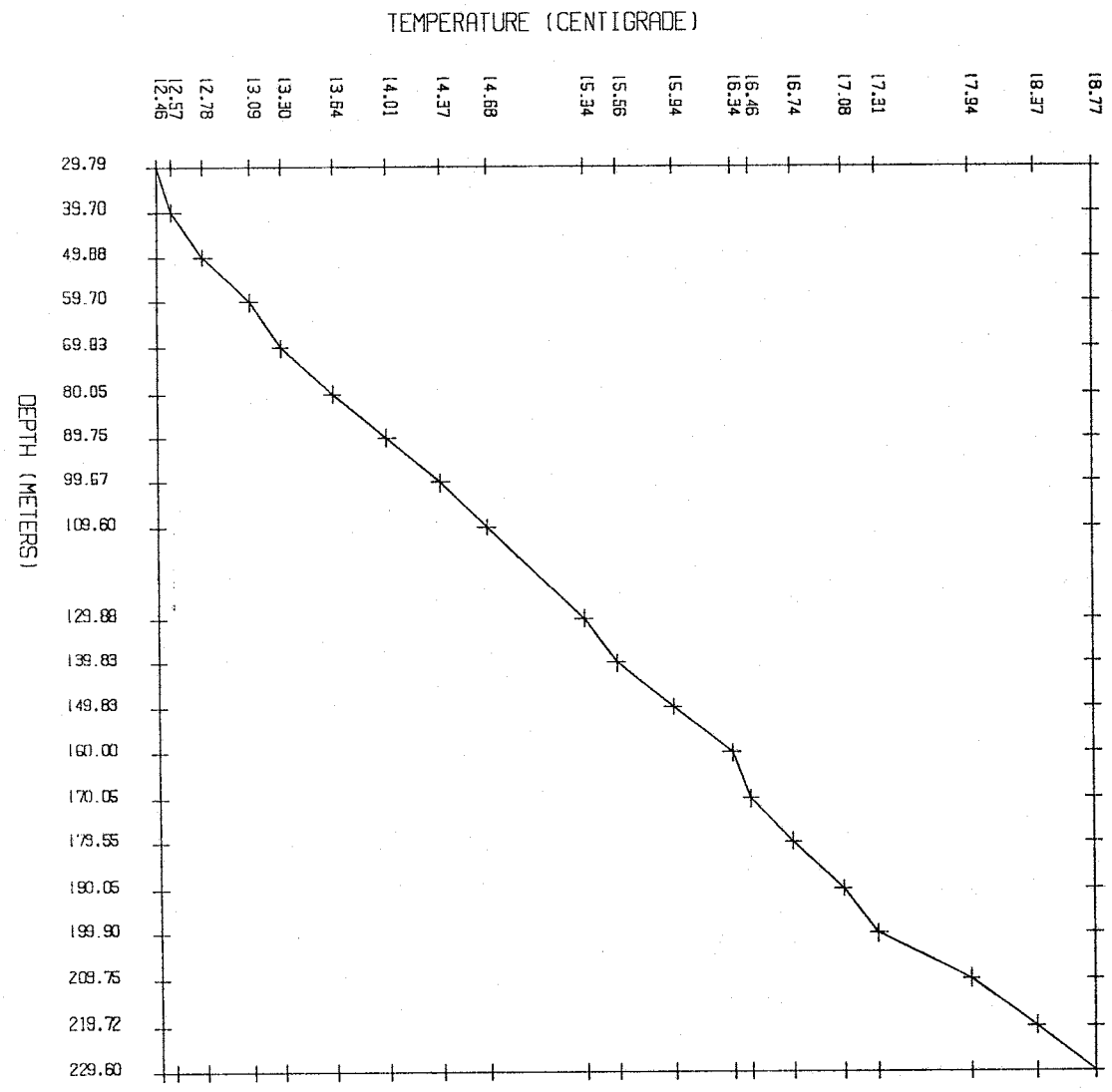

Half Lonesome Windmill 4N-18W-11
lat. 34.59
long. 108.69
depth to water: >55 m

Thermal Conductivity data

depth interval (feet)	rock type	Kr (W/mK)	porosity
95-130	sh	2.37	.13
130-165	sh	2.40	.11
165-180	sh	2.87	.15

Kr - measured values
porosity - from density log

Temperature Gradient data

depth (m)	temperature (degrees C)

date logged: 21 July 1983
tool: 100k ohm

30.00	12.616
40.00	12.717
50.00	12.922
55.00	13.011

HALF LONESOME WINDMILL 4N 18W 11

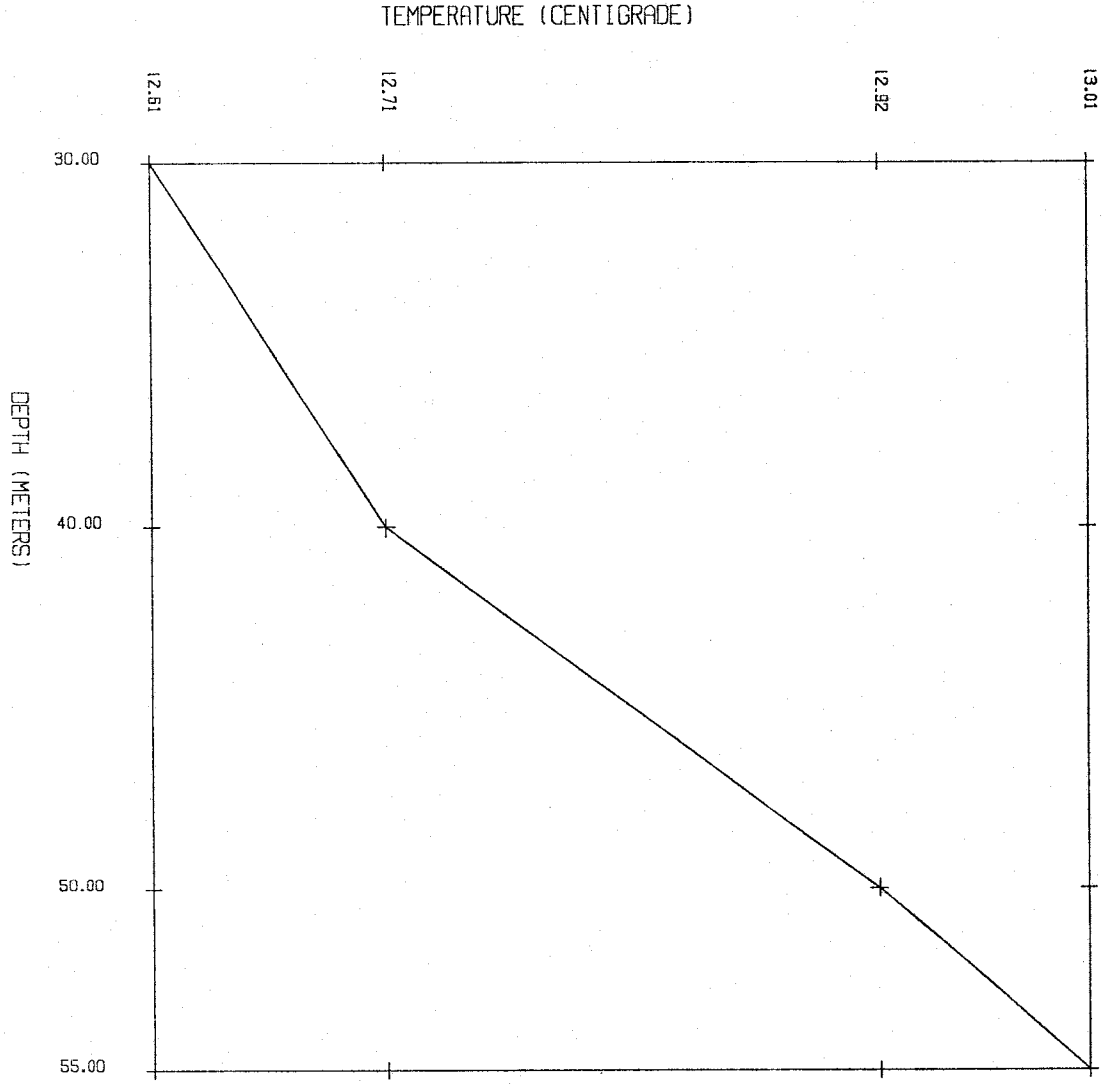

Red Hill 1N-20W-34
lat. 34.26
long. 108.93
depth to water: 60-65m

Thermal Conductivity data

depth interval (feet)	rock type	Kr (W/mK)	porosity
30- 50	sh/ss	2.18	.24
50- 60	sh/ss	2.44	.21
60- 80	sh	2.33	.18
80-106	sh/coal	1.23	.24
106-125	ss	5.05	.30
125-140	ss	5.91	.30
140-165	sh	2.21	.24
165-190	ss	3.58	.24
190-212	sh	2.38	.24
212-230	ss	4.72	.30
230-260	ss/sh	3.25	.21
260-275	ss/sh	3.70	.24
275-300	ss/sh	3.82	.21
300-320	ss/sh	3.46	.21
320-335	ss/sh	3.46	.18
335-350	sh	2.42	.18
350-365	sh	2.30	.18
365-385	sh	2.43	.15
385-410	sh	2.45	.15
410-430	sh	2.29	.15
430-450	sh	2.47	.15
450-470	sh	2.48	.15
470-493	sh	2.18	.15
493-520	sh/ss	2.53	.18
520-535	sh/ss	2.74	.21
535-550	ss/sh	3.11	.24
550-570	ss/sh	2.90	.21

Kr - measured values
porosity - from density log

Temperature Gradient data

depth (m)	temperature (degrees C)
9.05	14.057
13.85	14.261
18.85	14.324
23.80	14.407
28.85	14.577

date logged: 14 June 1984
tool: 4k ohm

33.85	14.750
38.85	14.871
43.82	15.032
48.82	15.283
53.93	15.561
58.95	15.742
63.82	16.098
68.80	16.432
73.85	16.633
78.75	16.837
83.75	17.312
88.85	17.249
93.75	17.394
98.82	17.467
103.85	17.636
108.85	17.831
113.90	18.097
118.88	18.377
123.88	18.815
128.98	19.307
133.88	19.795
138.77	20.129
143.77	20.426
148.85	21.058
153.80	21.069
158.77	21.075
168.85	21.456
173.85	21.577

date logged: 20 June 1984
tool: 100k ohm

48.13	16.406
53.18	16.197
58.25	16.068
63.30	16.071
68.32	16.192
73.35	16.279
78.36	16.436
83.44	16.737
88.50	16.809
93.48	17.131
98.77	17.248
103.54	17.514
108.55	17.605
113.64	17.790
118.59	18.121
123.72	18.452
128.65	19.104
133.73	19.235
138.74	19.298
143.83	20.043
148.88	20.249
153.98	20.284
158.87	20.319
163.91	20.496

RED HILL, NM 1N 20W 31

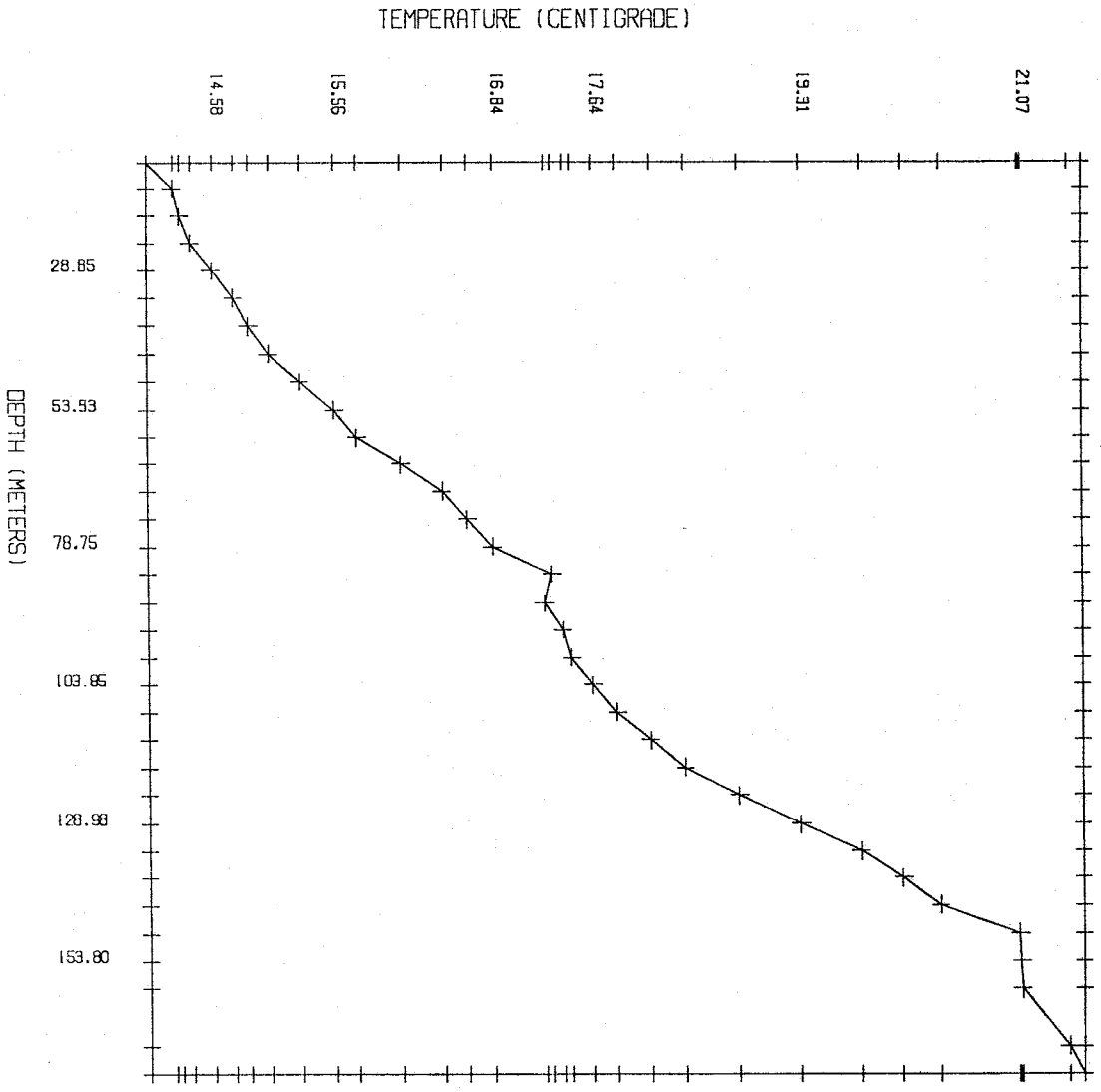

RED HILL, NM IN 20W 34

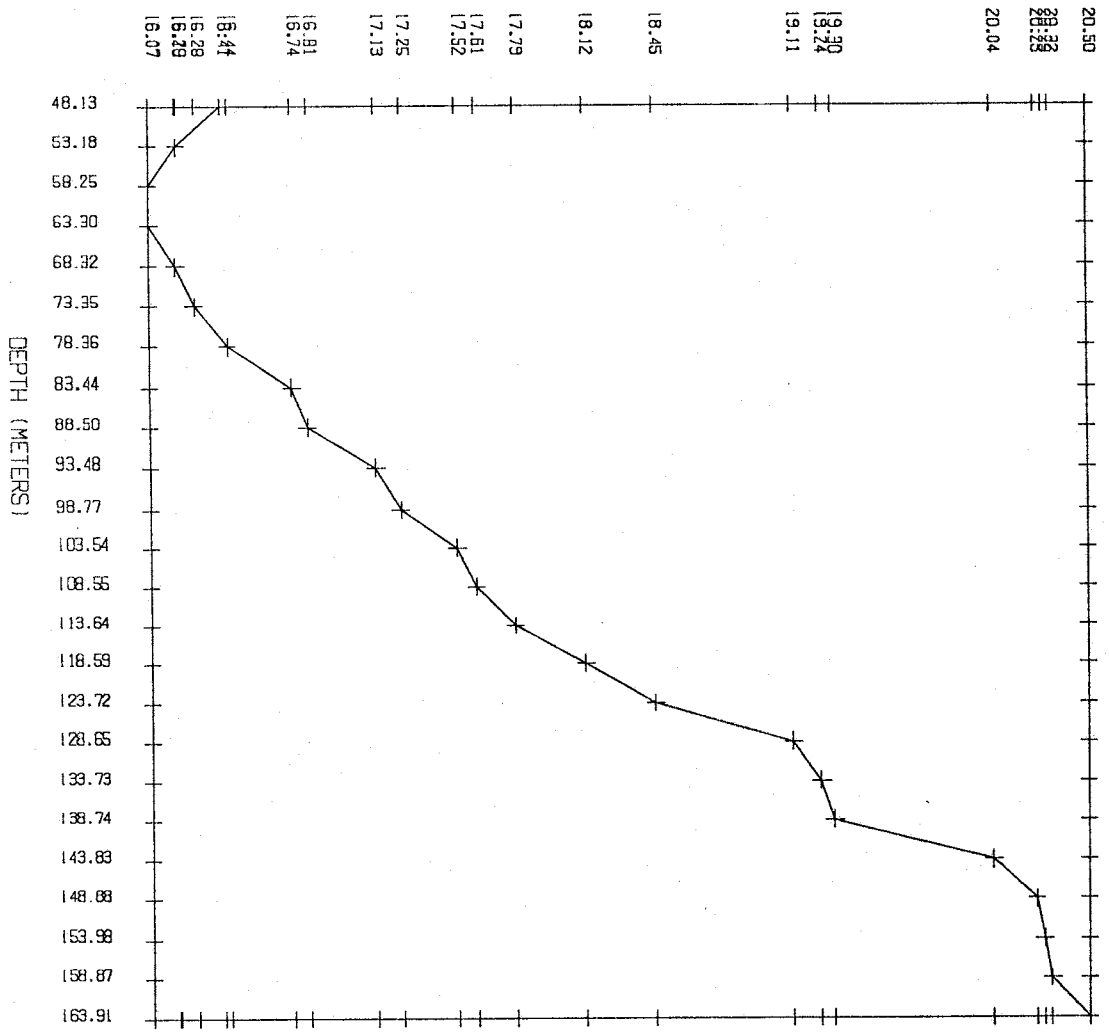

Route 32 2N-17W-9
lat. 34.40
long. 108.62
depth to water: 40-45m

Thermal Conductivity data

depth interval (feet)	rock type	Kr (W/mK)	porosity
140-147	sh	2.34	.18
147-151	sh/ss	2.89	.19
151-171	sh	2.34	.18
171-182	sh/ss	2.89	.19
182-218	sh	2.34	.18
218-228	sh/ss	2.89	.19
228-270	sh	2.34	.18
270-295	sh/ss	2.89	.19
295-360	sh	2.34	.18
360-370	sh/ss	2.89	.19
370-400	sh	2.34	.18
400-430	sh	2.23	.18
430-485	sh	2.46	.23
485-520	sh	2.42	.23
520-537	sh	2.82	.26
537-542	coal	0.36	.03
542-563	sh	2.25	.20
563-587	ss	3.18	.23

Kr - 140-400 feet, average values
400-587 feet, measured values
porosity - from density log
coal - Kr and porosity, average of measurements

Temperature Gradient data

depth (m)	temperature (degrees C)
42.86	15.759
48.06	15.731
52.80	15.681
57.98	15.877
63.15	16.058
68.02	16.155
73.08	16.377
78.14	16.597
83.32	16.776
88.17	16.923
93.31	17.088
98.19	17.275

date logged: 10 July 1984
tool: 100k ohm

103.25	17.486
108.33	17.709
113.32	17.877
118.39	18.122
123.32	18.398
128.48	18.643
133.43	18.848
138.51	19.085
143.46	19.317
148.63	19.538
153.50	19.766
158.60	20.004
163.61	20.288
168.72	20.656
173.66	20.872
178.61	20.999

ROUTE 32 2N 17W 9

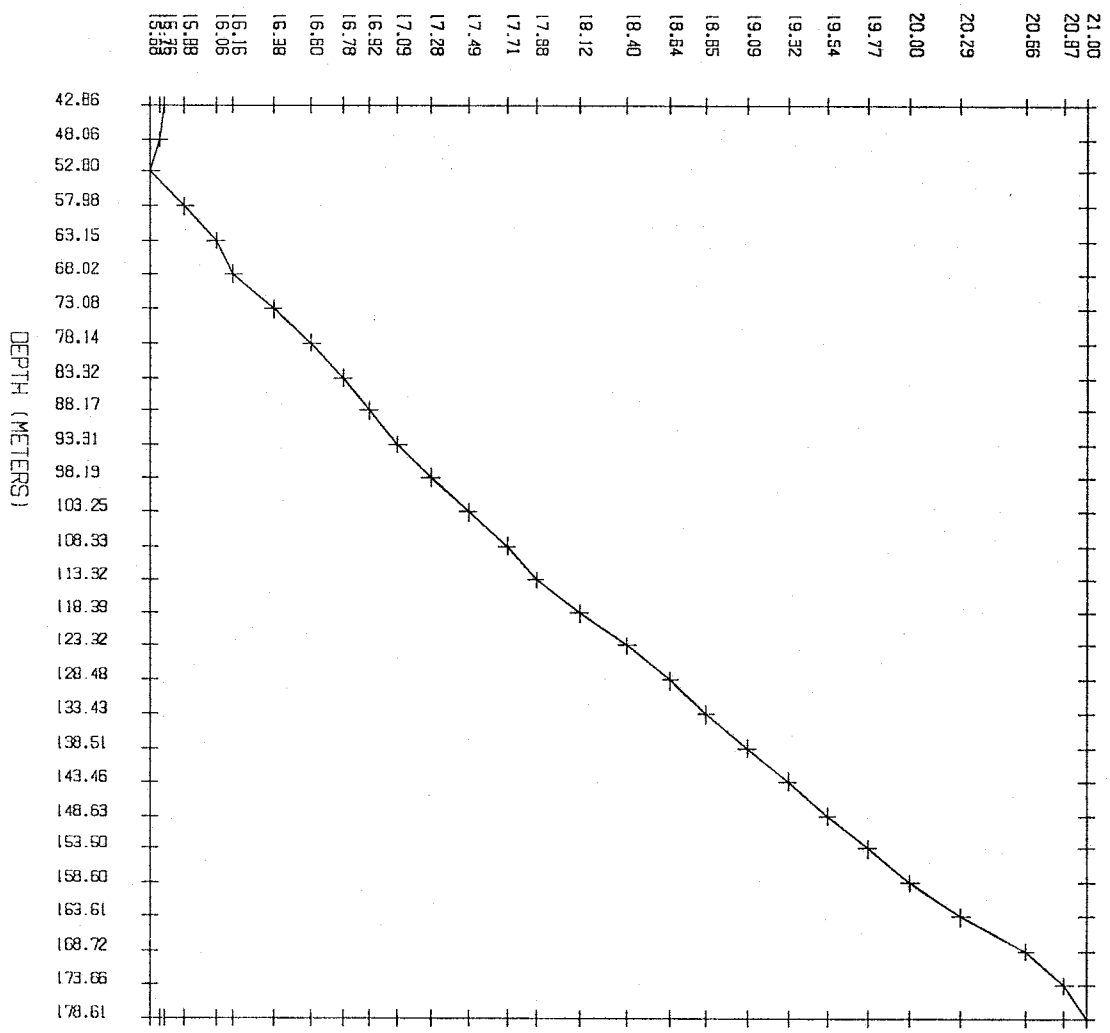

Zuni Salt Lake 1 2N-18W-13
lat. 34.40
long. 108.67
depth to water: >69m

Thermal Conductivity data

depth interval (feet)	rock type	Kr (W/mK)	porosity
30- 40	sh	2.13	.18
40- 50	sh	2.13	.18
50- 60	sh	2.40	.18
60- 70	sh	2.19	.18
70- 80	sh	2.07	.18
80- 90	sh	2.05	.18
90-100	sh	2.11	.18
100-110	sh/ss	2.83	.19
110-120	sh	2.18	.18
120-135	sh	2.15	.18
135-145	ss/sh	3.32	.19
145-155	ss/sh	3.26	.19
155-165	ss	3.92	.23
170-180	sh	2.82	.18
180-190	sh	2.96	.18
190-200	sh	1.83	.18
200-210	sh/ss	2.48	.19
210-220	ss	3.95	.23
220-230	ss	3.92	.23
230-235	ss	4.55	.23
240-250	sh	2.79	.18
250-260	sh	3.03	.18
260-270	sh/ss	2.58	.19
270-280	ss	4.38	.23

Kr - measured values
porosity - average values

Temperature Gradient data

depth (m)	temperature (degrees C)
date logged: 09 July 1984	
tool: 4k ohm	
8.92	14.985
10.85	14.738
13.00	14.569
15.00	14.407
17.03	14.427
18.92	14.403
20.90	14.415
22.92	14.462

24.92	14.517
26.92	14.573
28.87	14.641
31.03	14.713
32.90	14.782
34.97	14.863
37.00	14.940
38.92	15.102
41.00	15.238
42.97	15.387
44.95	15.590
47.00	15.678
48.90	15.687
50.90	15.687
52.92	15.712
54.95	15.758
56.95	15.822
58.92	15.894
60.97	16.056
62.97	16.185
64.95	16.319
66.95	16.467
68.92	16.527

ZUNI SALT LAKE 1 2N 18W 13

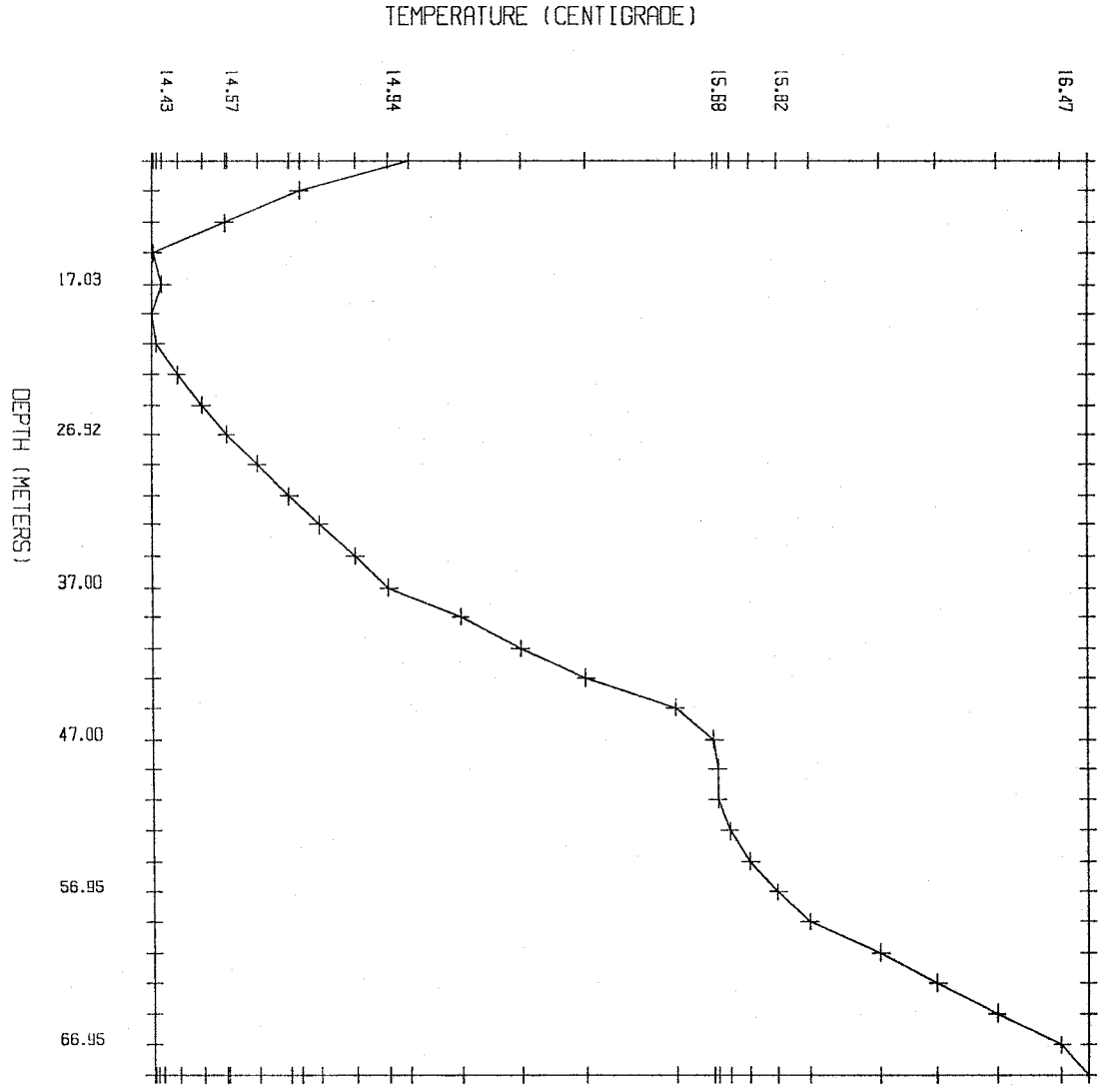

Zuni Salt Lake No. 2 2N-18W-15
lat. 34.41
long. 108.69
depth to water: > 85 m

Thermal Conductivity data

depth interval (feet)	rock type	Kr (W/mK)	porosity
50- 60	sh	2.13	.18
60- 70	sh	2.13	.18
70- 80	sh	2.40	.18
80- 90	sh	2.19	.18
90-100	sh	2.07	.18
100-110	sh	2.05	.18
110-120	sh	2.11	.18
120-130	sh/ss	2.83	.19
130-140	sh	2.18	.18
140-155	sh	2.15	.18
155-165	ss/sh	3.32	.19
165-175	ss/sh	3.26	.19
175-185	ss	3.92	.23
190-200	sh	2.82	.18
200-210	sh	2.96	.18
210-220	sh	1.83	.18
220-230	sh/ss	2.48	.19
230-240	ss	3.95	.23
240-250	ss	3.92	.23
250-255	ss	4.55	.23
260-270	sh	2.79	.18
270-280	sh	3.03	.18

Kr - measured from Zuni Salt Lake No. 1
porosity - average values

Temperature Gradient data

depth (m)	temperature (degrees C)
8.97	13.337
11.03	13.549
12.95	13.790
15.03	13.922
17.05	14.033
19.08	14.107
21.05	14.162
22.97	14.213
24.95	14.288
27.03	14.359

date logged: 11 July 1984
tool: 4k ohm

28.92	14.431
31.00	14.525
33.00	14.605
35.03	14.681
36.97	14.774
39.00	14.912
40.95	14.989
43.05	15.073
45.00	15.143
47.03	15.217
49.05	15.296
50.95	15.366
52.95	15.445
55.00	15.548
57.05	15.687
58.92	15.771
61.10	15.847
63.03	15.950
65.03	16.129
67.03	16.241
69.00	16.249
71.00	16.249
73.23	16.267
75.05	16.288
77.08	16.323
79.03	16.380
81.00	16.449
83.05	16.519
85.00	16.580

ZUNI SALT LAKE 2 2N 18W 15

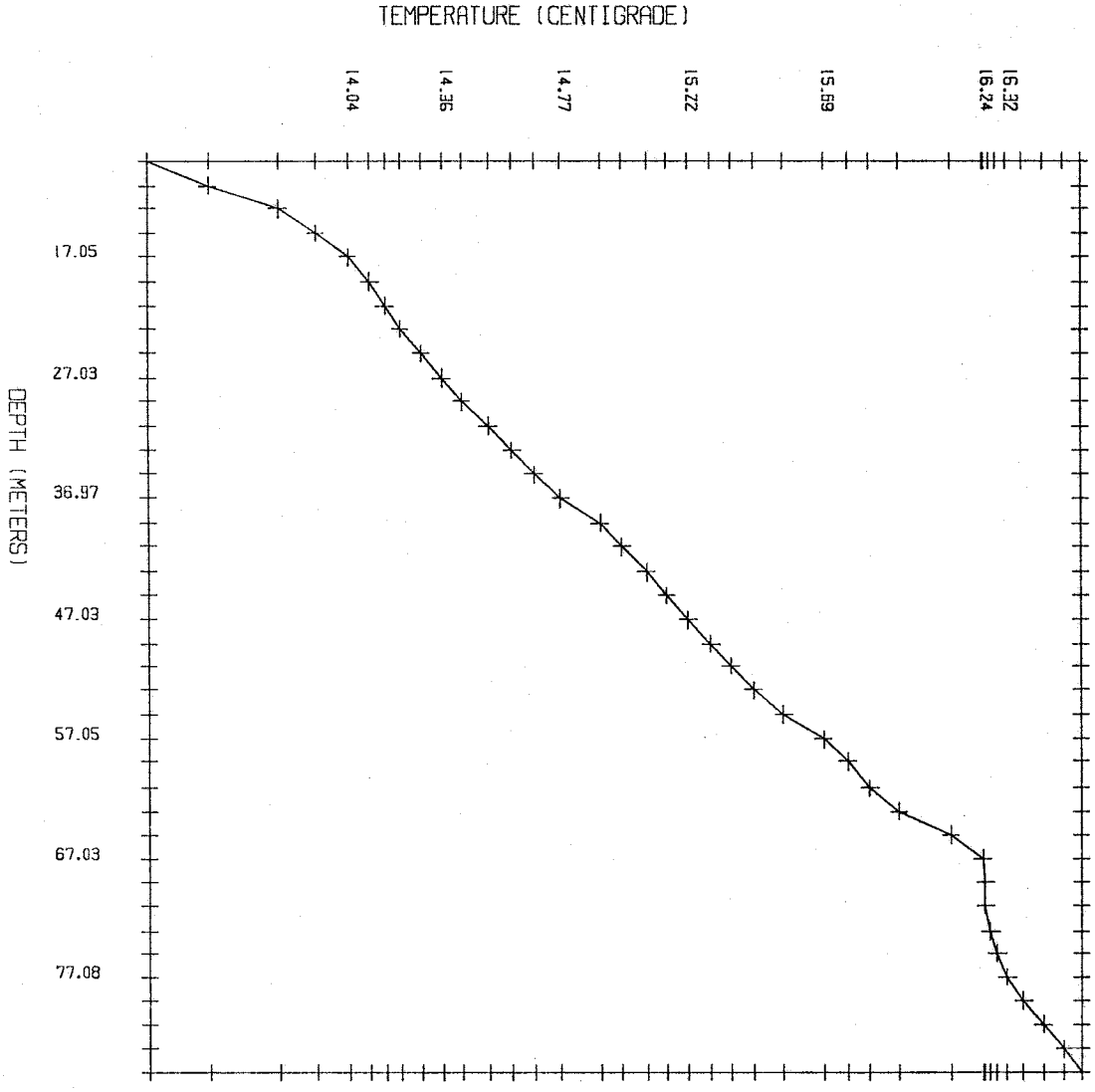

Zuni Salt Lake No. 3 2N-18W-11
lat. 34.40
long. 108.70
depth to water: > 57 m

Thermal Conductivity data

depth interval (feet)	rock type	Kr (W/mK)	porosity
30- 45	sh	2.15	.18
45- 55	ss/sh	3.32	.19
55- 65	ss/sh	3.26	.19
65- 75	ss	3.92	.23
80- 90	sh	2.82	.18
90-100	sh	2.96	.18
100-110	sh	1.83	.18
110-120	sh/ss	2.48	.19
120-130	ss	3.95	.23
130-140	ss	3.92	.23
140-145	ss	4.55	.23
150-160	sh	2.79	.18
160-170	sh	3.03	.18
170-180	sh/ss	2.58	.19
180-190	ss	4.38	.23

Kr - measured from Zuni Salt Lake No. 1
porosity - average values

Temperature Gradient data

depth (m)	temperature (degrees C)
date logged: 11 July 1984	
tool: 4k ohm	
9.00	13.914
11.00	14.147
12.92	14.308
14.97	14.470
16.97	14.553
18.92	14.621
20.97	14.709
22.92	14.778
24.92	14.843
26.95	14.977
28.90	15.028
31.00	15.110
32.90	15.197
35.05	15.279
36.95	15.387
38.95	15.483
40.97	15.577

43.05	15.649
44.90	15.729
46.97	15.822
48.90	15.898
51.05	15.984
52.97	16.047
54.95	16.154
56.92	16.301

ZUNI SALT LAKE 3 2N 18W 11

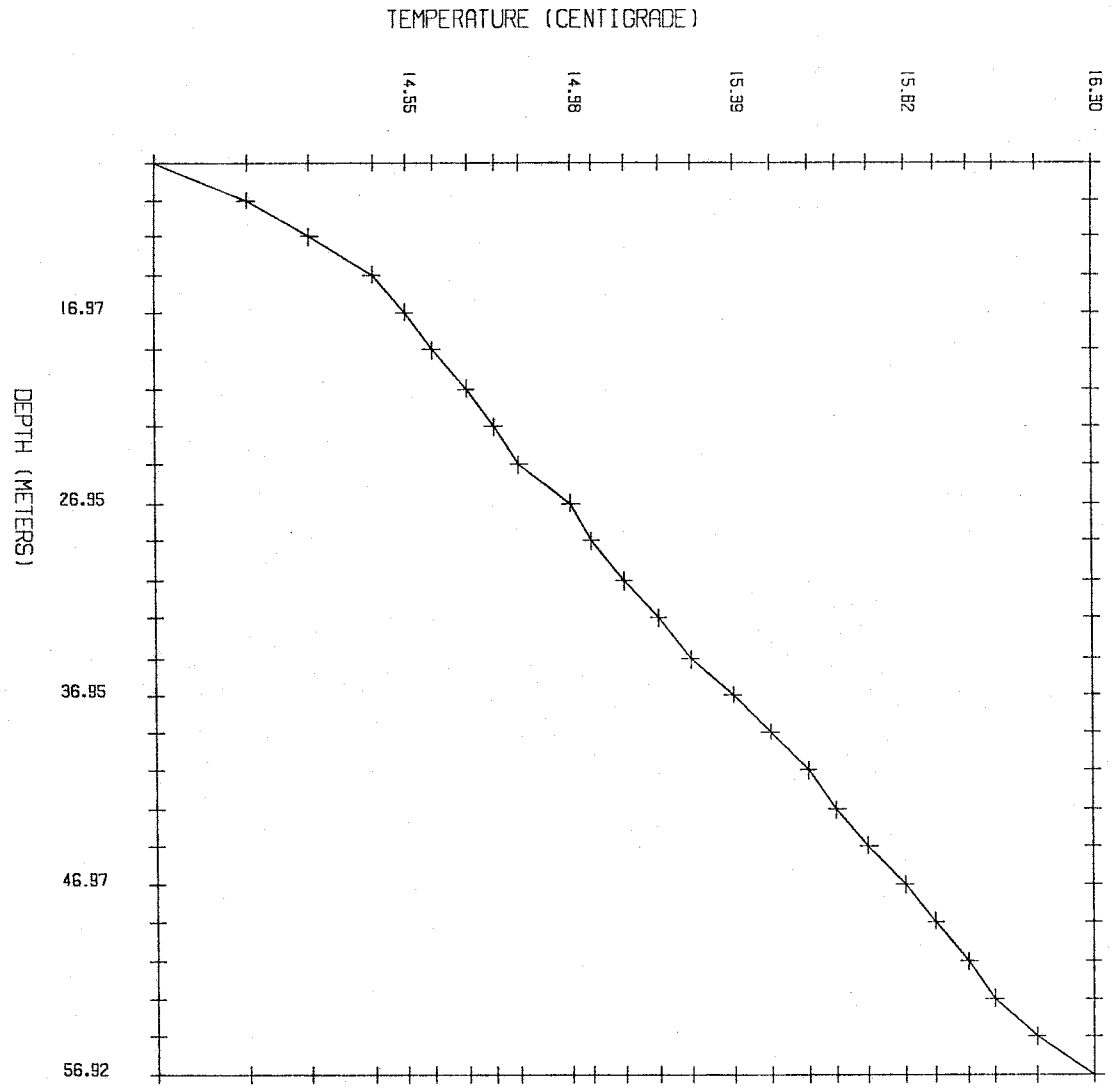

Los Alamos No. 1
lat. 34.12
long. 109.13
depth to water: not indicated

Thermal Conductivity data

depth interval (feet)	rock type
0- 13	sltstn
13- 15	ss
15- 23	sltstn
23- 25	ss
25- 33	sltstn
33- 35	ss
35- 43	sh
43- 45	ss
45-100	sltstn
100-121	sh
121-180	sltstn

Temperature Gradient data

depth (m)	temperature (degrees C)
9.10	16.06
15.20	16.08
21.30	16.18
30.50	16.80
36.60	17.35
42.70	17.84
51.80	18.44

LOS ALAMOS NO. 1

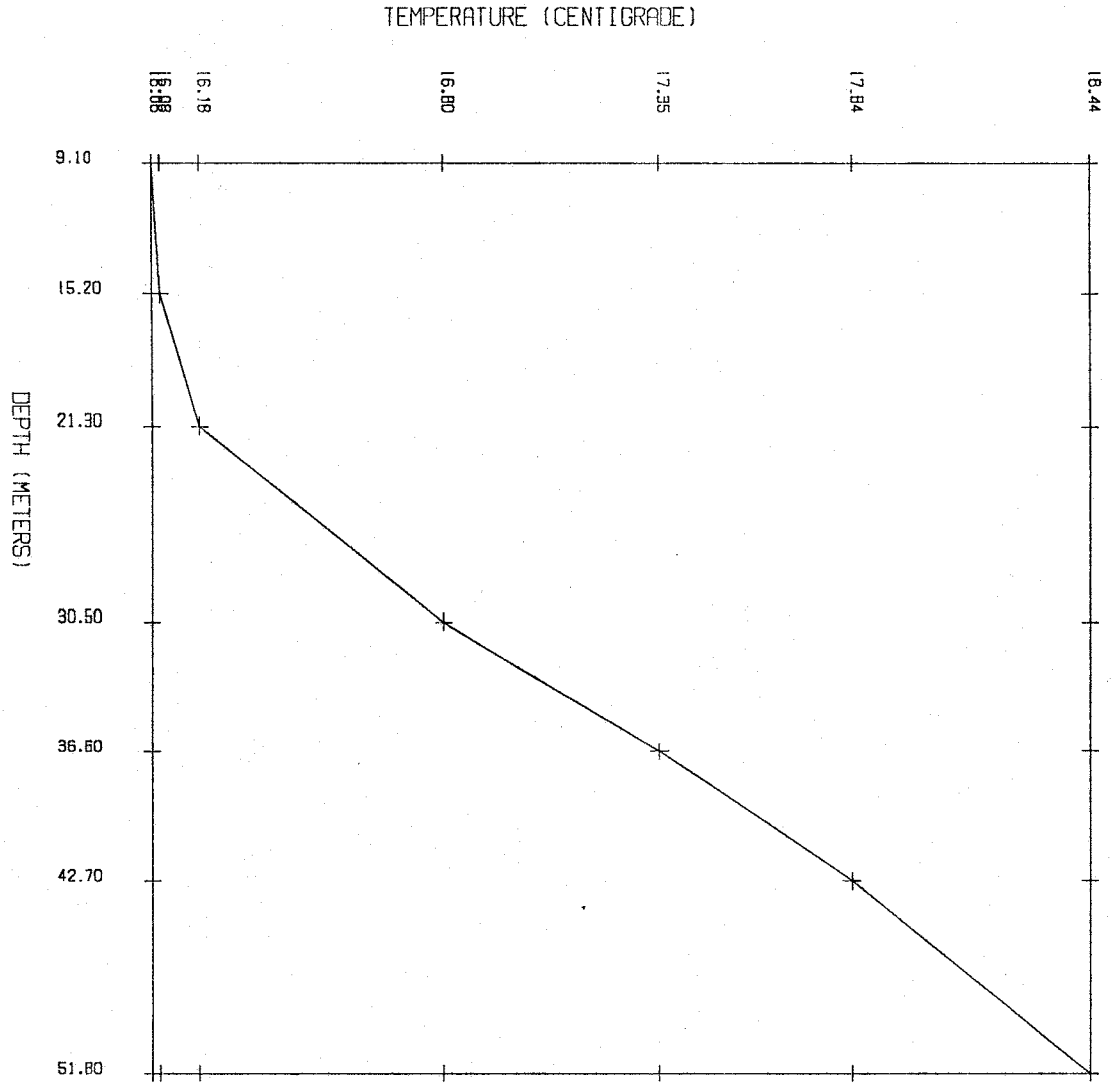

Los Alamos No. 2
lat. 34.14
long. 109.13
depth to water: not indicated

Thermal Conductivity data

depth interval (feet)	rock type
0- 30	sh
30- 50	ss
50- 77	sltstn
77-161	sh
161-200	silty ss
200-225	sh
225-230	ss
230-234	sh
234-237	ss
237-387	sh
387-390	ss
390-400	sltstn
400-405	ss
405-410	sh

Temperature Gradient data

depth (m)	temperature (degrees C)
9.10	16.04
15.20	16.42
21.30	16.82
30.50	18.46
36.60	19.48
42.70	20.70
48.80	21.87
54.90	22.66
61.00	23.26
67.10	23.85
73.10	24.41
79.20	25.10
85.30	26.24
91.40	27.35
100.60	28.54
103.90	28.89
109.70	29.56
116.10	30.22
121.90	30.81

LOS ALAMOS NO. 2

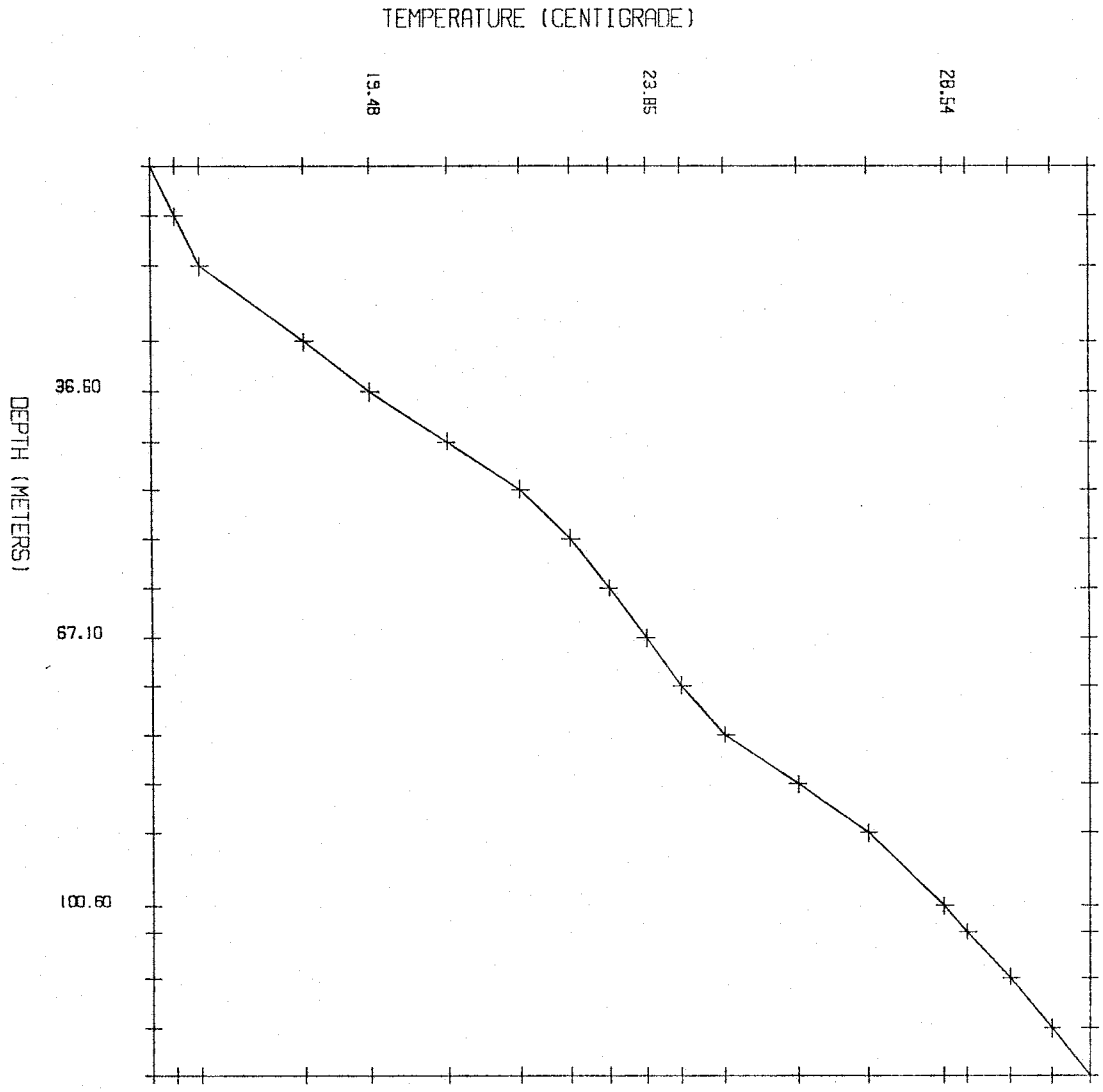

Los Alamos No. 3
lat. 34.29
long. 108.76
depth to water: not indicated

Thermal Conductivity data

none

Temperature Gradient data

depth (m)	temperature (degrees C)
6.10	12.08
12.20	12.73
18.30	12.84
24.40	13.06
30.50	13.24
36.60	13.48
42.70	13.60
48.80	13.95
54.90	14.12
61.00	14.34
67.10	14.53
73.20	14.68
79.20	14.86
85.30	15.14
91.40	15.36
97.50	15.66
103.60	15.90
109.70	16.11
115.80	16.36
121.90	16.54
128.00	16.76
134.10	16.98
140.20	17.18
146.30	17.47
152.40	17.71
158.50	17.93
164.60	18.13
170.70	18.35
176.80	18.58
182.90	18.84
189.00	19.11
195.10	19.35

LOS ALAMOS NO. 3

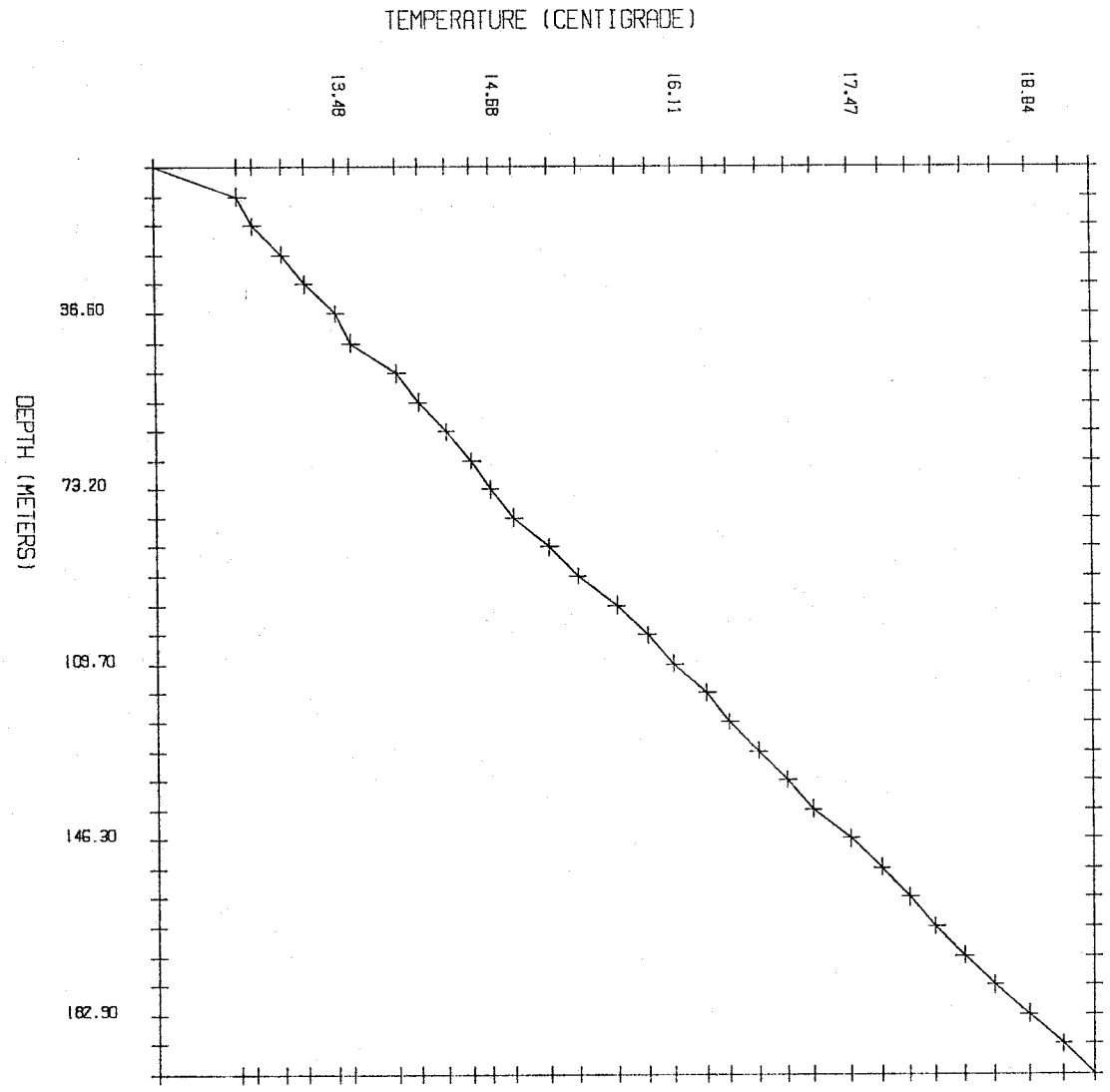

Los Alamos No. 4
lat. 34.27
long. 108.71
depth to water: 245 feet

Thermal Conductivity data

depth interval (feet)	rock type
0- 30	ss
30- 40	volc
40- 90	ss/volc
90-100	conglom
100-110	ss
110-120	volc
120-140	ss
140-160	conglom
160-180	ss
180-240	sltstn
240-250	ss
250-260	sh
260-280	ss
280-980	sh

Temperature Gradient data

depth (m)	temperature (degrees C)
6.10	15.82
12.20	15.41
18.30	15.06
24.40	14.96
30.50	15.20
36.60	15.23
42.70	15.00
48.80	15.30
54.90	15.42
61.00	15.57
67.10	15.84
73.20	16.06
79.20	16.23
85.30	16.24
91.40	16.06
97.50	16.36
103.60	16.54
109.70	16.72
115.80	16.98
121.90	17.14
128.00	17.34
134.10	17.61
140.20	17.88
146.30	17.94

152.40	18.16
158.50	18.32
164.60	18.46
170.70	18.71
176.80	18.92
182.90	19.12
189.00	19.35
195.10	19.65
201.20	19.90
207.30	20.13
213.40	20.41
219.50	20.65
225.60	20.66
231.60	20.92
237.70	21.08
243.80	21.31
249.90	21.61
256.00	21.89
262.10	22.14
268.20	22.26
274.30	22.43
280.40	22.68
286.50	22.92
292.60	22.97

LOS ALAMOS NO. 1

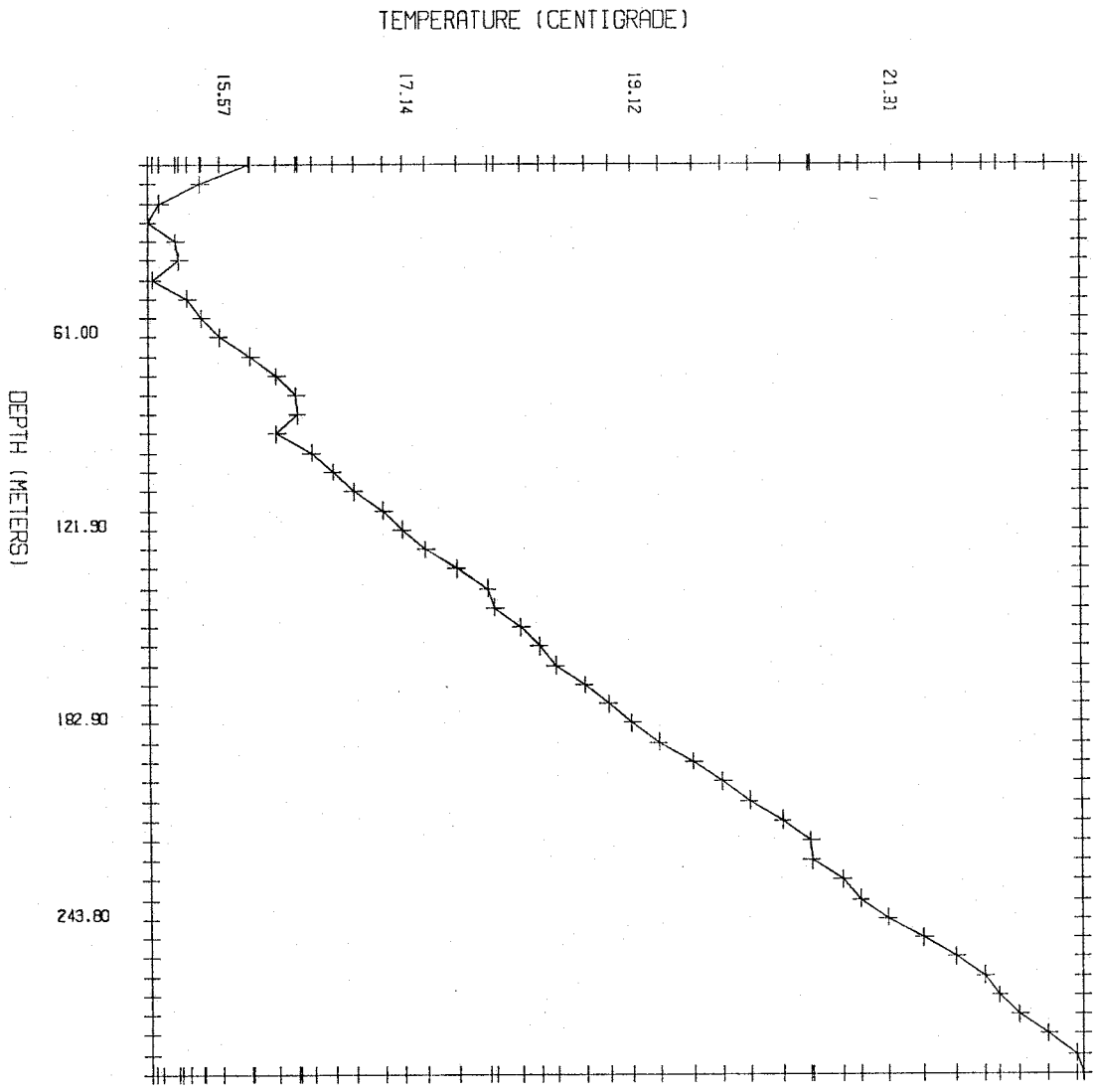

Los Alamos No. 8
lat. 34.91
long. 108.84
depth to water: not indicated

Thermal Conductivity data

depth interval (feet)	rock type
0- 35	sh
35-110	ss
110-120	sh
120-200	ss
200-400	sh
400-410	ss
410-440	sh

Temperature Gradient data

depth (m)	temperature (degrees C)
6.10	22.04
12.20	21.46
18.30	21.23
24.40	20.95
29.30	20.72
34.10	20.55
39.00	20.41
43.90	20.25
49.10	20.12
53.90	14.89
58.80	14.95
63.70	15.25
68.60	15.61
73.50	15.98
78.30	16.34
83.20	16.69
88.10	16.98
93.00	17.23
97.80	17.64
102.70	17.95
107.60	18.19
112.50	18.48
117.30	18.72
122.20	18.97
127.10	19.11

LOS ALAMOS NO. 8

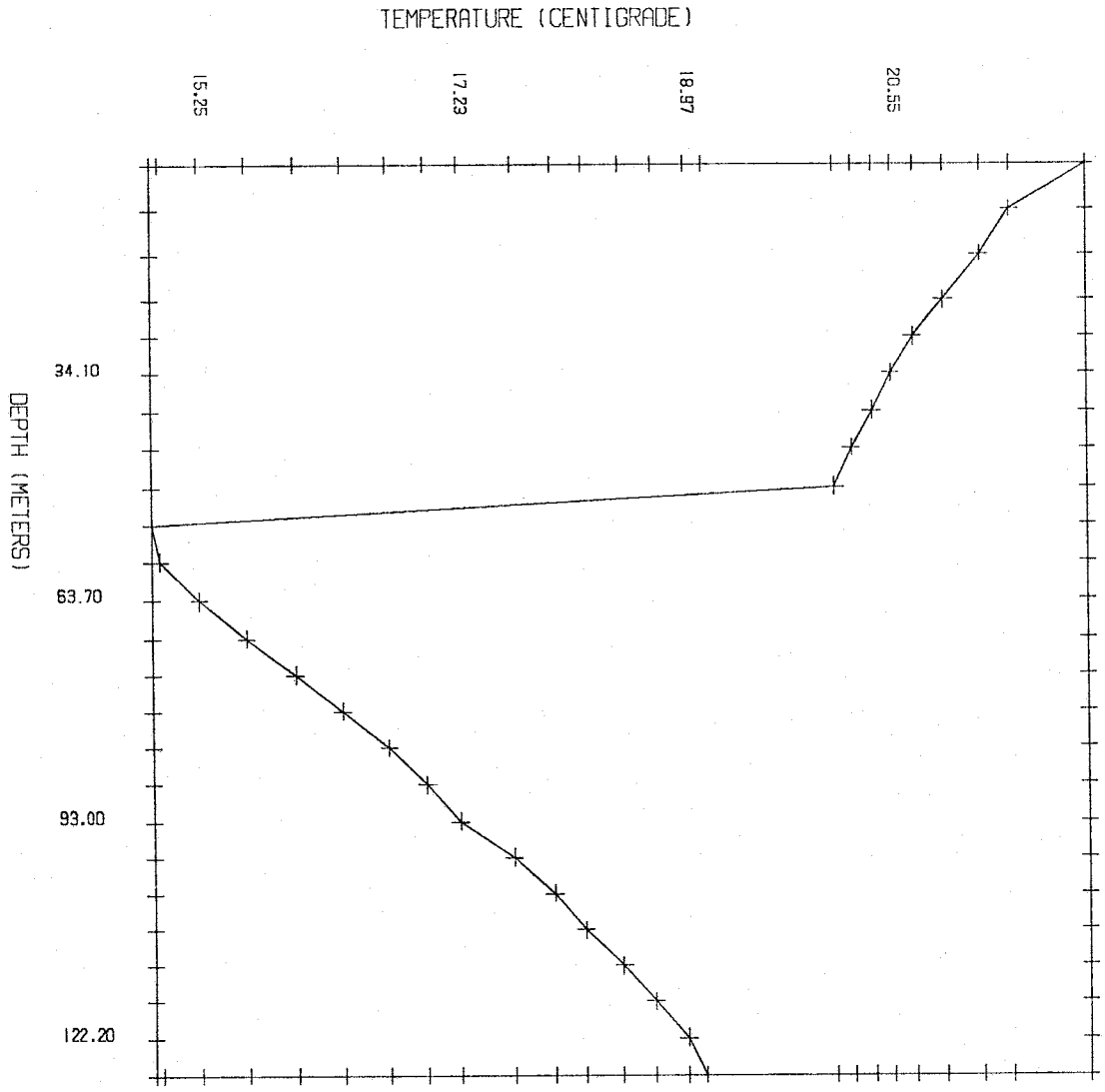

Los Alamos No. 10
lat. 34.92
long. 108.69
depth to water: not indicated

Thermal Conductivity data

depth interval (feet)	rock type
0- 65	sh
65- 75	ss
75-145	sh
145-170	ss
170-175	sh
175-550	ss

Temperature Gradient data

depth (m)	temperature (degrees C)
12.20	15.13
14.60	14.94
19.50	14.89
24.40	14.84
29.30	14.64
34.10	14.61
39.00	14.60
43.90	14.60
49.10	14.62
53.90	14.64
58.80	14.66
63.70	14.70
68.60	14.73
73.50	14.79
78.30	14.84
83.20	14.89
88.10	14.96
93.00	15.04
97.80	15.10
102.70	15.19
107.60	15.33
112.50	15.47
117.30	15.61
122.20	15.77
127.10	15.96
132.30	16.31
137.20	16.79
142.00	17.14
146.60	18.34
151.80	18.43
156.70	18.60

161.50 18.64

LOS ALAMOS NO. 1C

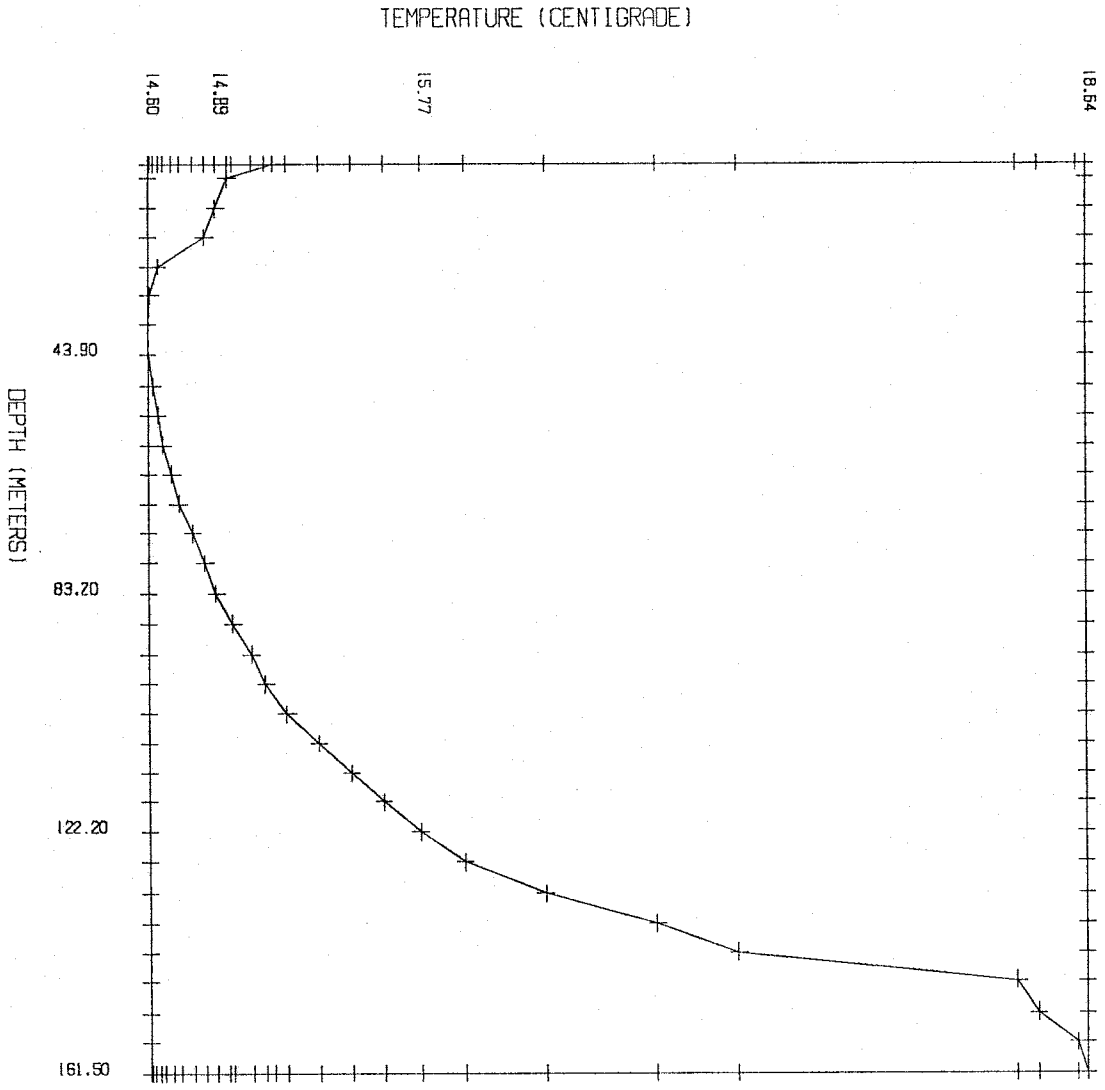

Los Alamos No. 12
lat. 35.14
long. 108.83
depth to water: not indicated

Thermal Conductivity data

depth interval (feet)	rock type
0- 870	ls
870-1180	ss

Temperature Gradient data

depth (m)	temperature (degrees C)
6.10	23.24
12.20	21.97
18.30	19.70
24.40	17.56
30.50	16.84
36.60	16.06
42.70	15.72
48.80	15.47
54.90	15.44
61.00	15.44
67.10	15.41
73.20	15.40
79.20	15.43
85.30	15.48
91.40	15.69
97.50	15.94
103.60	16.33
109.70	16.62
115.80	16.88
121.90	17.05
128.00	17.20
134.10	17.37
140.20	17.60
146.30	18.20
152.40	18.80
158.50	19.27
164.60	19.60
170.70	19.90
176.80	20.16
182.90	20.31
189.00	20.46
195.10	20.63
201.20	20.94
207.30	21.40
213.40	21.72
219.50	21.97

225.60	22.97
231.60	23.28
237.70	23.61
243.80	23.91
249.90	24.23
256.00	24.54
262.10	24.83
268.20	25.08
274.30	25.26
280.40	25.41
286.50	25.55
292.60	25.64
298.70	25.87
304.80	26.04
310.90	26.21
317.00	26.29
323.10	26.46
329.20	26.62
335.30	26.76
341.40	26.92
347.50	26.94

LOS ALAMOS NO. 12

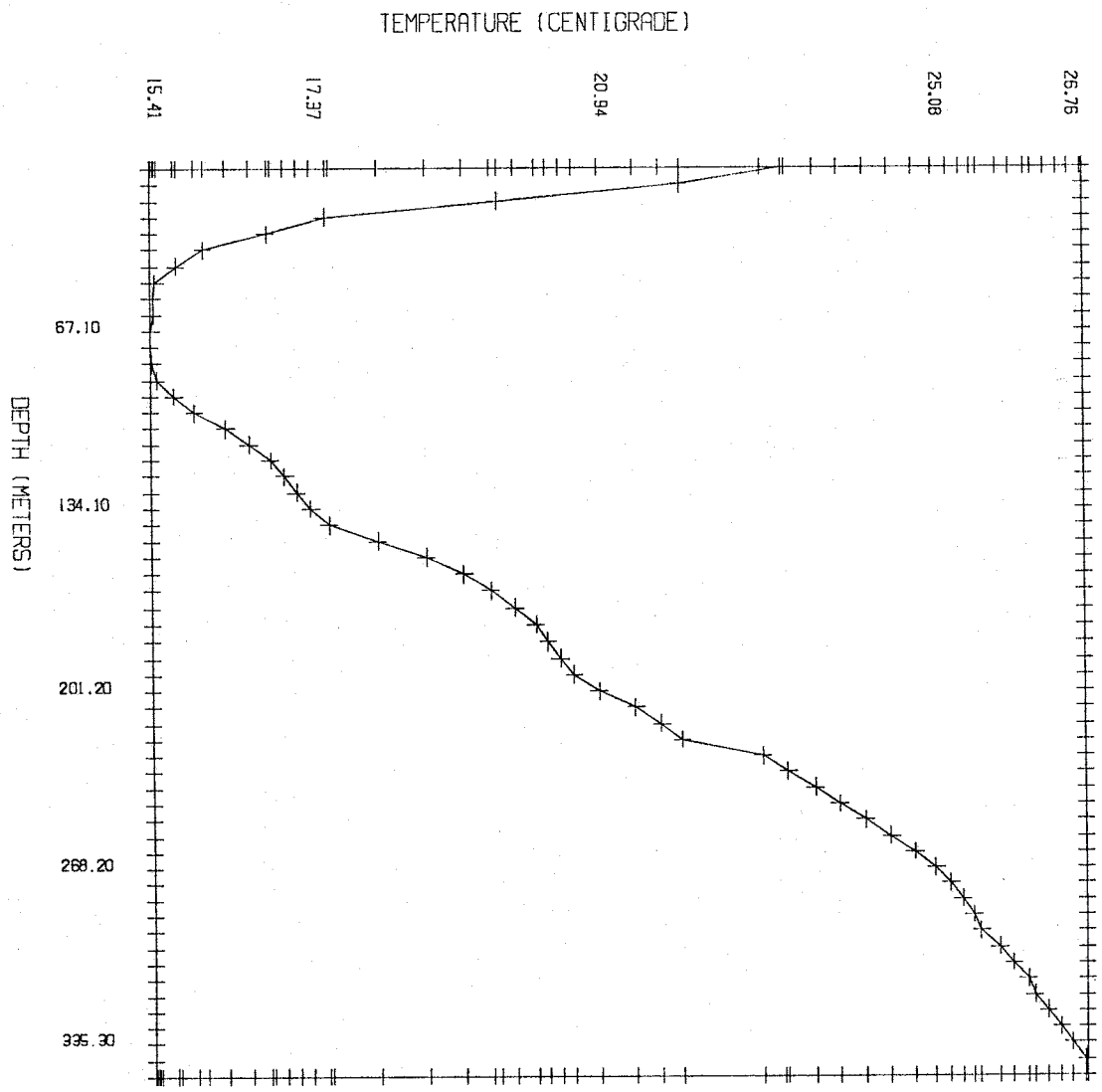

Los Alamos No. 13
lat. 35.11
long. 108.65
depth to water: not indicated

Thermal Conductivity data

depth interval (feet)	rock type
0- 65	sh
65- 80	ss
80-180	sh
180-190	ss
190-400	sh

Temperature Gradient data

depth (m)	temperature (degrees C)
9.80	19.04
12.20	18.66
14.60	18.09
17.10	17.58
19.50	17.14
21.90	16.68
24.40	16.56
26.80	16.45
29.30	16.34
31.70	16.10
34.10	15.91
36.60	15.78
39.00	15.64
41.50	15.55
43.90	15.45
46.30	15.38
49.10	15.33
51.50	15.28
53.90	15.25
56.40	15.23
58.80	15.21
61.30	15.23
63.70	15.25
66.10	15.28
68.60	15.34
71.00	15.39
73.50	15.54
75.90	15.61
78.30	15.68
80.80	15.77
83.20	15.90
85.60	16.04

88.10	16.24
90.50	16.44
93.00	16.63
95.40	16.76
97.80	16.92
100.30	17.12
102.70	17.26
105.20	17.38
107.60	18.46
110.00	18.56
112.50	18.76
114.90	18.86

LOS ALAMOS NO. 13

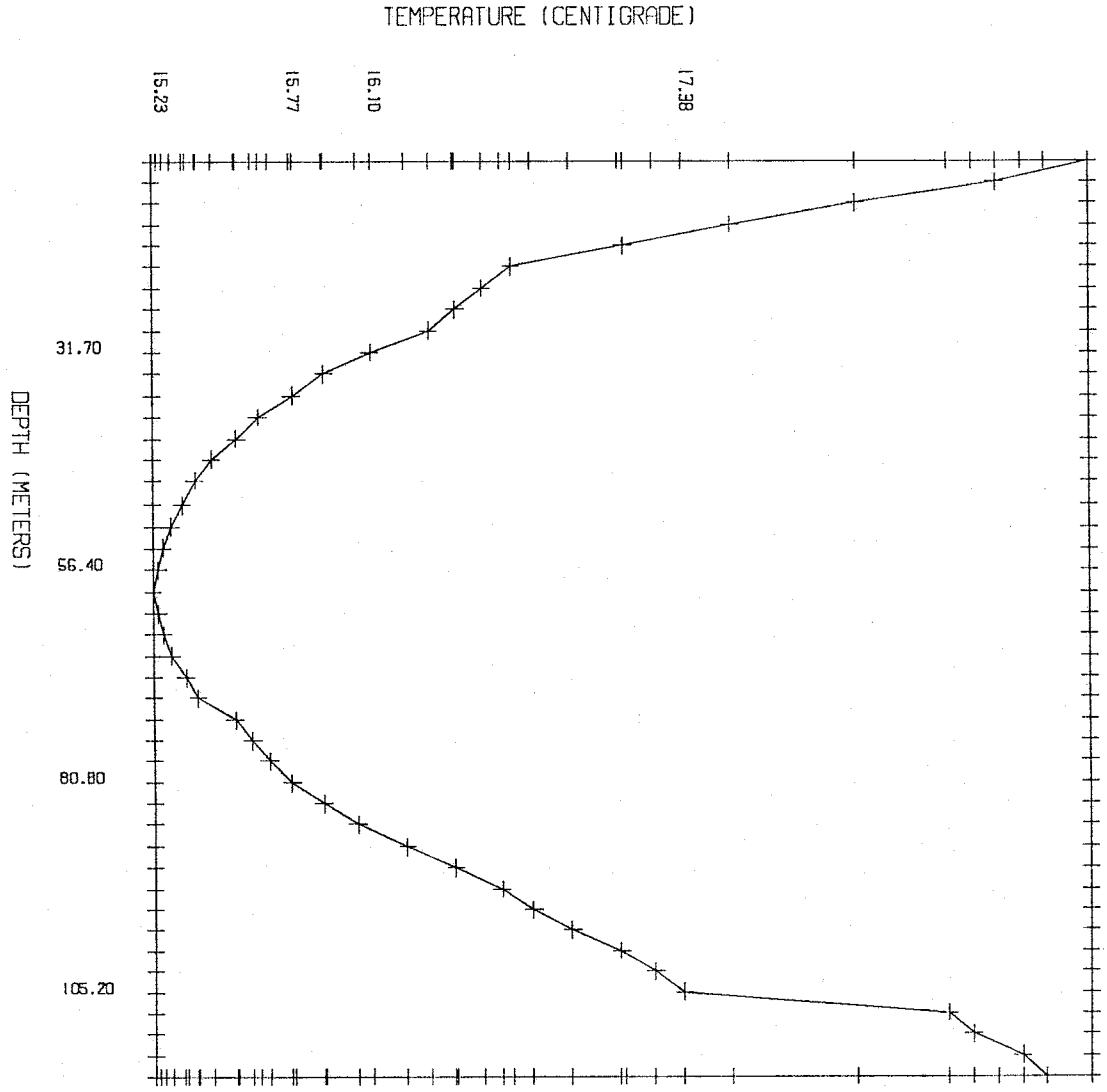

Los Alamos No. 15
lat. 35.27
long. 108.63
depth to water: not indicated

Thermal Conductivity data

depth interval (feet)	rock type
0- 15	sltstn
15- 40	ss
40- 45	sh
45- 54	ss
54- 85	sh
85- 87	ss
87- 95	sh
95- 97	ss
97- 98	sh
98- 99	ss
99-100	sh
100-102	ss
102-103	sh
103-104	ss
104-105	sh
105-107	ss
107-108	sh
108-110	ss
110-111	sh
111-112	ss
112-113	sh
113-114	ss
114-115	sh

Temperature Gradient data

depth (m)	temperature (degrees C)
2.40	16.83
4.90	16.71
9.80	11.62
12.20	11.43
14.60	11.46
17.10	11.54
19.50	11.63
21.90	11.71
24.40	11.79
29.30	11.94
33.50	12.09

LOS ALAMOS NO. 15

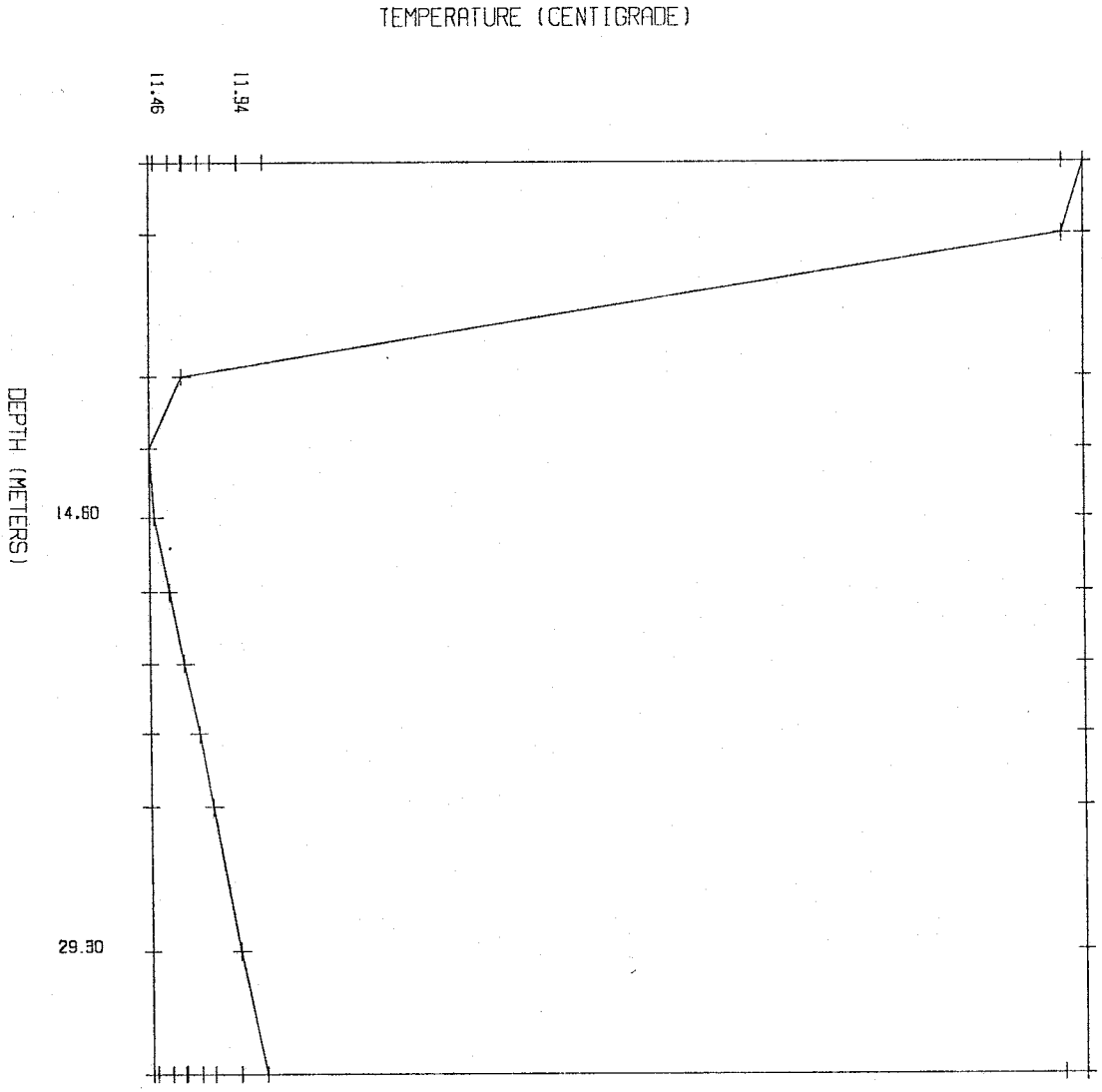

Los Alamos No. 18
lat. 35.23
long. 108.60
depth to water: not indicated

Thermal Conductivity data

depth interval (feet)	rock type
0- 35	ss
35-111	sh
111-112	coal
112-124.5	sh
124.5-125	coal
125-140	silty ss
140-155	sh

Temperature Gradient data

depth (m)	temperature (degrees C)
4.90	10.92
7.30	10.96
9.80	11.22
12.20	11.28
14.60	11.27
17.10	11.38
19.50	11.40
21.90	11.50
24.40	11.56
26.80	11.72
29.30	11.86
31.70	11.94
34.10	12.08
36.60	12.15
39.00	12.34
41.40	12.48
44.50	12.56

LOS ALAMOS NO. 18

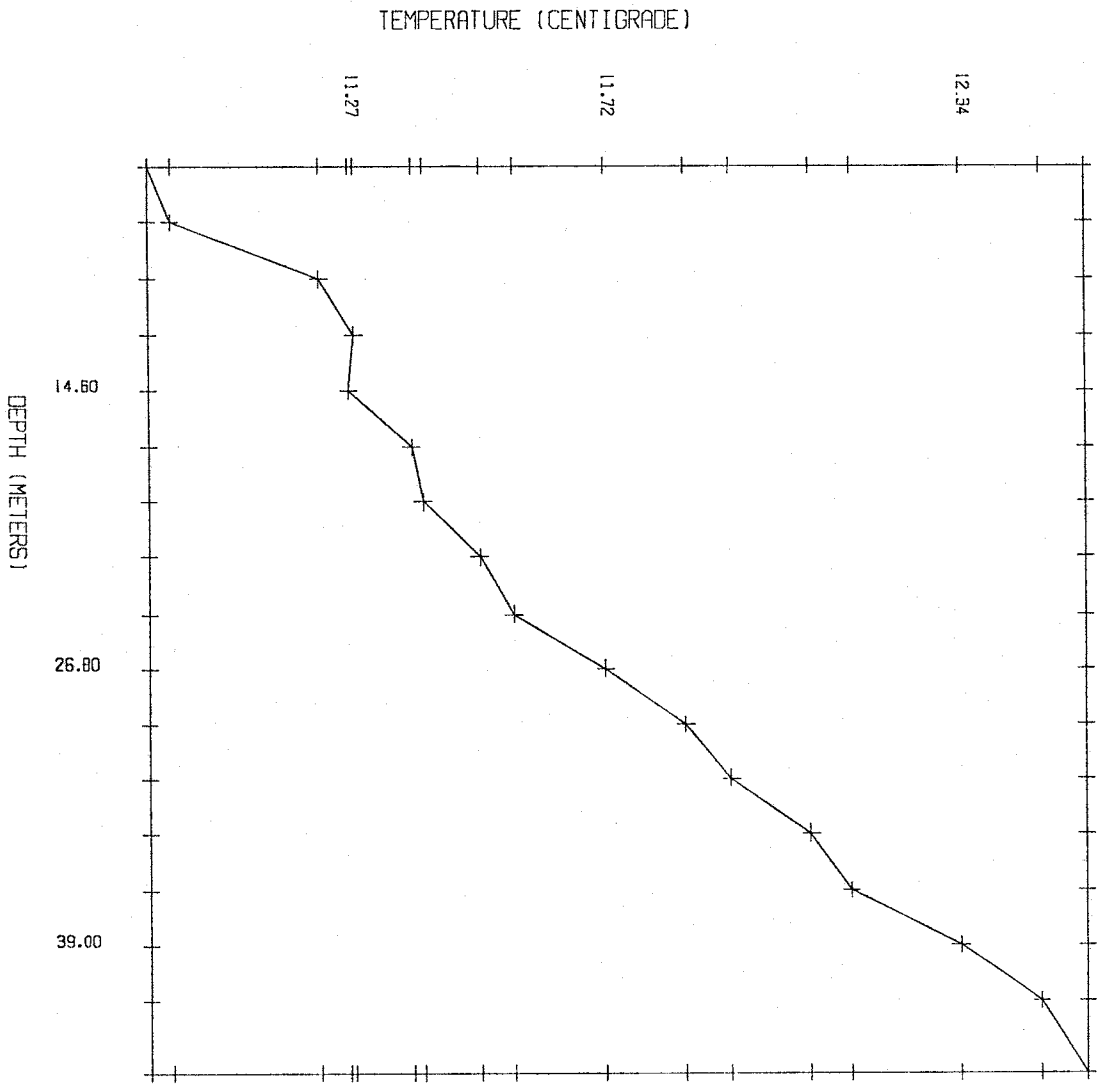

Los Alamos No. 20
lat. 35.59
long. 108.30
depth to water: 385 feet

Thermal Conductivity data

depth interval (feet)	rock type
0- 450	sh
450- 530	ss
530- 630	sandy sltstn
630- 790	ss
790- 800	sh
800- 810	ss
810- 830	sh
830- 850	ss
850- 860	sh
860- 870	ss
870- 880	sh
880- 900	ss
900-1160	ss
1160-1300	silty ss
1300-1340	ls
1340-1600	ss

Temperature Gradient data

depth (m)	temperature (degrees C)
12.20	15.06
24.40	13.04
36.60	12.88
48.80	12.76
61.00	12.74
73.20	12.86
85.30	13.04
97.50	13.20
103.60	13.41
109.70	13.69
115.80	13.87
121.90	14.50
128.00	14.65
134.10	14.83
140.20	15.01
146.30	15.19
152.40	15.38
158.50	15.66
164.60	15.99
170.70	16.33
176.80	16.82

182.90	17.64
189.00	18.43
195.10	18.42
201.20	18.90
207.30	19.15
213.40	19.34
219.50	19.60
225.60	19.79
231.60	19.98
237.70	20.10
243.80	20.20
249.90	20.32
256.00	20.38
262.10	20.39
268.20	20.44
274.30	20.49
280.40	20.70
286.50	20.89
292.60	20.98
298.70	21.10
304.80	21.10
310.90	21.20
317.00	21.40
323.10	21.39
329.20	21.50
335.30	21.62
341.40	21.84
347.50	21.95
353.60	22.07
359.70	22.19
365.80	22.35
371.90	22.52
378.00	22.57
384.00	22.65
390.10	22.78
396.20	22.82
402.30	22.91
408.40	22.98
414.50	23.05
420.60	23.11
426.70	23.11
432.80	23.16
438.90	23.23
445.00	23.31
451.10	23.52
457.20	23.64
463.30	23.76
469.40	23.82
475.50	23.87

LOS ALAMOS NO. 2C

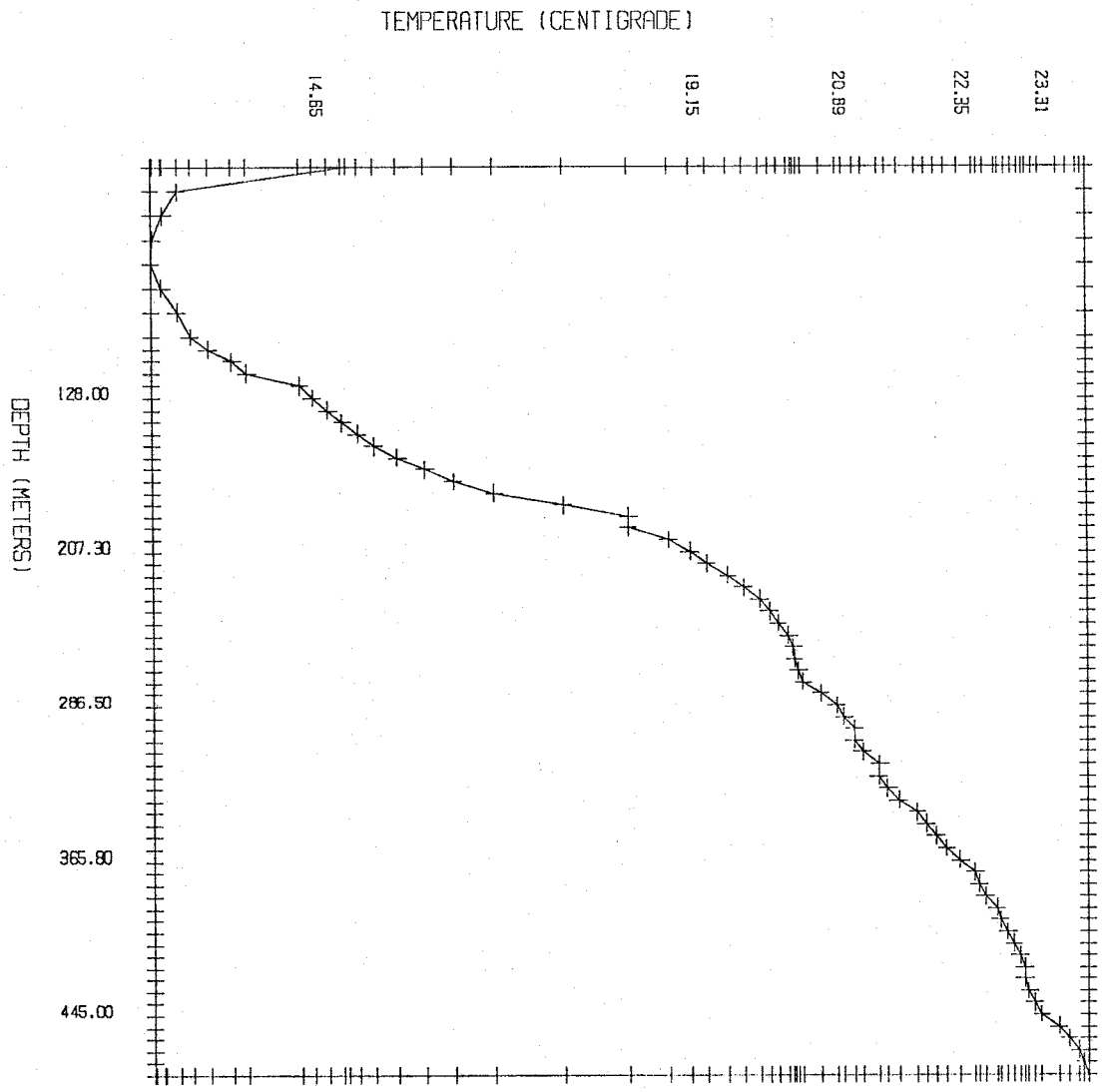

Los Alamos No. 21
lat. 35.59
long. 108.33
depth to water: not indicated

Thermal Conductivity data

depth interval (feet)	rock type
0- 450	sh
450- 700	ss
700- 760	conglom. ss
760-1280	silty ss
1280-1300	sh
1300-1340	silty ss
1340-1380	sh
1380-1420	silty ss
1420-1440	ls
1440-1600	ss

Temperature Gradient data

depth (m)	temperature (degrees C)
6.10	18.77
12.20	16.96
18.30	15.96
24.40	15.29
30.50	14.78
36.60	14.58
42.70	14.45
48.80	14.34
54.90	14.28
61.00	14.31
67.10	14.29
73.20	14.23
79.20	14.21
85.30	14.21
91.40	14.33
97.50	14.48
103.60	14.66
109.70	14.82
115.80	14.98
121.90	15.13
128.00	15.30
134.10	15.48
140.20	15.75
146.30	15.87
152.40	16.15
158.50	16.35
164.60	16.53

170.70	16.72
176.80	16.93
182.90	17.09
189.00	17.26
195.10	17.42
201.20	17.60
207.30	17.83
213.40	17.87
219.50	18.02
225.60	18.17
231.60	18.35
237.70	18.51
243.80	18.67
249.90	18.83
256.00	18.98
262.10	19.13
268.20	19.28
274.30	19.41
280.40	19.56
286.50	19.70
292.60	19.81
298.70	19.96
304.80	20.10
310.90	20.24
317.00	20.36
323.10	20.48
329.20	20.60
335.30	20.72
341.40	20.83
347.50	20.94
353.60	21.06
359.70	21.21
365.80	21.34
371.90	21.47
378.00	21.69
384.00	21.74
390.10	21.88
396.20	22.00
402.30	22.12
408.40	22.26
414.50	22.38
420.60	22.51
426.70	22.63
432.80	22.73
438.90	22.99
445.00	23.03
451.10	23.06
457.20	23.08
463.30	23.37
469.40	23.59
475.50	23.62
481.60	23.64

LOS ALAMOS NO. 21

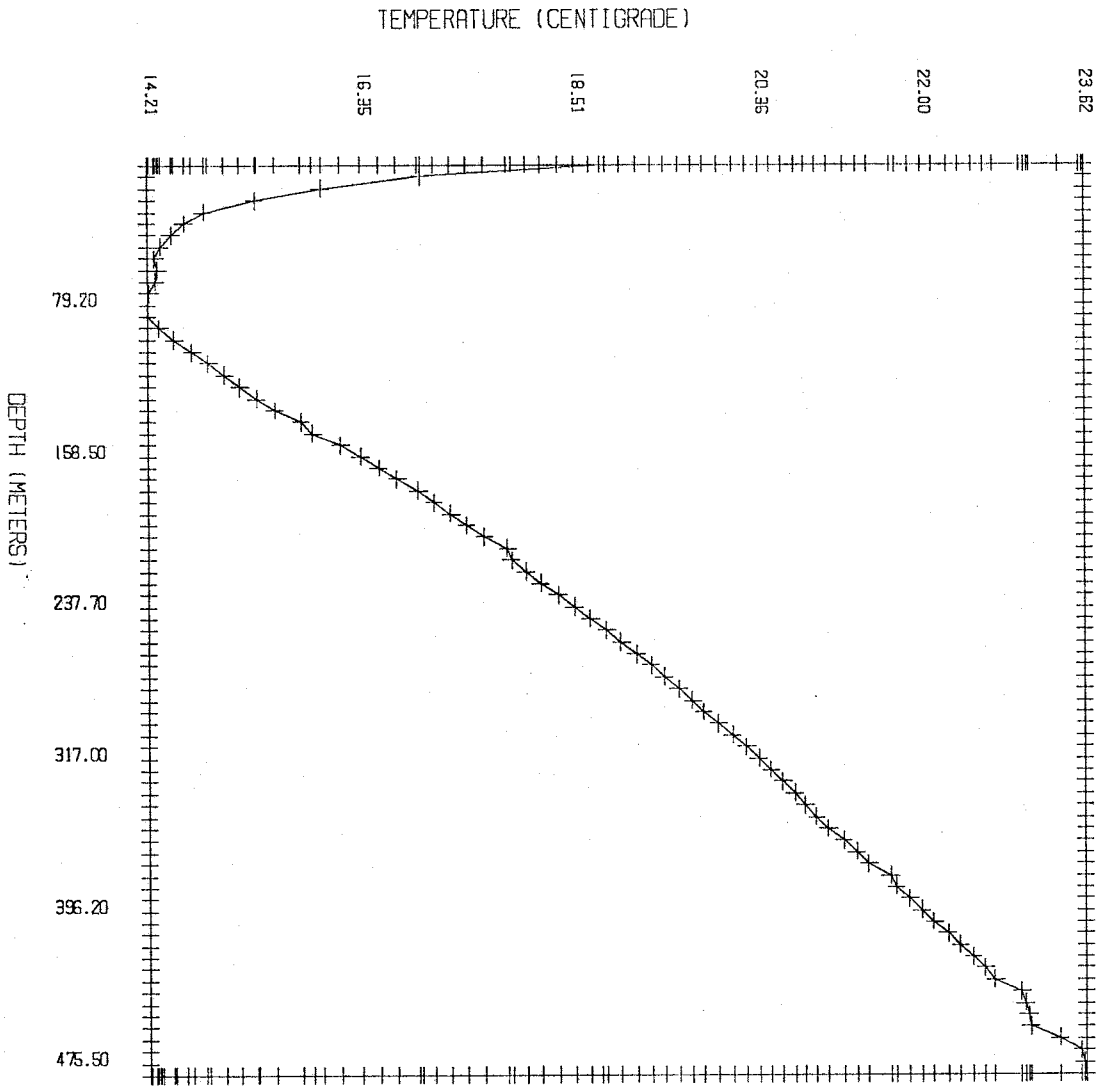

Los Alamos No. 24
lat. 35.49
long. 108.75
depth to water: 420 feet

Thermal Conductivity data

depth interval (feet)	rock type
0- 20	ss
20- 40	sh
40- 75	ss
75- 80	coal
80-115	sh
115-125	ss
125-195	sh
195-200	ss
200-230	sh
230-245	ss
245-265	sh
265-275	ss
275-290	sh
290-295	coal
295-325	ss
325-400	sh
400-440	ss

Temperature Gradient data

depth (m)	temperature (degrees C)
6.10	21.98
12.20	21.26
18.30	20.46
24.40	19.56
30.50	18.77
36.60	17.81
42.70	17.05
48.80	16.50
54.90	15.72
61.00	14.06
67.10	14.13
73.20	14.27
79.20	14.51
85.30	14.67
91.40	14.92
97.50	15.03
103.60	15.23
109.70	15.41
115.80	15.62

121.90	15.82
125.00	15.89
128.00	16.07
131.10	16.21

LOS ALAMOS NO. 21

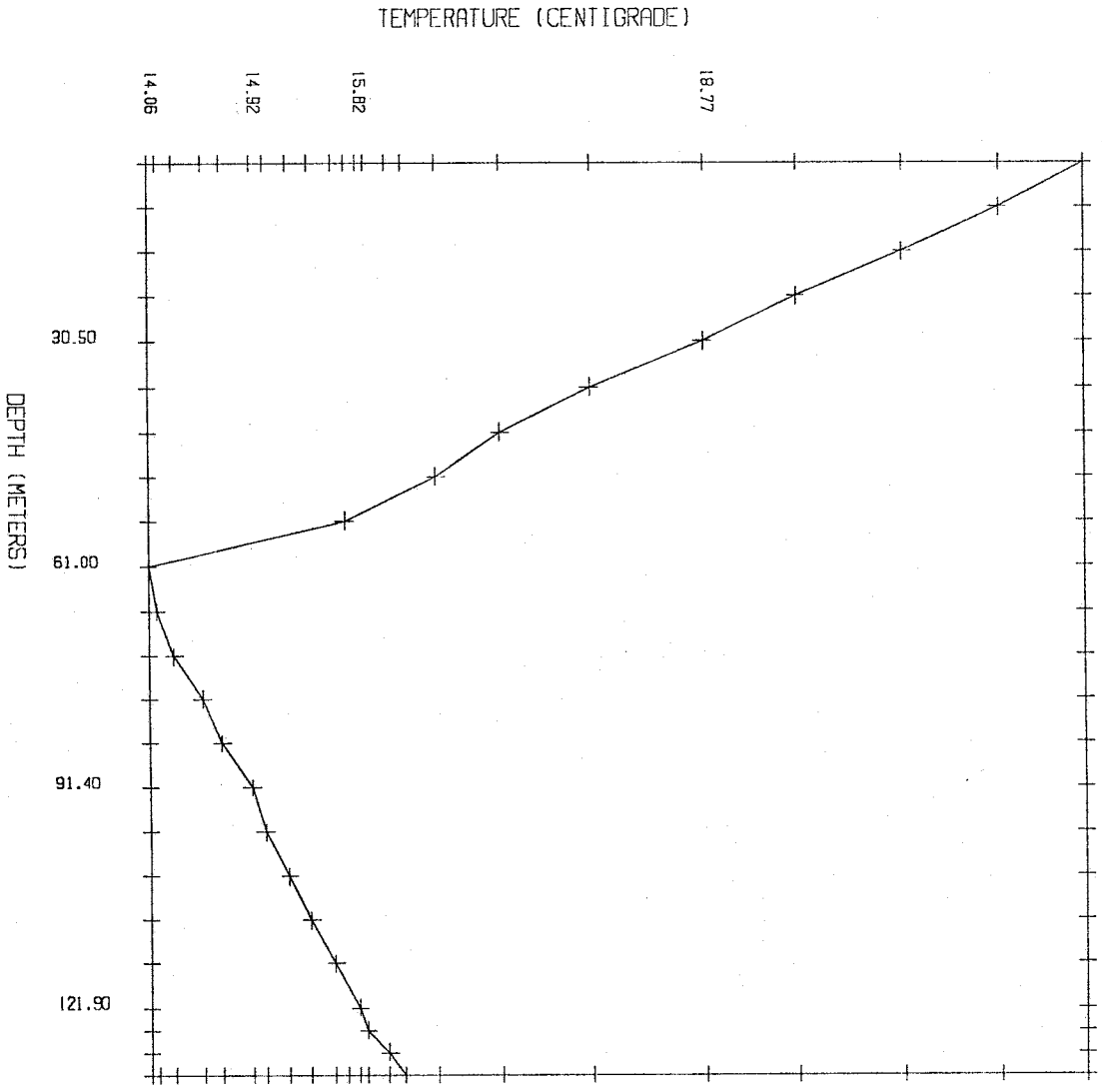

Los Alamos No. 25
lat. 35.50
long. 108.67
depth to water: not indicated

Thermal Conductivity data

depth interval (feet)	rock type
0- 45	sh
45- 50	ss
50-165	sh
165-190	ss
190-285	sh
285-290	coal
290-395	sh
395-425	ss

Temperature Gradient data

depth (m)	temperature (degrees C)
4.90	16.17
9.80	15.08
14.60	14.90
19.50	14.78
24.40	14.68
29.30	14.58
34.10	14.44
39.00	14.32
43.90	14.28
49.10	14.28
53.90	14.34
58.80	14.50
63.70	14.69
68.60	14.90
73.50	15.18
78.30	15.45
83.20	15.69
88.10	15.86
93.00	15.99
97.80	16.17
102.70	16.20
107.60	16.29
112.50	16.33
117.30	16.34
122.20	16.35
127.10	16.40

LOS ALAMOS NO. 25

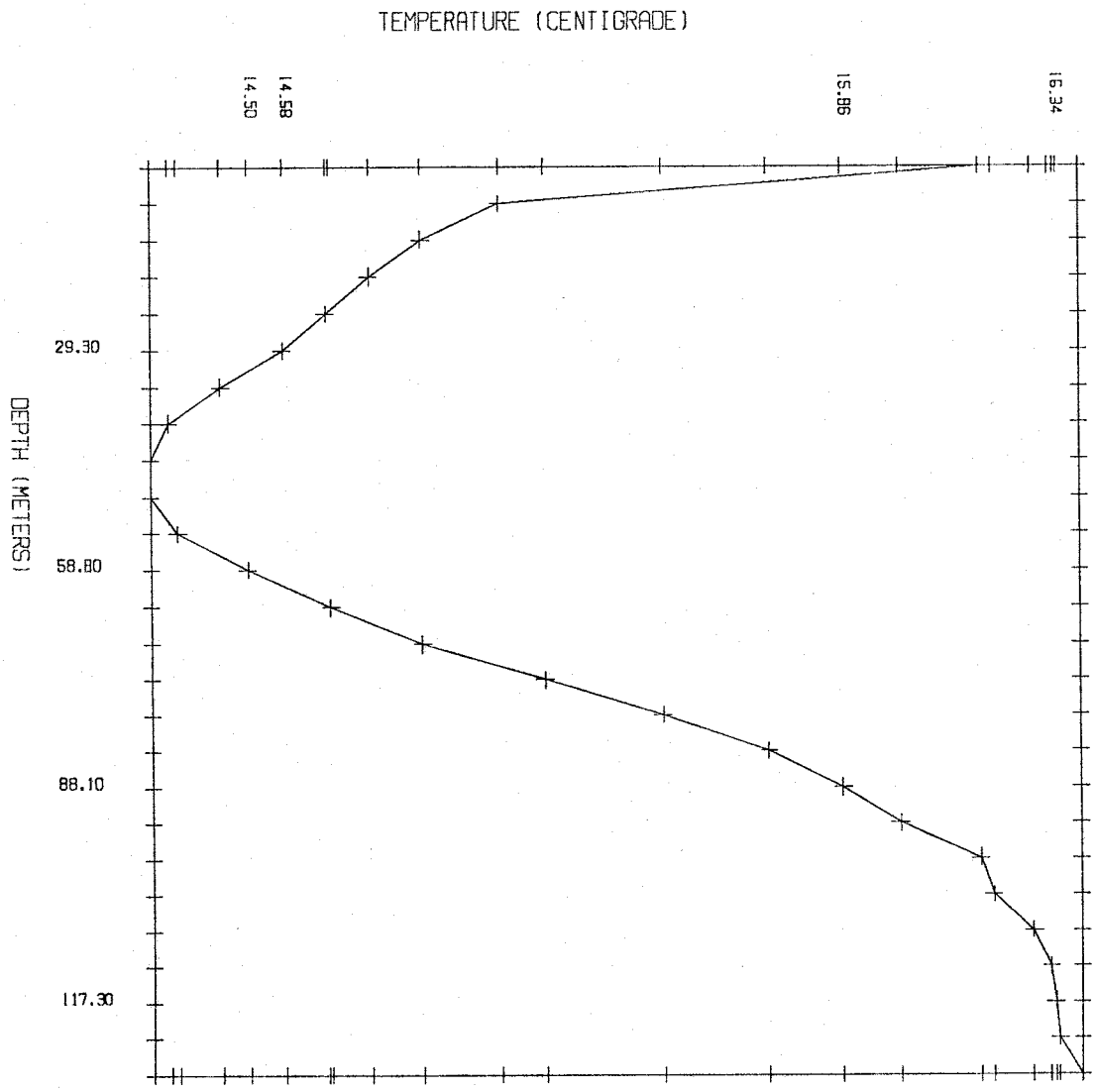

Los Alamos No. 26
lat. 35.54
long. 108.60
depth to water: 140 feet

Thermal Conductivity data

depth interval (feet)	rock type
0- 60	conglom
60-240	ss
240-270	sh
270-275	ss
275-280	sh
280-285	ss
285-290	sh
290-297	ss
297-300	sh
300-305	ss
305-320	sltstn
320-330	ss
330-360	sltstn
360-365	ss
365-370	sh
370-377	ss
377-380	sh
380-390	ss
390-397	sh
397-400	ss
400-420	sltstn
420-440	sh
440-445	ss
445-465	sh
465-470	ss
470-480	sh
480-485	ss
485-490	sh
490-500	ss
500-515	sh
515-520	ss
520-525	sh
525-530	ss
530-545	sltstn
545-560	sh
560-565	ss
565-580	sh
580-590	sltstn
590-605	sh
605-610	ss
610-620	sh

Temperature Gradient data

depth (m)	temperature (degrees C)
6.10	16.84
12.20	16.42
18.30	16.62
30.50	17.13
42.70	17.09
48.80	17.13
54.90	17.40
61.00	17.68
67.10	17.91
73.20	18.30
79.20	18.56
85.30	18.99
91.40	19.37
97.50	19.59
103.60	19.88
109.70	20.17
115.80	20.46
121.90	20.77
128.00	21.07
134.10	21.32
140.20	21.41
146.30	21.64
152.40	21.76
158.50	21.86
164.60	22.01
170.70	22.09
176.80	22.31
182.90	22.44

LOS ALAMOS NO. 26

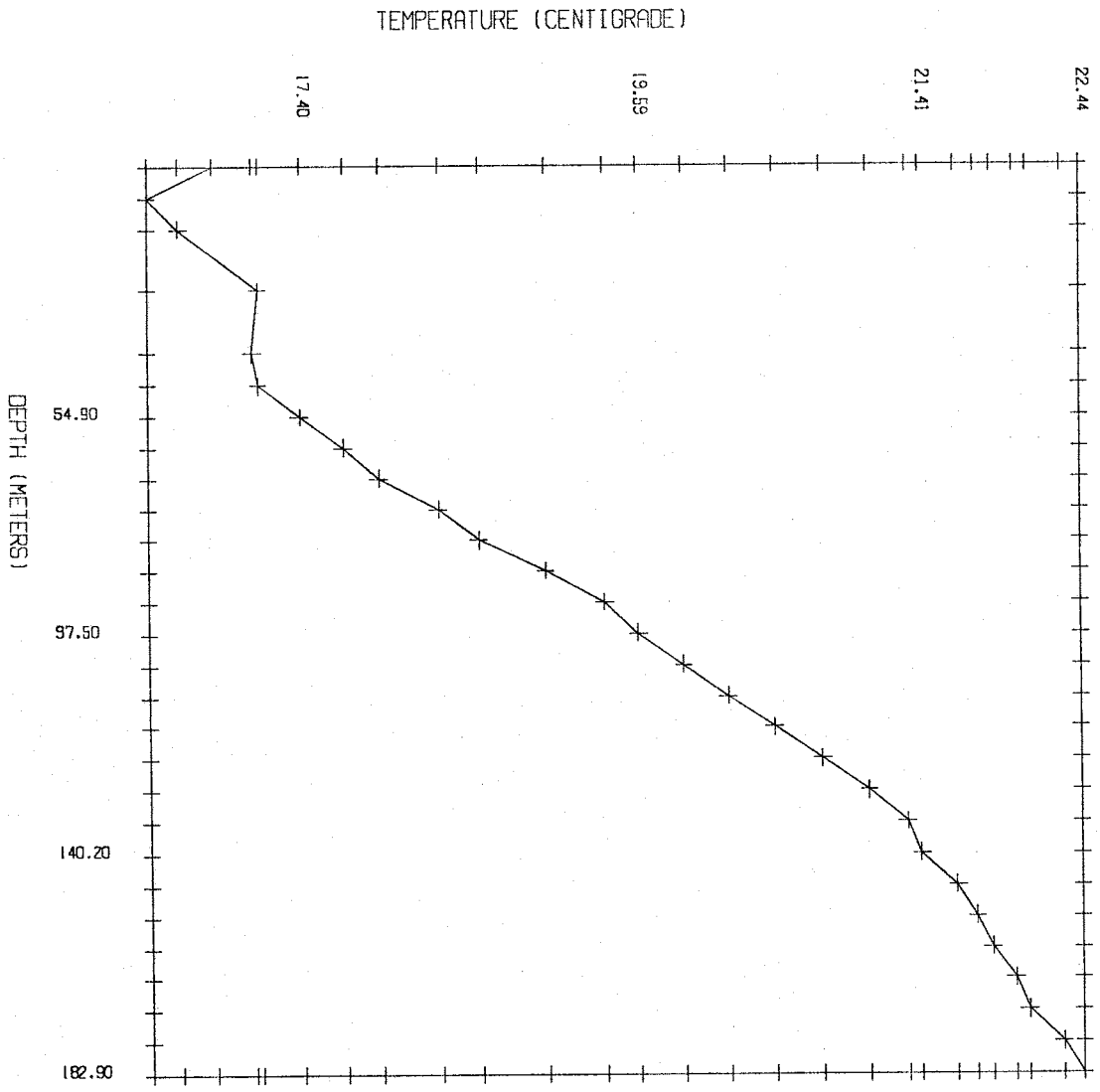

Los Alamos No. 28
lat. 35.50
long. 108.21
depth to water: 1200 feet

Thermal Conductivity data

depth interval (feet)	rock type
0- 40	sh
40- 200	ss
200- 340	sandy sltstn
340- 520	ss
520-1100	sandy shale
1100-1120	ls
1120-1280	ss
1280-1340	sh
1340-1360	ss
1360-1380	sh
1380-1400	ss
1400-1460	sh
1460-1490	ss
1490-1510	sh
1510-1550	ss
1550-1600	sh
1600-1640	ss
1640-1660	sh
1660-1690	ss
1690-1700	sh
1700-1720	ss
1720-1760	sh
1760-1810	ss
1810-1870	sh
1870-1890	ss
1890-1920	sh
1920-1950	ss
1950-1970	sh
1970-2000	ss
2000-2050	sh
2050-2080	ss
2080-2160	sh
2160-2180	ss
2180-2240	sh
2240-2270	ss
2270-2340	sh
2340-2360	ss
2360-2400	sh
2400-2420	ss
2420-2450	sh
2450-2470	ss
2470-2480	sh
2480-2500	ss
2500-2530	sh
2530-2550	ss

2550-2610	sh
2610-2650	ss

Temperature Gradient data

depth (m)	temperature (degrees C)
12.20	14.26
24.40	13.55
36.60	13.43
48.80	13.22
61.00	13.55
73.10	14.05
85.30	14.16
97.50	14.35
109.70	14.74
121.90	14.98
134.10	15.25
146.30	15.75
158.50	15.98
170.70	16.21
182.90	16.87
195.10	17.06
213.40	17.56
219.50	17.66
225.50	17.68
274.30	18.14
335.30	19.72
371.90	20.45
396.20	20.90
426.70	22.24
438.90	22.79
451.10	23.05
463.30	23.46
475.50	23.98
487.70	24.48
493.80	24.65
499.90	24.81
506.00	25.02
512.10	25.24
518.20	25.48
524.30	25.72
530.30	25.96
536.40	26.04
542.50	26.25
548.60	26.50
554.70	26.65
560.80	27.00
566.90	27.40
573.00	27.58
579.10	27.73
585.20	27.81
591.30	28.27
597.40	28.41
603.50	28.69
609.60	28.94
615.70	29.17

621.80	29.38
627.90	29.62
634.00	29.93
640.10	30.16
646.20	30.45
652.30	30.72
658.40	31.01
664.50	31.23
670.60	31.43
676.70	31.64
682.70	31.84
688.80	31.98
694.90	32.20
701.00	32.34
707.10	32.46
713.20	32.63
719.30	32.86
725.40	33.17
731.50	33.60
737.60	33.96
743.70	34.22
749.80	34.48
755.90	34.72
762.00	34.96
768.10	35.14
774.20	35.41
780.30	35.71
786.40	36.02
792.50	36.27

LOS ALAMOS NO. 28

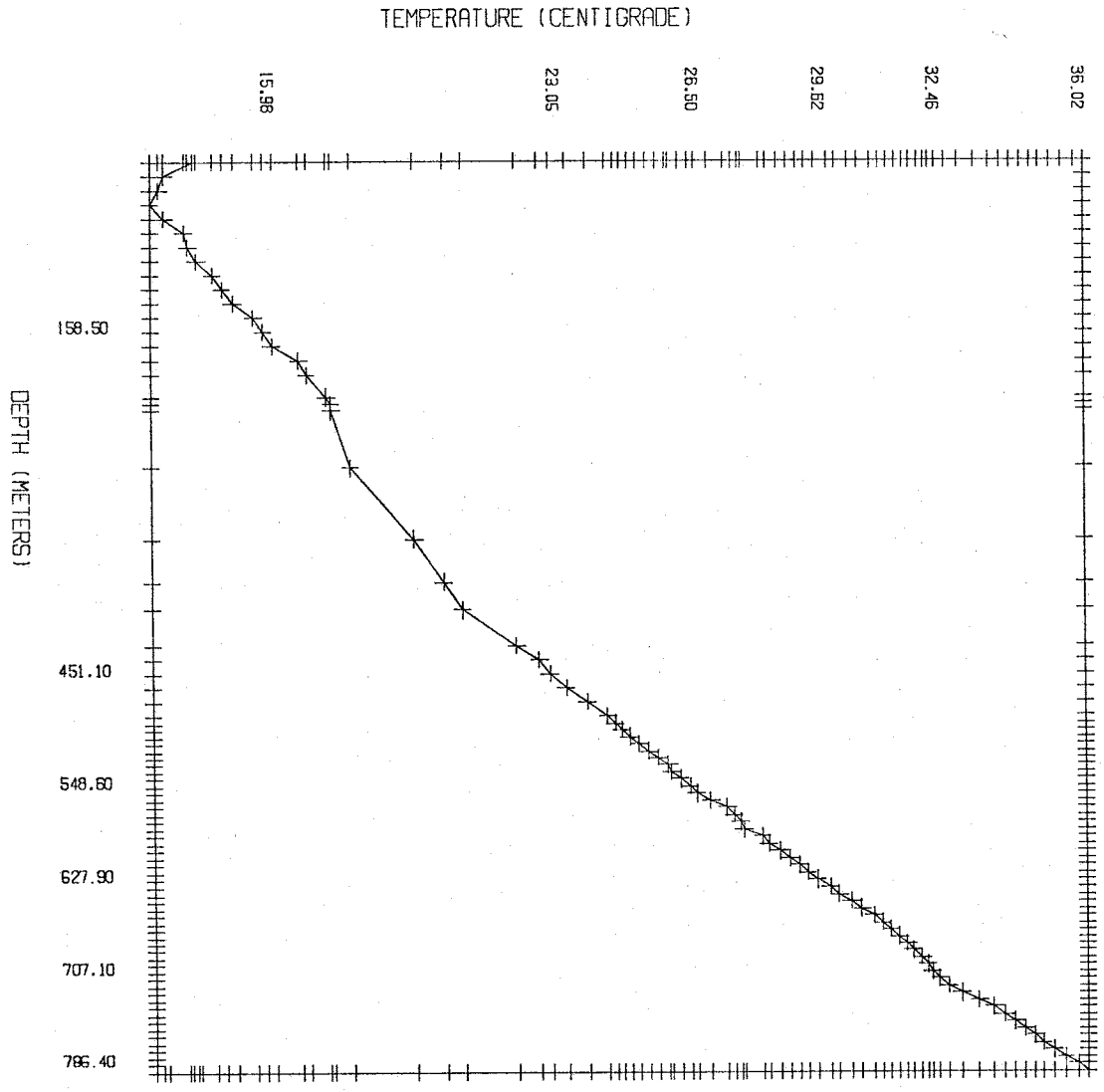

Los Alamos No. 29
lat. 35.53
long. 108.12
depth to water: 340 feet

Thermal Conductivity data

depth interval (feet)	rock type
0- 610	sh
610- 850	ss
850- 920	sandy sh
920- 960	silty ss
960-1010	conglom ss
1010-1020	silty ss
1020-1090	conglom ss
1090-1130	sltstn
1130-1160	ss
1160-1180	sh
1180-1200	ss
1200-1210	sltstn
1210-1220	ss
1220-1260	sh
1260-1280	ss
1280-1290	sltstn
1290-1300	ss
1300-1400	ss
1400-1440	silty ss
1440-1490	ss
1490-1550	silty ss
1550-1600	sh
1600-1640	silty ss
1640-1670	sh
1670-1680	ss
1680-1700	sh
1700-1760	silty ss
1760-1910	ls
1910-1980	ss

Temperature Gradient data

depth (m)	temperature (degrees C)
6.10	24.58
12.20	22.18
18.30	19.28
24.40	17.96
30.50	16.80
36.60	16.48
42.70	15.53
48.80	15.02

54.90	14.65
61.00	14.56
67.10	14.54
73.20	14.55
79.20	14.56
85.30	14.57
91.40	14.60
97.50	14.67
103.60	15.43
109.70	16.08
115.80	16.29
121.90	16.57
128.00	16.85
134.10	17.11
140.20	17.35
146.30	17.62
152.40	17.81
158.50	17.98
164.60	18.12
170.70	18.28
176.80	18.45
182.90	18.63
189.00	18.74
195.10	18.86
201.20	18.97
207.30	19.08
213.40	19.20
219.50	19.31
225.60	19.38
231.60	19.44
237.70	19.56
243.80	19.70
249.90	19.81
256.00	19.95
262.10	20.13
268.20	20.30
274.30	20.58
280.40	20.87
286.50	20.89
292.60	21.06
298.70	21.26
304.80	21.47
310.90	21.60
317.00	21.77
323.10	21.94
329.20	22.20
335.30	22.28
341.40	22.30
347.50	22.44
353.60	22.64
359.70	22.79
365.80	22.98
371.90	23.13
378.00	23.29
384.00	23.39
390.10	23.55
396.20	23.76
402.30	23.88
408.40	23.96
414.50	24.03

420.60	24.15
426.70	24.25
432.80	24.35
438.90	24.48
445.00	24.60
451.10	24.69
457.20	24.78
463.30	24.96
469.40	25.04
475.50	25.15
481.60	25.28
487.70	25.44
493.80	25.59
499.90	25.74
506.00	25.95
512.10	26.10
518.20	26.20
524.30	26.27
530.40	26.52
536.40	26.67
542.50	26.68
548.60	26.70
554.70	26.72
560.80	26.82
566.90	27.07
573.00	27.20
579.10	27.23
585.20	27.24
591.30	27.26

LOS ALAMOS NO. 29

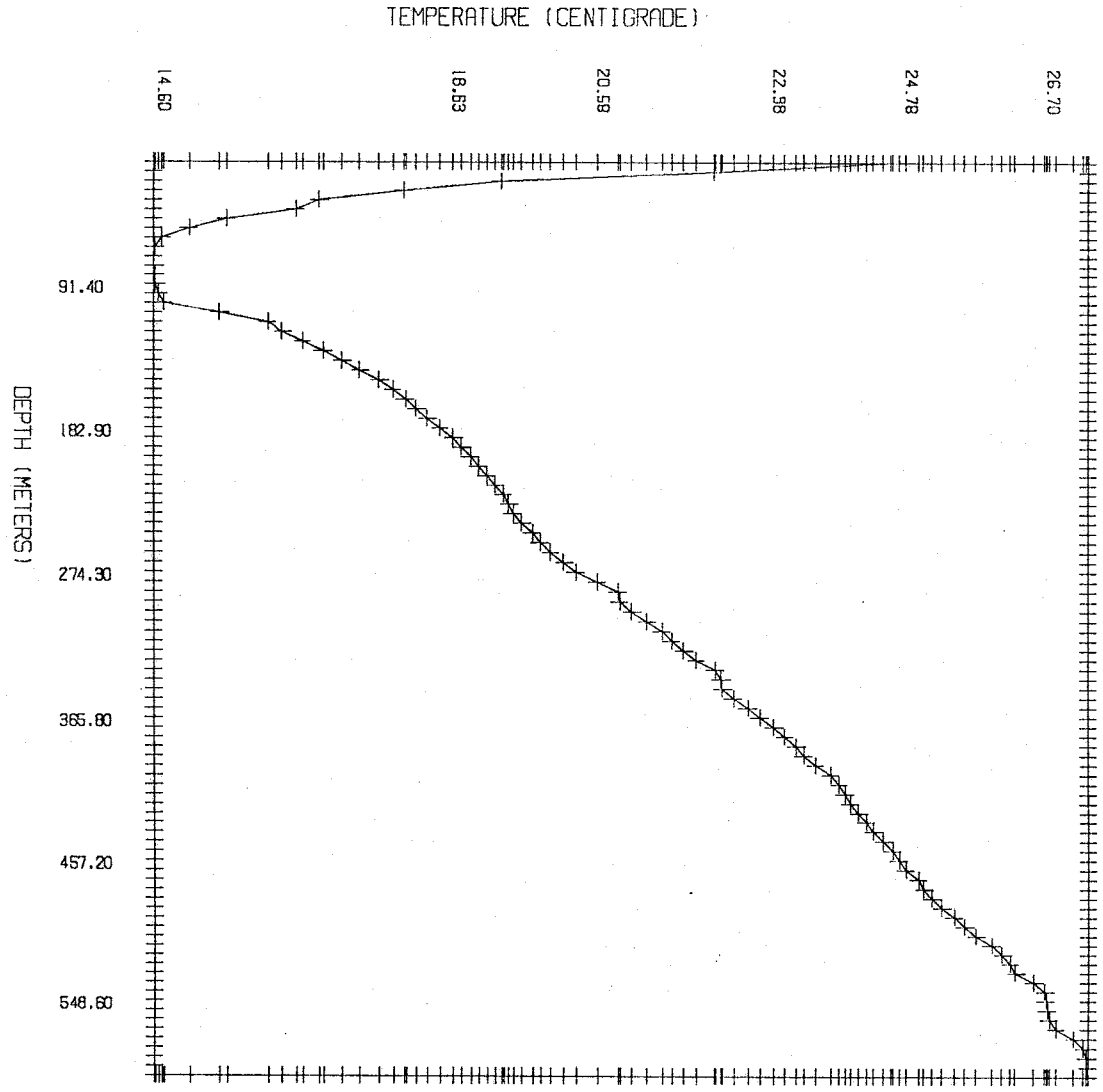

REFERENCES

Aldrich, M.J., Chapin, C.E., Laughlin, A.W. and Zoback, M.L., 1987, Colorado Plateau Oligocene to Quaternary stress history, Geol. Soc. Amer. Abstracts with Programs, 19, p. 569.

Aldrich, M.J. and Laughlin, A.W., 1984, A model for the tectonic development of the southeastern Colorado Plateau boundary, J. Geophys. Res., 89, 10,207-10,218.

Allen, J.E. and Balk, R., 1954, Mineral resources of Fort Defiance and Tohatchi quadrangles, Arizona and New Mexico, New Mexico Bur. Mines Mineral Resources Bull., 36, 192 p.

Ander, M.E., Goss, R. and Strangway, D.W., 1984, A detailed magnetotelluric/audiomagnetotelluric study of the Jemez volcanic zone, New Mexico, J. Geophys. Res., 89, 3335-3353.

Ander, M.E. and Heustis, S.P., 1982, Mafic intrusion beneath the Zuni-Bandera volcanic field, New Mexico, Geol. Soc. Amer. Bull., 93, 1142-1150.

Anderson, O.J., 1982, Geology and coal resources of Mesita de Yeso quadrangle, Cibola County, New Mexico, New Mexico Bur. Mines Mineral Resources Open-File Rep., 171, 31 p.

Anderson, O.J., 1983, Geology and coal resources of the Atarque Lake quadrangle, Cibola County, New Mexico, New Mexico Bur. Mines Mineral Resources Open-File Rep., 167, 26 p.

Anderson, O.J. and Frost, S.J., 1982, Geology and coal resources of the Twenty-two Spring 7.5' quadrangle, Catron and Cibola Counties, New Mexico, New Mexico Bur. Mines Mineral Resources Open-File Rep., 143, 6 p.

Anderson, O.J. and Mapel, W.J., 1983, Geology and coal resources, Shoemaker Canyon SE quadrangle, Cibola County, New Mexico, New Mexico Bur. Mines Mineral Resources Open-File Rep., 172, 34 p.

Armstrong, R.L., 1969, K-Ar dating of laccolithic centers of the Colorado Plateau and vicinity, Geol. Soc. Amer. Bull., 80, 2081-2086.

Aubele, J.C., Crumpler, L.S. and Shafiqullah, M., 1986, K-Ar ages of late Cenozoic rocks of the central and eastern parts of the Springerville volcanic field, east-central Arizona, Isochron/West, 46, 3-5.

Axelrod, D.I. and Bailey, H.P., 1976, Tertiary vegetation, climate, and altitude of the Rio Grande depression, New Mexico-Colorado, Paleobiology, 2, 235-254.

Baldridge, W.S., 1979, Lineament tectonics and the role of pre-existing structure on the Rio Grande rift, EOS, 60, p. 954.

Baldridge, W.S., Bartov, Y. and Kron, A., 1983, Geologic map of the Rio Grande rift and southeastern Colorado Plateau. New Mexico and Arizona, Amer. Geophys. U., 1:500,000

Berkowitz, N., 1979, An introduction to coal technology, Academic Press, New York, 345 p.

Bikerman, M., 1972, New K-Ar ages on volcanic rocks from Catron and Grant Counties, New Mexico, Isochron/West, 9-12.

Birch, F., 1948, The effects of Pleistocene climatic variations upon geothermal gradients, Amer. J. Sci., 246, 729-760.

Birch, F., 1950, Flow of heat in the Front Range, Colorado, Geol. Soc. Amer. Bull., 61, 567-630.

Bird, P., 1979, Continental delamination and the Colorado Plateau, J. Geophys. Res., 84, 7561-7571.

Bodell, J.M. and Chapman, D.S., 1982, Heat flow in the north-central Colorado Plateau, J. Geophys. Res., 87, 2869-2884.

Boyle, J.M. and Saleem, Z.A., 1979, Determination of recharge rates using temperature-depth profiles in wells, Water Resources Res., 15, 1616-1622.

Bradbury, J.P., 1966, Pleistocene-Recent geologic history of Zuni Salt Lake, New Mexico, New Mexico Geol. Soc. Gdbk., 17th Field Conf., 119.

Bredehoeft, J.D. and Papadopoulos, I.S., 1965, Rates of vertical groundwater movement estimated from the earth's thermal profile, Water Resources Res., 1, 325-328.

Brown, T.L. and Lemay, H.E., 1977, Chemistry, Prentice-Hall, Englewood Cliffs, NJ, 815 p.

Callender, J.F., Seager, W.R. and Swanberg, C.A., 1983, Late Tertiary and Quaternary tectonics and volcanism, map, New Mexico State Univ. Energy Inst., Las Cruces.

Campbell, F., 1981, Geology and coal resources of Cerro Prieto and The Dyke quadrangles, New Mexico Bur. Mines Mineral Resources Open-File Rep., 144, 44 p.

Campbell, F., 1984, Geology and coal resources of Cerro Prieto and The Dyke quadrangles, Cibola and Catron Counties, New Mexico, New Mexico Geology, February, 6-10.

Campbell, F. and Roybal, G.H., 1984, Geology and coal resources of the Fence Lake 1:50,000 quadrangle, Catron and Cibola Counties, New Mexico, New Mexico Bur. Mines Mineral Resources Open-File Rep., 207, 34 p.

Carslaw, H.S. and Jaeger, J.C., 1959, Conduction of heat in solids, Oxford Univ. Press, Oxford, 510 p.

Cather, S.M. and Johnson, B.D., 1984, Eocene tectonics and depositional setting of west-central New Mexico and eastern Arizona, New Mexico Bur. Mines Mineral Resources Circ., 192, 33 p.

Cather, S.M., McIntosh, W.C. and Chapin, C.E., 1987, Stratigraphy, age, and rates of deposition of the Datil Group (Upper Eocene-Lower Oligocene), west-central New Mexico, New Mexico Geology, 9, 50-54.

Chamberlin, R.M., 1981, Uranium potential of the Datil Mountains-Pietown area, Catron County, New Mexico, New Mexico Bur. Mines Mineral Resources Open-File Rep. 138, 51 p.

Chapman, D.S., Howell, J. and Sass, J.H., 1984, A note on drillhole depths required for reliable heat flow deter minations, Tectonophysics, 103, 11-18.

Chapin, C.E. and Cather, S.M., 1983, Eocene tectonics and sedimentation in the Colorado Plateau-Rocky Mountain area, in, Rocky Mountain Foreland Basins and Uplifts, J.D. Lowell, ed., Rocky Mtn. Assoc. Geol., Denver, 33-56.

Chapin, C.E., Chamberlin, R.M., Osburn, G.R., White, D.W. and Sanford, A.R., 1978, Exploration framework of the Socorro geothermal area, New Mexico, New Mexico Geol. Soc. Spec. Publ., 7, 114-129.

Chapin, C.E., Osburn, G.R., Hook, S.C., Massingill, G.L. and Frost, S.J., 1979, Coal, uranium, oil and gas potential of the Riley-Puertocito area, Socorro County, New Mexico, New Mexico Bur. Mines Mineral Resources Open-File Rep., 103, 38 p.

Chapin, C.E. and Seager, W.R., 1975, Evolution of the Rio Grande rift in the Socorro and Las Cruces areas, New Mexico Geol. Soc. Gdbk., 26th Field Conf., 297-321.

Chapman, D.S. and Pollack, H.N., 1977, Regional geotherms and lithospheric thickness, Geology, 5, 265-268.

Clark, S.P., 1966, Thermal conductivity, Geol. Soc. Amer. Mem., 97, 459-482.

Clarkson, G.W., 1984, Implications for thermal histories of the San Juan Basin and San Juan Mountains since late Cretaceous time, Ph.D. diss., New Mexico Institute of Mining and Technology, Socorro, 107 p.

Clauser, C., 1984, A climatic correction on temperature gradients using surface-temperature series of various periods, Tectonophysics, 103, 33-46.

Davis, G.H., 1978, Monocline fold pattern of the Colorado Plateau, Geol. Soc. Amer. Mem., 151, 215-233.

Decker, E.R. and Birch, F., 1974, Basic data for Colorado, New Mexico and Texas, U.S. Geol. Surv. Open-File Rep., 74-9, 5-1 - 5-59.

De Vries, D.A., 1958, Simultaneous transfer of heat and moisture in porous media, Trans. Amer. Geop. Union, 39, 909-916.

Dixon, W.J. and Massey, F.J., 1983, Introduction to statistical analyses, 4 ed., McGraw-Hill, New York.

Donaldson, I.G., 1962, Temperature gradients in the upper layers of the earth's crust due to convective water flows, J. Geophys. Res., 67, 3449-3459.

Dow, W., 1977, Kerogen studies and geological interpretations, J. Geochem. Expl., 7, 79-99.

Drury, M.J., 1984, Perturbations to temperature gradients by water flow in crystalline rock formations, Tectonophysics, 102, 19-32.

Eardley, A.J., 1962, Structural geology of North America, Harper and Row, New York, 743 p.

Eaton, G.P., 1979, A plate-tectonic model for late Cenozoic crustal spreading in the western United States, in, Rio Grande rift: tectonics and magmatism, R.E. Riecker, ed., Amer. Geophys. U., Washington, D.C., 7-32.

Eaton, G.P., 1986, A tectonic redefinition of the Southern Rocky Mountains, Tectonophysics, 132, 163-193.

Eggleston, R.E. and Reiter, M., 1984, Terrestrial heat-flow estimates from petroleum bottom-hole temperature data in the Colorado Plateau and the eastern Basin and Range province, Geol. Soc. Amer. Bull., 95, 1027-1034.

Elston, W.E., Rhodes, R.C., Coney, P.J. and Deal, E.G., 1976, Progress report on the Mogollon Plateau volcanic field, southwestern New Mexico, No. 3 - surface expression of a pluton, New Mexico Geol. Soc. Spec. Publ., 5, 3-28.

Fassett, J.E. and Hinds, J.S., 1971, Geology and fuel resources of the Fruitland Formation and Kirtland shale of the San Juan Basin, New Mexico and Colorado, U.S. Geol. Surv. Prof. Pap., 676, 76 p.

Fenwal Electronics, 1978, Isocurve thermistors catalog L-2B, Framingham, MA.

Fieldner, A.C., Cooper, H.M. and Osgood, F.D., 1936, Analyses of mine samples, U.S. Bur. Mines Tech. Pap., 569, 40-63.

Freeze, R.A. and Cherry, J.A., 1979, Groundwater, Prentice Hall, Englewood Cliffs, New Jersey, 604 p.

Frost, S.J., Tabet, D.E. and Campbell, F.W., 1979, Coal exploratory drilling in the Datil Mountains coal field, New Mexico Bur. Mines Mineral Resources Open-File Rep., 111, 49 p.

Gilluly, J., Waters, A.C. and Woodford, A.O., 1975, Principles of Geology, 4th ed., W.H. Freeman and Co., San Francisco.

Graybill, F.A., 1961, An introduction to linear statistical models, McGraw-Hill, New York.

Guilinger, D.R., 1982, Geology and uranium potential of the Tejana Mesa-Hubbell Draw area, Catron County, New Mexico, New Mexico Bur. Mines Mineral Resources Open-File Rep., 176, 129 p.

Heroux, Y., Chagnon, A. and Bertrand, R., 1979, Compilation and correlation of major thermal maturation indicators, Amer. Assoc. Petr. Geol. Bul., 63, 2128-2144.

Hook, S.C., 1983, Contributions to mid-Cretaceous paleontology and stratigraphy of New Mexico--part II, New Mexico Bureau of Mines and Mineral Resources Circular 185.

Jaeger, J.C., 1961, The effect of the drilling fluid on temperatures measured in bore holes, J. Geophys. Res., 66, 563-569,

Jaeger, J.C., 1964, Thermal effects of intrusion, Rev. Geophys. Space Phys., 2, 443-466.

Jeffreys, H., 1938, The disturbance of the temperature gradient in the earth's crust by inequalities of height, Monthly Notices Roy. Astron. Soc. Geophys. Suppl., 4, 309-312.

Keller, G.R., Braile, L.W. and Morgan, P., 1979a, Crustal structure, geophysical models and contemporary tectonism of the Colorado Plateau, Tectonophysics, 61, 131-147.

Kelley, V.C., 1955, Regional tectonics of the Colorado Plateau and relationship to the origin and distribution of uranium, Univ. New Mexico Press, Albuquerque, 120 p.

Kelley, V.C., 1979, Tectonics of the Colorado Plateau and new interpretation of its eastern boundary, Tectono physics, 61, 97-102.

Lachenbruch, A.H. and Brewer, M.C., 1959, Dissipation of the temperature effect of drilling a well in Arctic Alaska, U.S. Geol. Surv. Bull., 1083-C, 73-109.

Lachenbruch, A.H. and Sass, J.H., 1977, Heat flow in the United States and the thermal regime of the crust, Amer. Geophys. U. Mono., 20, 626-675.

Lachenbruch, A.H., Sass, J.H., Munroe, R.J. and Moses, T.H., Jr., 1976, Geothermal setting and simple heat conduction models for the Long Valley caldera, J. Geophys. Res., 81, 769-784.

Laughlin, A.W., Aldrich, M.J., Ander, M.E., Heiken, G.H. and Vaniman, D.T., 1982, Tectonic setting and history of late Cenozoic volcanism in west-central New Mexico, New Mexico Geol. Soc. Gdbk., 33rd field conff., 279-284.

Laughlin, A.W., Aldrich, M.J. and Vaniman, D.T., 1983, Tectonic implications of mid-Tertiary dikes in west-central New Mexico, Geology, 11, 45-48.

Laughlin, A.W., Brookins, D.G., Damon, P.E. and Shafiqullah, M., 1979, Late Cenozoic volcanism of the central Jemez zone, Arizona-New Mexico, Isochron/West, 25, 5-8.

Laughlin, A.W., Damon, P.E. and Shafiqullah, M., 1980, New K-Ar dates from the Springerville volcanic field, central Jemez zone, Apache County, Arizona, Isochron/West, 29, 3-4.

Lees, C.H., 1910, On the shape of the isogeotherms under mountain ranges in radioactive districts, Proc. Roy. Soc. London, A 83, 339-346.

Leopold, L.B., Wolman, M.G. and Miller, J.P., 1964, Fluvial processes in geomorphology, W.H. Freeman and Co., San Francisco, 52 p.

Levitte, D. and Gambill, D.T., 1980, Geothermal potential of west-central New Mexico from geochemical and thermal gradient data, Los Alamos Scientific Lab. Rep., LA-8608-MS, 102 p.

Lindgren, B.W., McElrath, G.W. and Berry, D.A., 1978, Introduction to probability and statistics, MacMillan Pub. Co., New York, 356 p.

Lipman, P.W. and Mehnert, H.H., 1979, Potassium-argon ages from the Mount Taylor volcanic field, New Mexico, U.S. Geol. Surv. Prof. Pap., 1124-B, B1-B8.

Luchitta, I. 1972, Early history of the Colorado River in the Basin and Range province, Geol. Soc. Amer. Bull., 83, 1933-1948.

Magara, K., 1980, Comparison of porosity-depth relationships of shale and sandstone, J. Petr. Geol., 3, 175-185.

Majorowicz, J.A. and Jessop, A.M., 1981, Regional heat flow patterns in the western Canadian sedimentary basin, Tectonophysics, 74, 209-238.

Mansure, A.J. and Reiter, M., 1979, A vertical groundwater movement correction for heat flow, J. Geophys. Res., 84, 3490-3496.

Mayo, E.B., 1958, Lineament tectonics and some ore districts of the southwest, Mining Engineering, 10, 1169-1175.

McKee, E.D. and McKee, E.H., 1972, Pliocene uplift of the Grand Canyon region - time of drainage adjustment, Geol. Soc. Amer. Bull., 83, 1923-1932.

Minier, J., Reiter, M., Shafiqullah, M. and Damon, P.E., 1987, Geothermal studies in the Quemado area, New Mexico, submitted for publication.

Molenaar, C.M., 1977, Stratigraphy and depositional history of upper Cretaceous rocks of the San Juan basin area, New Mexico and Colorado, with a note on economic resources, in New Mexico Geol. Soc. Gdbk., 28th Field Conf., 159-166.

Morrison, M.A., Thompson, R.N. and Dickin, A.P., 1985, Geochemical evidence for complex magmatic plumbing during development of a continental volcanic center, Geology, 13, 581-584.

Naeser, C.W., 1971, Geochemistry of the Navajo-Hopi dia tremes, Four Corners area, J. Geophys. Res., 76, 4978-4985.

Nichols, R.L., 1946, McCartys basalt flow, Valencia County, New Mexico, Geol. Soc. Amer. Bull., 86, 811-818.

Norton, D. and Knight, J., 1977, Transport phenomena in hydrothermal systems: cooling plutons, Amer. J. Sci., 277, 937-981.

Osburn, J.C., 1982, Geology and coal resources of three quadrangles in the central Datil Mountains coal field, Socorro County, New Mexico, New Mexico Bur. Mines Mineral Resources Open-File Rep., 164, 82 p.

Pakiser, L.C., 1963, Structure of the crust and upper mantle in the western United States, J. Geophys. Res., 68, 5747-5756.

Philip, J.R. and de Vries, D.A., 1957, Moisture movement in porous materials under temperature gradients, Trans. Amer. Geophys. U., 38, 222-232.

Pohlmann, H.F., 1967, The Navajo indian nation and Dineh bi Keyah, New Mexico Geol. Soc. Gdbk., 18th Field Conf., 63-69.

Reiter, M.A., 1969, Terrestrial heat flow and thermal conductivity in southwestern Virginia, Ph.D. diss., Virginia Polytechnic Inst., 106 p.

Reiter, M. and Clarkson, G., 1983, Geothermal studies in the San Juan basin and the Four Corners area of the Colorado Plateau II. Steady-state models of the thermal source of the San Juan volcanic field, Tectonophysics, 91, 253-269.

Reiter, M., Edwards, C.L., Hartman, H. and Weidman, C., 1975, Terrestrial heat flow along the Rio Grande rift, New Mexico and southern Colorado, Geol. Soc. Amer. Bull., 86, 811-818.

Reiter, M., Eggleston, R.E., Broadwell, B.R. and Minier, J., 1986, Estimates of terrestrial heat flow from deep petroleum tests along the Rio Grande rift in central and southern New Mexico, J. Geophys. Res., 91, 6225-6245.

Reiter, M. and Hartman, H., 1971, A new steady-state method for determining thermal conductivity, J. Geophys. Res., 76, 7047-7051.

Reiter, M. and Mansure, A.J., 1983, Geothermal studies in the San Juan basin and the Four Corners area of the Colorado Plateau I. terrestrial heat-flow measurements, Tectonophysics, 91, 233-251.

Reiter, M., Mansure, A.J. and Shearer, C., 1979, Geothermal characteristics of the Colorado Plateau, Tectonophysics, 61, 183-195.

Reiter, M. and Minier, J., 1985, Possible infuences of thermal stresses on Basin and Range faulting, J. Geo phys. Res., 90, 10,209-10,222.

Reiter, M., Minier, J. and Gutjahr, A., 1985, Variance analysis of estimates and measurements of terrestrial heat flow, Geothermics, 14, 499-509.

Reiter, M. and Shearer, C., 1979, Terrestrial heat flow in eastern Arizona: a first report, J. Geophys. Res., 84, 6115-6120.

Reiter, M., Shearer, C. and Edwards, C.L., 1978, Geothermal anomalies along the Rio Grane rift in New Mexico, Geology, 6,85-88.

Reiter, M. and Tovar R., J.C., 1982, Estimates of terrestrial heat flow in northern Chihuahua, Mexico, based upon petroleum bottom-hole temperatures, Geol. Soc. Amer. Bull., 93, 613-624.

Renault, J., 1970, Major-element variations in the Potrillo, Carrizozo, and McCartys basalt fields, New Mexico, New Mexico Bur. Mines Mineral Resources Circ., 113, 22 p.

Roy, R.F., Decker, E.R., Blackwell, D.D. and Birch, F., 1968, Heat flow in the United States, J. Geophys. Res., 73, 5207-5221.

Sammis, T.W., Evans, D.D. and Warrick, A.W., 1982, Com parison of methods to estimate deep percolation rates, Water Resources Res., 18, 465-470.

Sass, J.H., Lachenbruch, A.H. and Munroe, R.J., 1971, Thermal conductivity of rocks from measurements on fragments and its application to heat-flow determinations, J. Geophys. Res., 76, 3391-3401.

Sass, J.H., Stone, C. and Bills, D.J., 1982, Shallow subsurface temperatures and some estimates of heat flow from the Colorado Plateau of northeastern Arizona, U.S. Geol. Surv. Open-File Rep. 82-994, 112 p.

Shearer, C.R., 1979, A regional terrestrial heat-flow study in Arizona, Ph.D. diss., New Mexico Institute of Mining and Technology, Socorro, 184 p.

Smith, L. and Chapman, D.S., 1983, On the thermal effects of groundwater flow 1. regional scale systems, J. Geophys. Res., 88, 593-608.

Smith, R.B. and Sbar, M.L., 1974, Contemporaneous tectonics and seismicity of the western United States with emphasis on the Intermountain seismic belt, Geol. Soc. Amer. Bull., 85, 1205-1218.

Snedecor, G.W. and Cochran, W.G., 1973, Statistical methods, Iowa State Univ. Press, Ames, Iowa.

Sorey, M.L., 1971, Measurement of vertical groundwater velocity from temperature profiles in wells, Water Resources Res., 7, 963-970.

Stach, E., Mackowsky, M.T., Teichmuller, M., Taylor, G.H., Chandra, D. and Teichmuller, R., 1982, Coal Petrology, 3rd ed., Gebruder-Borntraeger, Berlin, 535 p.

Stallman, R.W., 1963, Computation of ground-water velocity from temperature data, U.S. Geol. Surv. Water Supply Pap., 1544-H, 36-46.

Steven, T.A., 1975, Mid-Tertiary volcanic field in the southern Rocky Mountains, Geol. Soc. Amer. Mem., 144, 74-94.

Stone, W.J., 1984, Recharge in the Salt Lake coal field based on chloride in the unsaturated zone, New Mexico Bur. Mines Mineral Resources Open-File Rep., 214, 64 p.

Stone, W.J. and McGurk, B.E., 1987, Hydrogeologic considerations in mining, Nations Draw Area, Salt Lake Coal Field, New Mexico, Guidebook Paper, Coal Division Field Trip, Geol. Soc. Amer. Annual Meeting, Phoenix.

Summers, W.K., 1972, Hydrogeology and water supply of the Pueblo of Zuni, McKinley and Valencia Counties, New Mexico, New Mexico Bur. Mines Mineral Resources Open-File Rep., 33.

Suppe, J., Powell, C. and Berry, R., 1975, Regional topography, seismicity, Quaternary volcanism and present-day tectonics of the western United States, Amer. J. Sci., 275A, 397-436.

Tabet, D., 1981, Geology and coal resources, Pinehaven quadrangle, New Mexico Bur. Mines Mineral Resources Open-File Rep., 154, 71 p.

Thompson, G.A. and Burke, D.B., 1974, Regional geophysics of the Basin and Range province, Ann. Rev. Earth Planet. Sci., 2, 213-238.

Thompson, G.A. and Zoback, M.L., 1979, Regional geophysics of the Colorado Plateau, Tectonophysics, 61, 149-181.

Ting, F.T.C., 1982, Coal macerals, in, Coal Structure, R.A. Meyers, ed., Academic Press, New York, 7-49.

Turcotte, D.L. and Schubert, G., Geodynamics, applications of continuum physics to geological problems, John Wiley and Sons, New York.

Van Krevelen, D.W., 1961, Coal, Elsevier, Amsterdam, 514 p.

Van Schmus, W.R. and Bickford, M.E., 1981, Proterozoic chronology and evolution of the mid-continent region, North America, in, Precambrian Plate Tectonics, A. Kroner, ed., Elsevier, Amsterdam, 261-296.

Waples, D.W., 1980, Time and temperature in petroleum formation: Application of Lopatin's method to petroleum exploration, Amer. Assoc. Petrol. Geol. Bull., 64, 916-926.

Waples, D., 1981, Organic geochemistry for exploration geologists, Burgess Pub. Co., Minneapolis, 151 p.

Ward, C.R., ed., 1984, Coal geology and coal technology, Blackwell Scientific Pub., Melbourne, 345 p.

Wilson, E.D., Moore, R.T. and Cooper, J.R., 1969, Geologic map of Arizona, 1:500,000, Arizona Bur. Mines and U.S. Geol. Surv.

Woodside, W. and Messmer, J.H., 1961, Thermal conductivity of porous media, J. Appl. Phys., 32, 1688-1706.

Zoback, M.L., Anderson, R.E. and Thompson, G.A., 1981, Cainozoic evolution of the state of stress and style of tectonism of the Basin and Range province of the western United States, Phil. Trans. Roy. Soc. London, A 300, 407-434.

Zoback, M.L. and Zoback, M., 1980, State of stress in the conterminous United States, J. Geophys. Res., 85, 6113--6156.

This dissertation is accepted on behalf of the faculty of the Institute by the following committee:

Advisor

Nov. 25, 1987
Date